A Study of Differential and Integral Operators in Linear Viscoelasticity

by

Faris Alzahrani

A thesis submitted for the degree of

Doctor of Philosophy

Cardiff University

School of Mathematics

2013

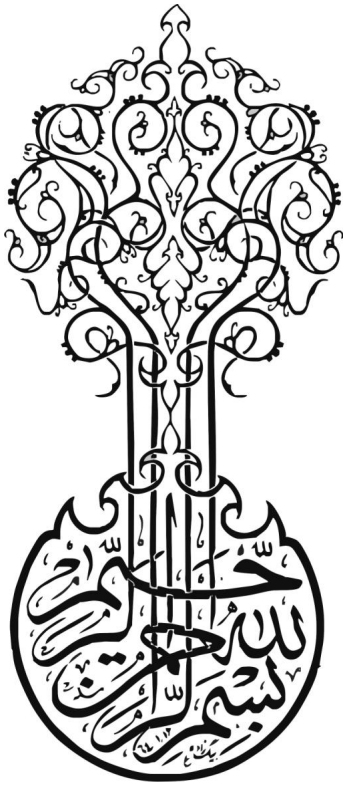

In the name of Allah
the Most Gracious, the Most Merciful

To
my late father, Saeed
and
my mother, Nourah.

DECLARATION

This work has not previously been submitted in substance for any other degree or award at this or any other university or place of learning, nor is being submitted concurrently in candidature for any degree or other award.

Signature ..... (F. Alzahrani) Date .....

STATEMENT 1

This thesis is being submitted in partial fulfillment of the requirements for the degree of PhD.

Signature ..... (F. Alzahrani) Date .....

STATEMENT 2

This thesis is the result of my own independent work/investigation, except where otherwise stated. Other sources are acknowledged by explicit references. The views expressed are my own.

Signature ..... (F. Alzahrani) Date .....

STATEMENT 3

I hereby give consent for my thesis, if accepted, to be available for photocopying and for inter-library loan, and for the title and summary to be made available to outside organisations.

Signature ..... (F. Alzahrani) Date .....

ACKNOWLEDGEMENTS

I will be forever grateful and indebted to Prof. Russell Davies, who has expertly supervised this thesis. He has always been there for me with his endless ideas and knowledge, despite his busy schedule as the Head of Mathematics School. This research project would certainly not have been possible without the help of Allah and then the continual guidance and advice of Prof. Davies. I consider myself extremely fortunate to have been his last PhD student, and I wish him all the best in his retirement.

I would also like to thank Dr. Karl Schmidt, who was willing to help whenever I asked. I especially thank him and Prof. William Evans for reviewing my thesis. Thanks should also be extended to Ms. Maureen Mills, the secretary of Prof. Davies, for being very helpful and friendly.

I gratefully acknowledge the generous financial support I have received from King Abdulaziz University in Saudi Arabia.

My sincerest and deepest gratitude goes to my beloved mother, whose constant prayers for me have been a great source of strength throughout this study. I thank her for everything she has done for me. My brothers (Nasir, Fahad and Bandar) and my sisters also deserve great gratitude for their support and well wishes. I should also mention my father-in-law Mr. Muidh Alzahrani for his encouragement.

Last but by no means least, I owe a very special debt of gratitude to my lovely wife Najah, who has experienced many ups and downs of this academic adventure. I thank her not only for her sacrifices, patience and understanding, but also for taking care of our beautiful daughter, Tala.

ABSTRACT

This thesis identifies and explores a link between the theory of linear viscoelasticity and the spectral theory of Sturm-Liouville problems.

The thesis is divided into five chapters. Chapter 1 gives a brief account of the relevant parts of the theory of linear viscoelasticity and lays the foundation for making the link with spectral theory. Chapter 2 is concerned with the construction of approximate Dirichlet series for completely monotonic functions. The chapter introduces various connections between non-negative measures, orthogonal polynomials, moment problems, and the Stieltjes continued fraction. Several interlacing properties for discrete relaxation and retardation times are also proved.

The link between linear viscoelasticity and spectral theory is studied in detail in Chapter 3. The stepwise spectral functions associated with some elementary viscoelastic models are derived and their Sturm-Liouville potentials are explicitly found by using the Gelfand-Levitan method for inverse spectral problems.

Chapter 4 presents a new family of exact solutions to the nonlinear integro-differential A-equation, which is the main equation in a recent method proposed by Barry Simon for solving inverse spectral problems. Starting from the A-amplitude $A(t) = A(t, 0)$ which is determined by the spectral function, the solution $A(t, x)$ of the A-equation identifies the potential $q(x)$ as $A(0, x)$.

Finally, Chapter 5 deals with two numerical approaches for solving an inverse spectral problem with a viscoelastic continuous spectral function. In the first approach, the A-equation is solved by reducing it to a system of Riccati equations using expansions in terms of shifted Chebyshev polynomials. In the second approach, the spectral function is approximated by stepwise spectral functions whose potentials, obtained using the Gelfand-Levitan method, serve as approximations for the underlying potential.

CONTENTS

LIST OF FIGURES

LIST OF TABLES

1

INTRODUCTION

1.1 Linear viscoelasticity

Viscoelasticity is the theory that describes the behaviour of materials which display a time-dependent relationship between stress and strain. In a viscoelastic material, the strain at a given point and at a given time is specified by a strain tensor, γ_{ij}, $i, j = 1, 2, 3$. For an infinitesimal deformation, in terms of Cartesian coordinates, the strain tensor takes the simple form

$$\gamma_{ij} = \frac{1}{2}\left(\frac{\partial u_i}{\partial x_j} + \frac{\partial u_j}{\partial x_i}\right),$$

where x_i is a component of position and u_i is a component of displacement. The rate of strain tensor, $\dot{\gamma}_{ij}$, is formulated similarly with u_i replaced by v_i, the velocity of displacement. For large deformation, the definition of strain becomes much more complicated and will not be addressed in this thesis.

In the theory of linear viscoelasticity, the relationship between stress in a viscoelastic material (specified by a tensor σ_{ij}) and strain, γ_{ij}, is linear. For small uniform shear deformations, the stress and strain components are independent of position. Furthermore, for incompressible deformations, the stress and strain tensors are symmetric. For small incompressible shear deformations, it is only the time-dependent shear components σ_{12} and γ_{12} which play a role and it is customary to drop the index notation. We shall write $\sigma_{12} = \sigma(t)$ and $\gamma_{12} = \gamma(t)$. The relationship between stress and strain is modelled by linear integral or differential equations and it is the detailed study of the nature of these integral and differential operators which will be the subject of this thesis.

In what follows, we will look at different well-known viscoelastic models used to describe linear viscoelasticity. The simplest model for a linear viscoelastic material undergoing incompressible shear deformation was proposed in 1867 by James Clerk Maxwell [21]. In this model, the relationship between the stress and strain

reads

$$\sigma + \tau\dot{\sigma} = \eta\dot{\gamma}, \tag{1.1}$$

where the positive constants τ and η denote, respectively, a relaxation time and a viscosity. The solution of this differential equation, with $\sigma(-\infty) = 0$, is given by

$$\sigma(t) = \frac{\eta}{\tau}\int_{-\infty}^{t} \exp\left[-\frac{(t-t')}{\tau}\right]\dot{\gamma}(t')\,dt', \tag{1.2}$$

where t and t' denote the present and the earlier times, respectively.

In 1874, Ludwig Boltzmann proposed a general linear integral model [25]. In the context of simple shear, this may be written in the form [11]

$$\sigma(t) = \int_{-\infty}^{t} G(t-t')\dot{\gamma}(t')\,dt'. \tag{1.3}$$

The kernel function $G(t)$ is monotonically decreasing and is known as the relaxation function for the material. Equation (1.3) shows that the current stress of a viscoelastic material depends on the complete past history of the strain-rate experienced by the material. For this reason, viscoelastic materials are often referred to as materials with memory. Writing (1.3) in the form

$$\sigma(t) = \int_{0}^{\infty} G(s)\dot{\gamma}(t-s)\,ds, \qquad s = t - t',$$

it follows, since $G(s)$ is monotonically decreasing with increasing time-lapse s, that $\sigma(t)$ depends more on the recent past than the distant past. This property is known as the principle of fading memory.

It is inherent in Boltzmann's classical formulation of the theory of linear viscoelasticity that for fixed pressure and temperature, every material possesses a unique relaxation function $G(t)$. This is a key material function which is of vital importance in the characterization of modern advanced materials. In practice, the function is determined experimentally. By comparing (1.2) and (1.3), we see immediately that for the Maxwell model, the corresponding relaxation function

takes the form

$$G(t) = g \exp\left(-\frac{t}{\tau}\right), \qquad g = \frac{\eta}{\tau},$$

where the constant g is called the elastic modulus of the material.

Equation (1.1) can be generalized for a number, n, of Maxwell elements using the principle of superposition, giving the so-called multi-mode Maxwell model. The stress in this case has the form

$$\sigma(t) = \sum_{i=1}^{n} \sigma_i(t), \tag{1.4a}$$

where each σ_i satisfies (1.1) with different τ_i and η_i, i.e.,

$$\sigma_i + \tau_i \dot{\sigma}_i = \eta_i \dot{\gamma}, \qquad i = 1, \ldots, n. \tag{1.4b}$$

Consequently, from (1.2), we find that

$$\sigma(t) = \sum_{i=1}^{n} \frac{\eta_i}{\tau_i} \int_{-\infty}^{t} \exp\left[-\frac{(t-t')}{\tau_i}\right] \dot{\gamma}(t')\, dt',$$

which gives the following relaxation function

$$G(t) = \sum_{i=1}^{n} g_i \exp\left(-\frac{t}{\tau_i}\right), \qquad g_i = \frac{\eta_i}{\tau_i}. \tag{1.5}$$

The differential system (1.4b) can be replaced by a single differential equation in σ of order n. The most general differential equation for linear viscoelasticity takes the form [2]

$$\left[1 + \sum_{i=1}^{n} \alpha_i D^i\right] \sigma = \left[\beta_0 + \sum_{i=1}^{m} \beta_i D^i\right] \gamma, \tag{1.6}$$

where $n = m$ or $n = m - 1$. In this equation, D denotes the differential operator d/dt and α_i, β_i are constants. For the case of the multi-mode Maxwell model, we

have $\beta_0 = 0$ and the coefficients α_i are determined from the identity

$$1 + \sum_{i=1}^{n} \alpha_i x^i = \prod_{i=1}^{n} (1 + \tau_i x).$$

Two further special cases of (1.6) need to be introduced here. The first one corresponds to $n = 0$, $m = 1$, $\beta_0 = 0$ and is the constitutive equation proposed by Isaac Newton (1642-1727) as the model for a purely viscous fluid

$$\sigma = \eta_1 \dot{\gamma}. \tag{1.7}$$

There is no memory in this model, since the stress depends only on the current rate of strain. The relaxation function here is simply

$$G(t) = \eta_1 \delta(t),$$

where $\delta(t)$ denotes the Dirac delta function.

The second special case is the constitutive equation for the Oldroyd-B model [23]. The form of such an equation reads

$$\sigma + \tau_2 \dot{\sigma} = \eta \dot{\gamma} + \eta_1 \tau_2 \ddot{\gamma}, \tag{1.8a}$$

and may be decomposed as follows

$$\sigma = \sigma_1 + \sigma_2, \qquad \eta = \eta_1 + \eta_2, \tag{1.8b}$$

where

$$\sigma_1 = \eta_1 \dot{\gamma}, \qquad \sigma_2 + \tau_2 \dot{\sigma}_2 = \eta_2 \dot{\gamma}.$$

In this case, the relaxation function is given by

$$G(t) = \eta_1 \delta(t) + g_2 \exp\left(-\frac{t}{\tau_2}\right), \qquad g_2 = \frac{\eta_2}{\tau_2}.$$

1.2 Complete monotonicity and the relaxation spectrum

Boltzmann's equation (1.3), upon integration by parts and assuming $\gamma(-\infty) = 0$, may be rewritten in the form

$$\sigma(t) = G(0)\gamma(t) - \int_{-\infty}^{t} M(t-t')\gamma(t')\,dt',$$

where

$$M(t) = -\frac{dG(t)}{dt},$$

is called the memory function of the material. $M(t)$ is positive and, in accord with the principle of fading memory, is again monotonically decreasing. Thus, fading memory demands that $G(t)$ is monotonically decreasing and $\dot{G}(t)$ is monotonically increasing.

We next consider the much more restrictive assumption that $G(t)$ is completely monotonic, i.e.,

$$(-1)^n \frac{d^n G(t)}{dt^n} \geq 0, \qquad n \geq 0, \qquad t \geq 0.$$

According to Bernstein's theorem [28], $G(t)$ is completely monotonic on $[0, \infty)$ if and only if it can be represented as the Laplace transform of a non-negative measure, i.e.,

$$G(t) = \int_0^\infty \exp(-st)\,d\mu(s), \tag{1.9}$$

where $\mu(s)$ is bounded and non-decreasing and the integral converges for all $t \geq 0$.

Since, in equation (1.5), the constants g_i and τ_i are positive, it follows that the relaxation function for the multi-mode Maxwell model is completely monotonic. Furthermore, by making the change of variable $s = \tau^{-1}$, the appropriate measure $d\mu(s)$ is given by

$$d\mu(s) = \frac{1}{\tau}\sum_{i=1}^{n} \eta_i \delta(\tau - \tau_i)\,d\tau. \tag{1.10}$$

In the literature on linear viscoelasticity, the distribution

$$H(\tau) = \sum_{i=1}^{n} \eta_i \delta(\tau - \tau_i),$$

is called the discrete relaxation spectrum of a material. There is a huge literature on various methods for determining the discrete relaxation spectra from experimental data. A recent account is given by Davies and Goulding [7].

As we have stated, the measure (1.10) associated with the multi-mode Maxwell model gives rise to a discrete spectrum of relaxation times which may be used to characterize a viscoelastic material. On the other hand, if the measure for $G(t)$ is continuous or piecewise continuous, then there is an associated non-negative continuous relaxation spectrum, $H(\tau)$, given by

$$d\mu(s) = \tau H(\tau)\, ds, \qquad s = \tau^{-1}. \tag{1.11}$$

Equation (1.9) may then be rewritten in the form

$$G(t) = \int_0^\infty \exp\left(-\frac{t}{\tau}\right) \frac{H(\tau)}{\tau}\, d\tau, \tag{1.12}$$

which is the conventional form found in the literature on linear viscoelasticity [11].

Whether or not the spectrum is discrete or continuous, the total viscosity of the material being modelled is expressed as

$$\eta = \int_0^\infty H(\tau)\, d\tau. \tag{1.13}$$

This is the zeroth moment of the relaxation spectrum. Provided $G(t)$ has no term in $\delta(t)$, the first negative moment

$$\mu_0 = \int_0^\infty \tau^{-1} H(\tau)\, d\tau,$$

always exists and takes the value $G(0)$. The other negative moments

$$\mu_n = \int_0^\infty \tau^{-(n+1)} H(\tau)\, d\tau, \qquad n = 1, 2, 3, \ldots,$$

always exist for a discrete spectrum, but may not always exist for a continuous spectrum. If $G(t)$ has a representation as a Maclaurin series, then all negative moments exist and take the values

$$\mu_n = (-1)^n G^{(n)}(0).$$

A proof of this is given in the appendix.

Finally, in Table 1.1 below, we collect the formulae for the relaxation functions and discrete relaxation spectra for the models introduced in the previous section.

Model	**Equation**	$G(t)$	$H(\tau)$
Newtonian	(1.7)	$\eta_1 \delta(t)$	$\eta_1 \delta(\tau)$
Maxwell	(1.1)	$\frac{\eta_1}{\tau_1} \exp\left(-\frac{t}{\tau_1}\right)$	$\eta_1 \delta(\tau - \tau_1)$
Oldroyd-B	(1.8)	$\eta_1 \delta(t) + \frac{\eta_2}{\tau_2} \exp\left(-\frac{t}{\tau_2}\right)$	$\eta_1 \delta(\tau) + \eta_2 \delta(\tau - \tau_2)$
Multi-mode Maxwell	(1.4)	$\sum_{i=1}^{n} \frac{\eta_i}{\tau_i} \exp\left(-\frac{t}{\tau_i}\right)$	$\sum_{i=1}^{n} \eta_i \delta(\tau - \tau_i)$

Table 1.1: Relaxation functions and discrete relaxation spectra for four well-known models.

1.3 Ill-posedness

Equation (1.12) and its Laplace transform equivalent

$$G(t) = \int_0^\infty \exp(-st)\, s^{-1} H(s^{-1})\, ds,$$

are both examples of a Fredholm integral equation of the first kind with smooth kernel. For such equations the problem of determining $H(\tau)$ from $G(t)$ is ill-posed in the sense of Hadamard. Let us assume that $H(\tau)$ exists and is unique for a given $G(t)$. The problem of finding $H(\tau)$ from $G(t)$ is ill-posed if a small perturbation in $G(t)$ leads to an arbitrarily large perturbation in $H(\tau)$, i.e., the inverse of the integral operator is not continuous. The ill-posedness of the inverse Laplace transform has been well documented (see, for instance, Epstein and Schotland [9]). It is known to be exponentially ill-posed.

We can demonstrate the ill-posedness of problem (1.12) by choosing a simple example. Let ϵ be small and positive, and let $H^\epsilon(\tau)$ be the box spectrum

$$H^\epsilon(\tau) = \begin{cases} \dfrac{1}{\epsilon}, & 1 \le \tau \le 1+\epsilon^2, \\ 0, & \text{otherwise.} \end{cases}$$

Then $G^\epsilon(t)$ has the form

$$G^\epsilon(t) = \frac{1}{\epsilon}\left[\mathrm{Ei}\left(\frac{t}{1+\epsilon^2}\right) - \mathrm{Ei}(t)\right], \tag{1.14}$$

where Ei is the exponential integral defined by

$$\mathrm{Ei}(t) = \int_1^\infty \frac{1}{x}\exp(-xt)\,dx. \tag{1.15}$$

The right-hand side of (1.14) may be expanded as a series in ϵ to give

$$G^\epsilon(t) = \exp(-t)\epsilon + \frac{1}{2}(t-1)\exp(-t)\epsilon^3 + O(\epsilon^5).$$

The function $G^\epsilon(t)$ is completely monotonic, although if the series is truncated to more than one term, the truncated series is not completely monotonic. By taking a perturbation in $G(t)$ of the form (1.14) of order ϵ in supremum norm, the corresponding perturbation in $H(\tau)$ will be of order ϵ^{-1} measured in supremum norm.

1.4 Relaxation and creep compliance functions

In this section, we consider the physical meaning of the relaxation function and show that is connected to the phenomenon of creep. The connection is made through the creep compliance function, $J(t)$.

The relaxation function $G(t)$ has the physical interpretation that it depicts the way in which the stress relaxes upon imposing a step-strain

$$\gamma(t) = \begin{cases} \gamma_0 & \text{if} \quad t \geq 0, \\ 0 & \text{if} \quad t < 0. \end{cases} \tag{1.16}$$

To prove this, we rewrite the Boltzmann equation (1.3) as

$$\sigma(t) = \gamma(0)G(t) + \int_0^t G(t-t')\dot{\gamma}(t')\,dt', \tag{1.17}$$

where we have assumed that $\gamma(t) = 0$ when $t < 0$. Substituting (1.16) into (1.17) yields

$$G(t) = \frac{\sigma(t)}{\gamma_0}, \qquad t \geq 0.$$

On the other hand, if, instead of (1.16), one considers an imposed step-stress

$$\sigma(t) = \begin{cases} \sigma_0 & \text{if} \quad t \geq 0, \\ 0 & \text{if} \quad t < 0, \end{cases} \tag{1.18}$$

then the Laplace transform $\widehat{\gamma}(s)$ of $\gamma(t)$ may be found from (1.17) in the form

$$\widehat{\gamma}(s) = \frac{\sigma_0}{s^2\widehat{G}(s)}.$$

By introducing the new function $\widehat{J}(s)$ such that

$$\widehat{G}(s)\widehat{J}(s) = \frac{1}{s^2}, \tag{1.19}$$

it follows that

$$J(t) = \frac{\gamma(t)}{\sigma_0}, \qquad t \geq 0.$$

The function $J(t)$ is called the creep compliance function since it describes the strain (creep) resulting from the imposed step-stress (1.18).

Equation (1.19) is simply the Laplace transform of the following integral equation, known as the interconversion equation, which establishes the relationship between $G(t)$ and $J(t)$ [11]

$$\int_0^t G(t-t')J(t')\,dt' = \int_0^t J(t-t')G(t')\,dt' = t. \tag{1.20}$$

1.5 The retardation spectrum

The Laplace transform of equation (1.12) reads

$$\widehat{G}(s) = \int_0^\infty \frac{H(\tau)}{\tau s + 1}\,d\tau, \qquad \mathrm{Re}(s) > 0. \tag{1.21}$$

Under the simple change of variable $s = -z^{-1}$, we obtain

$$-z^{-1}\widehat{G}\left(-z^{-1}\right) = \int_0^\infty \frac{H(\tau)}{\tau - z}\,d\tau, \qquad \mathrm{Re}(z) < 0, \tag{1.22}$$

which means that $-z^{-1}\widehat{G}\left(-z^{-1}\right)$ corresponds to the Stieltjes transform of the relaxation spectrum in the left half-plane. The Stieltjes transform is analytic in the upper half-plane. This means that $-z^{-1}\widehat{G}\left(-z^{-1}\right)$ can be analytically continued into the upper half-plane with

$$\mathrm{Im}\Big(-z^{-1}\widehat{G}\left(-z^{-1}\right)\Big) > 0, \qquad \text{for} \qquad \mathrm{Im}(z) > 0.$$

These two properties imply that $-z^{-1}\widehat{G}\left(-z^{-1}\right)$ is a Herglotz function [1]. Using the important property of Herglotz functions that if $F(z)$ is Herglotz, then so is

$-F(z)^{-1}$, we find from (1.19) that

$$z^{-1}\widehat{J}\big(-z^{-1}\big) = \frac{1}{z^{-1}\widehat{G}\big(-z^{-1}\big)}, \qquad z = -s^{-1}, \tag{1.23}$$

is also a Herglotz function. Being Herglotz means that there exists a monotone non-decreasing function $\mu_J(\lambda)$ with the following property

$$\int_0^\infty \frac{d\mu_J(\lambda)}{1+\lambda^2} < \infty,$$

and related to $z^{-1}\widehat{J}\big(-z^{-1}\big)$ via the integral

$$z^{-1}\widehat{J}\big(-z^{-1}\big) = \alpha + \beta z + \int_0^\infty \left[\frac{1}{\lambda - z} - \frac{\lambda}{1+\lambda^2}\right] d\mu_J(\lambda), \tag{1.24}$$

where

$$\alpha = \mathrm{Re}\Big(-i\widehat{J}(i)\Big), \qquad \text{and} \qquad \beta = \lim_{z\to\infty} z^{-2}\widehat{J}\big(-z^{-1}\big) \geq 0.$$

Equation (1.24), upon changing the variable back to s and rearranging, reads

$$\widehat{J}(s) = -\left[\alpha + \int_0^\infty \frac{d\mu_J(\lambda)}{\lambda(1+\lambda^2)}\right]\frac{1}{s} + \frac{\beta}{s^2} + \int_0^\infty \left[\frac{1}{\lambda s} - \frac{1}{\lambda s + 1}\right] d\mu_J(\lambda),$$

which is the Laplace transform of

$$J(t) = -\left[\alpha + \int_0^\infty \frac{d\mu_J(\lambda)}{\lambda(1+\lambda^2)}\right] + \beta t + \int_0^\infty \left[1 - \exp\left(-\frac{t}{\lambda}\right)\right]\frac{d\mu_J(\lambda)}{\lambda}. \tag{1.25}$$

From (1.13), (1.21) and (1.23), it follows that

$$\beta = \frac{1}{\eta}.$$

Furthermore, if we write $J(0) = j_0$ and introduce the continuous retardation spectrum, $L(\lambda)$, defined by

$$d\mu_J(\lambda) = L(\lambda)\, d\lambda,$$

equation (1.25) will then reduce to the conventional form found in the literature on linear viscoelasticity [11]

$$J(t) = j_0 + \frac{t}{\eta} + \int_0^\infty \left[1 - \exp\left(-\frac{t}{\lambda}\right)\right] \frac{L(\lambda)}{\lambda}\, d\lambda,$$

where λ denotes a retardation time.

For each discrete relaxation spectrum, there exists a corresponding discrete retardation spectrum. The discrete retardation spectra for the models introduced in Section 1.1 are listed in Table 1.2 below together with their corresponding creep compliance functions.

Model	**Equation**	$J(t)$	$L(\lambda)$
Newtonian	(1.7)	$\frac{t}{\eta_1}$	0
Maxwell	(1.1)	$\frac{\tau_1}{\eta_1} + \frac{t}{\eta_1}$	0
Oldroyd-B	(1.8)	$\frac{t}{\eta} + j_1\left[1 - \exp\left(-\frac{t}{\lambda_1}\right)\right]$	$j_1\lambda_1\delta(\lambda - \lambda_1)$
Multi-mode Maxwell	(1.4)	$j_0 + \frac{t}{\eta} + \sum_{i=1}^{n-1} j_i\left[1 - \exp\left(-\frac{t}{\lambda_i}\right)\right]$	$\sum_{i=1}^{n-1} j_i\lambda_i\delta(\lambda - \lambda_i)$

Table 1.2: Creep compliance functions and discrete retardation spectra for four well-known models. For the Oldroyd-B model, we have $j_1 = \eta_2\tau_2/\eta^2$ and $\lambda_1 = \eta_1\tau_2/\eta$. For the multi-mode Maxwell model, we have $\eta = \sum_{i=1}^{n} \eta_i$.

Tables 1.1 and 1.2 show that for the case of the multi-mode Maxwell model, $G(t)$ has n relaxation times, whereas $J(t)$ has $n-1$ retardation times. These relaxation and retardation times, as will be proved in the next chapter, separate each other as follows [22]

$$\tau_1 < \lambda_1 < \tau_2 < \cdots < \tau_{n-1} < \lambda_{n-1} < \tau_n, \tag{1.26}$$

a property known as the interlacing property.

1.6 Connection with Weyl-Titchmarsh theory

It is known from the Weyl-Titchmarsh theory (see, for instance, [8] and [17]) that for the Sturm-Liouville problem

$$\begin{cases} -y''(x,z) + q(x)y(x,z) = zy(x,z), & x \geq 0, \\ y(0,z) = 0, \end{cases} \tag{1.27}$$

there exists a Herglotz function, $m(z)$, called the Weyl-Titchmarsh function. Such a function has the representation

$$m(z) = \mathrm{Re}(m(i)) + \int_{-\infty}^{\infty} \left[\frac{1}{\tau - z} - \frac{\tau}{1+\tau^2} \right] d\rho(\tau), \qquad \mathrm{Im}(z) > 0,$$

where $\rho(\tau)$ is called the spectral function of the problem (1.27). Everitt [10] has shown that

$$m(z) = iz^{1/2} + o(1), \quad \text{as} \quad |z| \to \infty, \quad 0 < \epsilon < \arg(z) < \pi - \epsilon.$$

If we return to the Herglotz function $-z^{-1}\widehat{G}(-z^{-1})$ given by (1.22), then we find

$$-z^{-1}\widehat{G}(-z^{-1}) = o(1), \quad \text{as} \quad |z| \to \infty.$$

One of the purposes of this thesis is to investigate the question of whether there exists a certain Sturm-Liouville problem of the form (1.27) whose Weyl-Titchmarsh function is

$$m(z) = iz^{1/2} - z^{-1}\widehat{G}(-z^{-1}), \qquad \mathrm{Im}(z) > 0. \tag{1.28}$$

We will show in a later chapter that the answer to this question is yes. This important result will lead us to the study of the inverse spectral problem of recovering the potential $q(x)$ from the spectral function associated with (1.28).

1.7 Thesis outline

The rest of this thesis is organized as follows:

Chapter 2: Constructing Dirichlet series for completely monotonic functions

In this chapter, a particular kind of continued fraction, namely the S-fraction, is used to construct Dirichlet series approximations for the relaxation function which is assumed to be completely monotonic. Each approximation generates its own discrete relaxation spectrum representation for the underlying continuous relaxation spectrum.

Chapter 3: Linear viscoelasticity and spectral theory

In this chapter, we relate for the first time the spectral and Weyl-Titchmarsh functions to the theory of linear viscoelasticity. Another topic considered in this chapter is formulating and explicitly solving inverse spectral problems corresponding to three well-known viscoelastic models.

Chapter 4: A new family of exact solutions to the A-equation

In this chapter, we derive a new family of exact solutions $A(t, x)$ to a particular nonlinear integro-differential equation, the A-equation. Such an equation corresponds to a Sturm-Liouville problem with potential $q(x) = A(0, x)$.

Chapter 5: An inverse spectral problem with continuous spectral function

In this final chapter, we study a viscoelastic inverse spectral problem in which the spectral function is continuous. It is not possible to solve this problem explicitly, and we look at two numerical approaches to solve the problem.

2

CONSTRUCTING DIRICHLET SERIES FOR COMPLETELY MONOTONIC FUNCTIONS

2.1 Introduction

The discrete relaxation spectrum representation is closely related to the problem of approximating the relaxation function, $G(t)$, by a general Dirichlet series of the form

$$G_n(t) = a_{n,0} + \sum_{i=1}^{n} a_{n,i} \exp(-b_{n,i}t), \qquad t \geq 0, \tag{2.1}$$

where the coefficients $a_{n,0}, a_{n,i}$ are non-negative and $b_{n,i}$ are distinct positive. In his paper [20], Liu proved the following: *a function, defined on* $[0, \infty)$*, can be approximated by a Dirichlet series of the form* (2.1) *on supremum norm on* $[0, \infty)$ *if and only if it is completely monotonic on* $[0, \infty)$. This is an extension of a theorem due to Bernstein [3] which may be stated in the form: *every function which is completely monotonic on* $[0, \infty)$ *is the limit as* $n \to \infty$ *of a sum of exponentials of the form* (2.1).

This chapter is essentially concerned with a method for constructing Dirichlet series approximations of the form (2.1) to completely monotonic functions. The method is based on constructing a continued fraction approximation to the Laplace transform of $G(t)$ and related functions. The type of continued fraction is originally due to Stieltjes and is known as an S-fraction. Each approximation generates its own discrete relaxation spectrum representation for the underlying continuous relaxation spectrum $H(\tau)$.

Given any one value of n, we shall show that the S-fraction method can be made to generate more than one discrete relaxation spectrum, and more than one Dirichlet series for $G(t)$. We also show the equivalence of the S-fraction approach to the solution of certain moment problems.

To our knowledge, the S-fraction approach developed in this chapter is the only method for constructing Dirichlet series approximations which does not rely on directly fitting the function being approximated. It has not previously been used to generate discrete relaxation spectra. Bernstein's approach was based on collocation and all conventional methods of fitting are based on sampling the data.

In practice, experimentalists can measure either $G(t)$, the relaxation function, or $J(t)$, the creep compliance function. Most viscoelastic materials respond best either to a step-strain experiment (which gives discrete sampled values of $G(t)$) or to a step-stress experiment (which gives discrete sampled values of $J(t)$). The experimental data is always contaminated by noise. Sums of exponentials are then fitted to $G(t)$ or $J(t)$. Whichever function is fitted, the interconversion equation (1.20) may be solved to find the other.

The most popular methods of fitting experimental data are methods based on constrained non-linear least-squares. Details may be found in Liu [18, 19]. Perhaps the most crucial observation to be made here is that every method delivers a different Dirichlet series and consequently a different discrete spectrum. Also, working with noisy data means that one has to restrict the numbers of terms in the sums to prevent over-fitting or fitting the noise. It is never possible to determine a large number of terms.

The organization of the chapter is as follows. The main idea of the S-fraction method, which consists in expanding the Laplace transform of $G(t)$ into an S-fraction, is presented in Section 2.2. The section also shows that such an expansion has rational approximants, $\widehat{G}_n(s)$, in which the denominator for each n has real and simple zeros different from those of the numerator. The S-fraction method, as shown in Section 2.3, proceeds by exploiting the partial fraction decomposition of $\widehat{G}_n(s)$ which can then be conveniently transformed to the time domain to give the desired Dirichlet series approximations for $G(t)$. In Section 2.4, we describe the connection with the Stieltjes moment problem.

The obtained approximations for $G(t)$ are used in Section 2.5 as input functions to solve the interconversion equation and determine the corresponding approximations for the creep compliance function. Section 2.6 proves some interlacing properties satisfied by the relaxation and retardation times. Finally, the numerical examples provided in Section 2.7 show the accuracy of the S-fraction method as well as the ill-posedness inherent in its construction.

2.2 The S-fraction

2.2.1 The S-fraction for $\widehat{G}(s)$

In this subsection, we derive an S-fraction expansion for the Laplace transform of the relaxation function

$$G(t) = \int_0^\infty \exp\left(-\frac{t}{\tau}\right) \frac{H(\tau)}{\tau}\, d\tau. \tag{2.2}$$

This is the main step in the S-fraction method suggested for approximating $G(t)$ by Dirichlet series. We shall assume throughout that $G(t)$ is completely monotonic. This is the case if and only if the relaxation spectrum is non-negative. We also make the additional assumption that $G(t)$ has a Maclaurin series which is convergent in a neighborhood of the origin $t = 0$. This is more restrictive than the assumption made in the theorem of the appendix, which requires only that $G(t)$ has a formal power series about the origin. It then follows that the Laplace transform of $G(t)$,

$$\widehat{G}(s) = \int_0^\infty \frac{H(\tau)}{\tau s + 1}\, d\tau,$$

has a formal power series

$$\widehat{G}(s) = \sum_{n=0}^{\infty} (-1)^n \frac{\mu_n}{s^{n+1}}, \tag{2.3}$$

where

$$\mu_n = (-1)^n G^{(n)}(0), \qquad n = 0, 1, 2, \ldots. \tag{2.4}$$

In particular, all the negative moments of $H(\tau)$ exist:

$$\mu_n = \int_0^\infty \tau^{-(n+1)} H(\tau)\, d\tau, \qquad n = 0, 1, 2, \ldots. \tag{2.5}$$

The desired continued fraction representation for $\widehat{G}(s)$ may be obtained from (2.3) by using successive reciprocal series

$$\begin{aligned}
\widehat{G}(s) &= \frac{\mu_0}{s}\left[1 - \frac{\mu_1}{\mu_0 s} + \frac{\mu_2}{\mu_0 s^2} - \frac{\mu_3}{\mu_0 s^3} + \cdots\right] \\
&= \frac{\mu_0}{s}\left[1 + \frac{\mu_0^{(1)}}{s} + \frac{\mu_1^{(1)}}{s^2} + \frac{\mu_2^{(1)}}{s^3} + \cdots\right]^{-1} \\
&= \frac{\mu_0}{s}\left[1 + \frac{\mu_0^{(1)}}{s}\left(1 + \frac{\mu_1^{(1)}}{\mu_0^{(1)} s} + \frac{\mu_2^{(1)}}{\mu_0^{(1)} s^2} + \cdots\right)\right]^{-1} \\
&= \frac{\mu_0}{s}\left[1 + \frac{\mu_0^{(1)}}{s}\left(1 + \frac{\mu_0^{(2)}}{s} + \frac{\mu_1^{(2)}}{s^2} + \cdots\right)^{-1}\right]^{-1}.
\end{aligned}$$

Continuing this process, and denoting

$$\alpha_1 = \mu_0 \qquad \text{and} \qquad \alpha_n = \mu_0^{(n-1)}, \qquad n \geq 2,$$

we arrive at the following continued fraction

$$\widehat{G}(s) = \cfrac{\alpha_1}{s + \cfrac{\alpha_2}{1 + \cfrac{\alpha_3}{s + \cfrac{\alpha_4}{1 + \ddots}}}}$$

which has the conventional notation

$$\widehat{G}(s) = \frac{\alpha_1}{s} + \frac{\alpha_2}{1} + \frac{\alpha_3}{s} + \frac{\alpha_4}{1} + \cdots. \tag{2.6}$$

A continued fraction of the form (2.6) is called a Stieltjes continued fraction or just an *S*-fraction if the coefficients α_n are all positive (see, for instance, Henrici [15]). Such a condition, as we will show in what follows, is indeed fulfilled.

The coefficients of the continued fraction (2.6) can be obtained from those of the series (2.3) using the following formulae:

$$\alpha_1 = \Delta_1^{(0)}, \qquad \alpha_{2k} = \frac{\Delta_{k-1}^{(0)}\Delta_k^{(1)}}{\Delta_k^{(0)}\Delta_{k-1}^{(1)}}, \qquad \alpha_{2k+1} = \frac{\Delta_{k+1}^{(0)}\Delta_{k-1}^{(1)}}{\Delta_k^{(0)}\Delta_k^{(1)}}, \tag{2.7}$$

for $k \geq 1$, where $\Delta_k^{(n)}$ is the Hankel determinant defined by

$$\Delta_k^{(n)} = \begin{vmatrix} \mu_n & \mu_{n+1} & \cdots & \mu_{n+k-1} \\ \mu_{n+1} & \mu_{n+2} & \cdots & \mu_{n+k} \\ \vdots & \vdots & & \vdots \\ \mu_{n+k-1} & \mu_{n+k} & \cdots & \mu_{n+2k-2} \end{vmatrix}, \tag{2.8}$$

with $\Delta_0^{(n)} = 1$.

Remark 2.1. The formulae (2.7) are quoted, without proof, by Van Deun [26]. He claims that they follow from an application of Theorem 7.2 in Jones and Thron [16]. Analogous formulae to (2.7) are also derived by Henrici [15, Chapter 12] in his study of continued fractions.

We now prove the following theorem.

Theorem 2.1. *The Hankel determinants* (2.8) *satisfy*

$$\Delta_k^{(n)} > 0, \qquad \textit{for all} \qquad n \geq 0 \qquad \textit{and} \qquad k \geq 1.$$

Proof. It is sufficient to show that the following quadratic form satisfies

$$\sum_{i=0}^{k-1}\sum_{j=0}^{k-1} \mu_{n+i+j}\, x_i\, x_j > 0,$$

where x_i are real and not all zero. Using (2.5), we find

$$\sum_{i=0}^{k-1}\sum_{j=0}^{k-1}\mu_{n+i+j}x_ix_j = \int_0^\infty \tau^{-(n+1)}\left(\sum_{i=0}^{k-1}x_i\tau^{-i}\right)^2 H(\tau)\,d\tau. \tag{2.9}$$

The existence of all μ_n implies that the integral in (2.9) is convergent. The integral is non-negative since $H(\tau)$ is non-negative. Also, the integral vanishes if and only if $H(\tau)$ or the sum $\sum_{i=0}^{k-1}x_i\tau^{-i}$ vanishes for all $\tau > 0$. This sum cannot vanish for all $\tau > 0$ since the x_i are not all zero. Hence, the quadratic form is strictly positive. □

From the above theorem it follows immediately that the coefficients α_n given by (2.7) satisfy

$$\alpha_n > 0, \qquad \text{for all} \qquad n \geq 1,$$

and consequently, the continued fraction expansion (2.6) for $\widehat{G}(s)$ is an S-fraction.

2.2.2 Approximants of $\widehat{G}(s)$

The nth approximant of $\widehat{G}(s)$ is a finite continued fraction of the form

$$\widehat{G}_n(s) = \cfrac{\alpha_1}{s}\Bigg|+\cfrac{\alpha_2}{1}\Bigg|+\cdots+\cfrac{\alpha_n}{\epsilon_n}\Bigg|, \qquad n \geq 1, \tag{2.10}$$

where

$$\epsilon_n = \begin{cases} 1, & n = 2k, \\ s, & n = 2k+1, \end{cases}$$

and is obtained by truncating the infinite S-fraction (2.6). Such an approximant may also be written as a rational function

$$\widehat{G}_n(s) = \frac{P_n(s)}{Q_n(s)}, \qquad n \geq 1, \tag{2.11}$$

where the degrees of the polynomials $P_n(s)$ and $Q_n(s)$ depend on n in the following way:

$$\deg(P_n) = \begin{cases} k-1, & n = 2k, \\ k, & n = 2k+1, \end{cases} \qquad \deg(Q_n) = \begin{cases} k, & n = 2k, \\ k+1, & n = 2k+1. \end{cases}$$

Furthermore, the coefficients $\alpha_1, \alpha_2, \ldots, \alpha_n$ in (2.10) are constructed in such a way that the series expansion of (2.11) has the form

$$\widehat{G}_n(s) = \sum_{i=0}^{n-1} (-1)^i \frac{\mu_i}{s^{i+1}} + O\big(s^{-(n+1)}\big),$$

i.e., the first n terms in the series expansion of $\widehat{G}_n(s)$ agree with the first n terms of the series (2.3) for $\widehat{G}(s)$. In particular,

$$\begin{aligned} &\alpha_1 = \mu_0, && P_1(s) = \alpha_1, && Q_1(s) = s, \\ &\alpha_2 = \frac{\mu_1}{\mu_0}, && P_2(s) = \alpha_1, && Q_2(s) = s + \alpha_2, \\ &\alpha_3 = \frac{\mu_0\mu_2 - \mu_1^2}{\mu_0\mu_1}, && P_3(s) = \alpha_1(s + \alpha_3), && Q_3(s) = s(s + \alpha_1 + \alpha_3). \end{aligned}$$

More generally, the polynomials $P_n(s)$ and $Q_n(s)$ satisfy the following three-term recurrence relations

$$\begin{cases} P_n = \alpha_n P_{n-2} + \epsilon_n P_{n-1}, & n \geq 1, \\ P_{-1} = 1, \quad P_0 = 0, \end{cases}$$

$$\begin{cases} Q_n = \alpha_n Q_{n-2} + \epsilon_n Q_{n-1}, & n \geq 1, \\ Q_{-1} = 0, \quad Q_0 = 1. \end{cases}$$

The above recurrence relations show that $P_n(s)$ and $Q_n(s)$ have only positive coefficients and are of the forms

$$\begin{aligned} P_{2k} &= \alpha_1\big(a_{2k,0} + a_{2k,1}s + \ldots + a_{2k,k-2}s^{k-2} + s^{k-1}\big), && k \geq 1, \\ Q_{2k} &= b_{2k,0} + b_{2k,1}s + \ldots + b_{2k,k-1}s^{k-1} + s^k, && k \geq 1, \\ P_{2k+1} &= \alpha_1\big(a_{2k+1,0} + a_{2k+1,1}s + \ldots + a_{2k+1,k-1}s^{k-1} + s^k\big), && k \geq 1, \\ Q_{2k+1} &= s\big(b_{2k+1,0} + b_{2k+1,1}s + \ldots + b_{2k+1,k-1}s^{k-1} + s^k\big), && k \geq 1. \end{aligned}$$

The recurrence relations also show that the following two relations hold:

$$P_{2k}Q_{2k+2} - P_{2k+2}Q_{2k} = -\alpha_1\alpha_2\ldots\alpha_{2k+1}, \qquad k \geq 0, \tag{2.12a}$$

$$P_{2k+1}Q_{2k+3} - P_{2k+3}Q_{2k+1} = s\,\alpha_1\alpha_2\ldots\alpha_{2k+2}, \qquad k \geq 0. \tag{2.12b}$$

2.2.3 Zeros and poles of the approximants

Here, we focus on the zeros and poles of $\widehat{G}_n(s)$. In other words, the zeros of $P_n(s)$ and $Q_n(s)$ as they will play an important role in the S-fraction method.

The following theorem is due to Henrici [15].

Theorem 2.2. *Let $\mu(s)$ be a bounded and non-decreasing function on $[0,\infty)$. Then for $n = 0, 1, \ldots$, the following relation holds:*

$$\int_0^\infty s^i Q_n(-s)\,d\mu(s) = \begin{cases} 0, & i = 0, 1, \ldots, n-k-1, \\ (-1)^k\alpha_1\alpha_2\ldots\alpha_{n+1}, & i = n-k, \end{cases} \tag{2.13}$$

where k is the degree of Q_n.

Remark 2.2. In this theorem, $d\mu(s)$ is a non-negative measure with nth moment

$$\mu_n = \int_0^\infty s^n\,d\mu(s).$$

Recalling that Q_{2k} is of degree k, relation (2.13) in terms of the non-negative measure $d\mu(s)$ given by (1.11) reads

$$\int_0^\infty s^i Q_{2k}(-s)\left[s^{-1}H(s^{-1})\right] ds = \begin{cases} 0, & i = 0, 1, \ldots, k-1, \\ (-1)^k \alpha_1 \alpha_2 \ldots \alpha_{2k+1}, & i = k. \end{cases}$$

This is equivalent to saying that $\left\{Q_{2k}(-s)\right\}_{k\geq 1}$ forms a sequence of orthogonal polynomials on $[0,\infty)$ with respect to $s^{-1}H(s^{-1})$. On the other hand, since Q_{2k+1} is of degree $k+1$ and has a factor of s, the new polynomials

$$\widetilde{Q}_{2k+1}(s) = \frac{Q_{2k+1}(s)}{s}, \qquad k \geq 1, \tag{2.14}$$

are of degree k. It then follows from (1.11) and (2.13) that

$$\int_0^\infty s^i \widetilde{Q}_{2k+1}(-s) H(s^{-1})\, ds = \begin{cases} 0, & i = 0, 1, \ldots, k-1, \\ (-1)^k \alpha_1 \alpha_2 \ldots \alpha_{2k+2}, & i = k. \end{cases}$$

This relation implies that the sequence $\left\{\widetilde{Q}_{2k+1}(-s)\right\}_{k\geq 1}$ is also orthogonal on $[0,\infty)$, but with respect to $H(s^{-1})$.

Through the above orthogonality relations, we will be able to know some basic properties of the zeros of Q_n. This is due to the next theorem which can be found in any text on the theory of orthogonal polynomials (see, for instance, Chihara [6]).

Theorem 2.3. *If $\left\{f_n(s)\right\}_{n\geq 0}$ is a sequence of polynomials orthogonal on the interval I with respect to some measure, then the zeros of f_n are all real, simple and are contained in I. Moreover, they interlace with those of f_{n+1}, i.e.,*

$$s_{n+1,1} < s_{n,1} < s_{n+1,2} < \cdots < s_{n+1,n} < s_{n,n} < s_{n+1,n+1},$$

where $s_{n,i}$, $i = 1, 2, \ldots, n$, and $s_{n+1,i}$, $i = 1, 2, \ldots, n+1$, are the zeros of f_n and f_{n+1}, respectively.

Using the above theorem, we easily obtain the following result.

Theorem 2.4. *For $k = 1, 2, \ldots$,*

(i) The k zeros of the polynomial $Q_{2k}(s)$ are all real, simple, negative and are interlaced with those of $Q_{2k+2}(s)$.

(ii) Besides the zero at the origin, the polynomial $Q_{2k+1}(s)$ has k real, simple, negative zeros interlacing those of $Q_{2k+3}(s)$.

(iii) If the support of $H(s^{-1})$ is the finite interval $[a, b]$, then the zeros of $Q_n(s)$ lie in $[-b, -a]$.

Let us now turn our attention to the study of the zeros of the polynomials $P_n(s)$.

Theorem 2.5. *For $k = 1, 2, \ldots$,*

(i) The polynomial $P_{2k}(s)$ has $k - 1$ real, simple and negative zeros. Moreover, they interlace with those of $P_{2k+2}(s)$ and $Q_{2k}(s)$.

(ii) The polynomial $P_{2k+1}(s)$ has k real, simple and negative zeros. Moreover, they interlace with those of $P_{2k+3}(s)$ and $Q_{2k+1}(s)$.

Proof.

(i) The proof requires the relation (2.12a), i.e.,

$$P_{2k}Q_{2k+2} - P_{2k+2}Q_{2k} = -\alpha_1\alpha_2 \ldots \alpha_{2k+1}, \qquad k \geq 0.$$

It follows from this relation that P_{2k} and Q_{2k+2} have different signs at the zeros of Q_{2k}. This together with the fact that the zeros of Q_{2k+2} and Q_{2k} interlace imply that P_{2k} has $k - 1$ real, simple and negative zeros interlacing those of Q_{2k}.

Similarly, the above relation shows that P_{2k} and Q_{2k+2} are of opposite signs at the zeros of P_{2k+2}. Since the zeros of Q_{2k+2} interlace with those of P_{2k+2}, it follows that the zeros of P_{2k} and P_{2k+2} are interlaced.

(ii) Recall the relation (2.12b), i.e.,

$$P_{2k+1}Q_{2k+3} - P_{2k+3}Q_{2k+1} = s\,\alpha_1\alpha_2\ldots\alpha_{2k+2}, \qquad k \geq 0.$$

This relation shows that P_{2k+1} and Q_{2k+3} have different signs at the negative zeros of Q_{2k+1}. Combining this with the interlacing property satisfied by the zeros of Q_{2k+3} and Q_{2k+1}, we find that the k zeros of P_{2k+1} are real, simple, negative and are interlaced with those of Q_{2k+1}.

Similarly, it follows from the above relation that P_{2k+1} and Q_{2k+3} are of opposite signs at the zeros of P_{2k+3}. The interlacing property of the zeros of P_{2k+1} and P_{2k+3} then follows from the interlacing property satisfied by the zeros of Q_{2k+3} and P_{2k+3}.

□

2.3 Approximating $G(t)$ by Dirichlet series

2.3.1 Approximants of $G(t)$

This subsection shows how the S-fraction method can be used to generate Dirichlet series approximations for the relaxation function.

In the previous section, we have shown that the nth approximant for the Laplace transform of $G(t)$ has a rational representation

$$\widehat{G}_n(s) = \frac{P_n(s)}{Q_n(s)}, \qquad n \geq 1,$$

in which $\deg(Q_n) = \deg(P_n) + 1$ and all the zeros of $Q_n(s)$ are real and non-positive. In particular, we may write

$$Q_{2k}(s) = \prod_{i=1}^{k}\left(s + \frac{1}{\tau_{2k,i}}\right), \quad 0 < \tau_{2k,1} < \tau_{2k,2} < \cdots < \tau_{2k,k}, \quad k \geq 1,$$

and

$$Q_{2k+1}(s) = s\prod_{i=1}^{k}\left(s+\frac{1}{\tau_{2k+1,i}}\right), \quad 0<\tau_{2k+1,1}<\tau_{2k+1,2}<\cdots<\tau_{2k+1,k}, \quad k\geq 1.$$

The reason for writing the zeros of $Q_n(s)$ as reciprocals will become clear shortly. It then follows, since $Q_n(s)$ and $P_n(s)$ have no common zeros, that the approximants $\widehat{G}_n(s)$ can be expanded into two partial fractions of the form

$$\widehat{G}_{2k}(s) = \sum_{i=1}^{k}\frac{g_{2k,i}}{s+1/\tau_{2k,i}}, \qquad k\geq 1, \tag{2.15}$$

where

$$g_{2k,i} = \frac{P_{2k}(-1/\tau_{2k,i})}{Q'_{2k}(-1/\tau_{2k,i})}, \qquad i=1,2,\ldots,k,$$

and

$$\widehat{G}_{2k+1}(s) = \frac{g_{2k+1,0}}{s} + \sum_{i=1}^{k}\frac{g_{2k+1,i}}{s+1/\tau_{2k+1,i}}, \qquad k\geq 1, \tag{2.16}$$

where

$$g_{2k+1,0} = \frac{P_{2k+1}(0)}{Q'_{2k+1}(0)}, \qquad g_{2k+1,i} = \frac{P_{2k+1}(-1/\tau_{2k+1,i})}{Q'_{2k+1}(-1/\tau_{2k+1,i})}, \quad i=1,2,\ldots,k.$$

At this point, one can conveniently apply the inverse Laplace transform to obtain

$$G_{2k}(t) = \sum_{i=1}^{k} g_{2k,i}\exp\left(-\frac{t}{\tau_{2k,i}}\right), \qquad k\geq 1, \tag{2.17}$$

and

$$G_{2k+1}(t) = g_{2k+1,0} + \sum_{i=1}^{k} g_{2k+1,i}\exp\left(-\frac{t}{\tau_{2k+1,i}}\right), \qquad k\geq 1, \tag{2.18}$$

which are the desired Dirichlet series approximations for $G(t)$. We note that the positive constants $\tau_{n,i}$ represent the relaxation times. Regarding the signs of the other constants, we prove the following theorem.

Theorem 2.6. *The constants $g_{2k,i}$, $g_{2k+1,0}$ and $g_{2k+1,i}$, $i = 1, 2, \ldots, k$, are all positive.*

Proof. The positivity of $P_{2k}(0)$ and $Q_{2k}(0)$ together with the interlacing property of the zeros of P_{2k} and Q_{2k} imply that P_{2k} has the same sign as Q'_{2k} at the zeros of Q_{2k}. Thus, $g_{2k,i} > 0$ for $i = 1, 2, \ldots, k$.

For the odd constants, it follows from (2.14) that

$$g_{2k+1,0} = \frac{P_{2k+1}(0)}{\widetilde{Q}_{2k+1}(0)} > 0,$$

since both $P_{2k+1}(0)$ and $\widetilde{Q}_{2k+1}(0)$ are positive. Combining this latter fact with the interlacing property satisfied by the zeros of P_{2k+1} and Q_{2k+1}, we find that P_{2k+1} and Q'_{2k+1} have the same sign at the negative zeros of Q_{2k+1}. Thus, $g_{2k+1,i} > 0$ for $i = 1, 2, \ldots, k$. □

Comparing (2.2) with (2.17) and (2.18), we find that $G_{2k}(t)$ and $G_{2k+1}(t)$ correspond, respectively, to the following discrete relaxation spectra

$$H_{2k}(\tau) = \sum_{i=1}^{k} \eta_{2k,i}\, \delta(\tau - \tau_{2k,i}), \qquad k \geq 1, \tag{2.19}$$

and

$$H_{2k+1}(\tau) = g_{2k+1,0}\tau^{-1}\delta(\tau^{-1}) + \sum_{i=1}^{k} \eta_{2k+1,i}\, \delta(\tau - \tau_{2k+1,i}), \qquad k \geq 1, \tag{2.20}$$

where $\eta_{n,i} = g_{n,i}\tau_{n,i}$.

Remark 2.3 (Solids and liquids: limiting cases)**.**
Let $G_\infty = \lim_{t\to\infty} G(t)$. For a linear viscoelastic solid, it is well-known [11] that $G_\infty > 0$, while for a linear viscoelastic liquid, $G_\infty = 0$. For a viscoelastic solid, the series (2.17) has the properties

$$g_{2k,k} \to G_\infty \qquad \text{and} \qquad \tau_{2k,k} \to \infty, \qquad \text{as} \qquad k \to \infty,$$

while the series (2.18) has the property

$$g_{2k+1,0} \to G_\infty, \qquad \text{as} \qquad k \to \infty.$$

For a viscoelastic liquid, the series (2.18) has the property

$$g_{2k+1,0} \to 0, \qquad \text{as} \qquad k \to \infty.$$

More generally, referring to (1.9), the measure $d\mu(s)$ must contain a term of the form $G_\infty \delta(s)$, although this term vanishes for a liquid. A solid, therefore, has an infinite relaxation time. For completeness, we note that a model of the form

$$G(t) = G_\infty + \sum_{i=1}^{k} g_i \exp\left(-\frac{t}{\tau_i}\right),$$

is called a generalized Kelvin-Voigt model [11].

2.3.2 Convergence of the S-fraction

Under the simple change of variable $s = \tau^{-1}$, equation (2.2) becomes

$$G(t) = \int_0^\infty \exp(-st)\, s^{-1} H(s^{-1})\, ds.$$

Applying the Laplace transform to the above equation, with transformation variable x, yields

$$\widehat{G}(x) = \int_0^\infty \frac{s^{-1} H(s^{-1})}{x+s}\, ds, \tag{2.21}$$

which means that $\widehat{G}(x)$ is the Stieltjes transform of $s^{-1}H(s^{-1})$. It follows, then, from Henrici [15, Theorem 12.11d] that for all $x > 0$ and $k \geq 0$, the approximants of the S-fraction expansion of $\widehat{G}(x)$ satisfy the following inequality

$$\widehat{G}_{2k}(x) < \widehat{G}(x) < \widehat{G}_{2k+1}(x). \tag{2.22}$$

We may develop (2.22) further and obtain

Theorem 2.7. *For all $x > 0$, we have*

$$\widehat{G}_0(x) < \widehat{G}_2(x) < \cdots < \widehat{G}(x) < \cdots < \widehat{G}_3(x) < \widehat{G}_1(x). \tag{2.23}$$

Proof. We only need to show that the even and odd approximants form increasing and decreasing sequences, respectively. From (2.11) and (2.12a), it follows that

$$\widehat{G}_{2k}(x) - \widehat{G}_{2k+2}(x) = -\frac{\alpha_1\alpha_2\ldots\alpha_{2k+1}}{Q_{2k}(x)Q_{2k+2}(x)}.$$

We note that the denominator of the right-hand side is a polynomial with positive coefficients and consequently

$$\widehat{G}_{2k}(x) < \widehat{G}_{2k+2}(x), \qquad \text{for all} \qquad x > 0 \qquad \text{and} \qquad k \geq 0.$$

Similarly, (2.11) and (2.12b) implies that

$$\widehat{G}_{2k+3}(x) - \widehat{G}_{2k+1}(x) = -\frac{x\alpha_1\alpha_2\ldots\alpha_{2k+2}}{Q_{2k+1}(x)Q_{2k+3}(x)}.$$

Since $Q_{2m+1}Q_{2m+3}$ is again a polynomial with positive coefficients, it follows that

$$\widehat{G}_{2k+3}(x) < \widehat{G}_{2k+1}(x), \qquad \text{for all} \qquad x > 0 \qquad \text{and} \qquad k \geq 0.$$

□

Theorem 2.7 tells us that the subsequence of even approximants $\{\widehat{G}_{2k}(x)\}$ converges to an upper limit function $f^+(x)$, say, while the subsequence of odd approximants $\{\widehat{G}_{2k+1}(x)\}$ converges to a lower limit function $f^-(x)$. We may also deduce from (2.23) that

$$f^+(x) \leq \widehat{G}(x) \leq f^-(x), \qquad \text{for all} \qquad x > 0.$$

A sufficient condition for the convergence of the full sequence $\left\{\widehat{G}_n(x)\right\}_{n\geq 1}$ is

$$\sum_{n=1}^{\infty} \mu_n^{-1/2n} = \infty, \tag{2.24}$$

a condition known as the Carleman condition (see Henrici [15]). We may therefore deduce that if (2.24) holds, then

$$f^+(x) = \widehat{G}(x) = f^-(x), \qquad \text{for all} \qquad x > 0,$$

since every subsequence of a convergent sequence must converge to the same limit.

Remark 2.4 (The Carleman condition and discrete spectra)**.**
Consider a discrete relaxation spectrum

$$H(\tau) = \sum_{i=1}^{k} \eta_i \delta(\tau - \tau_i), \qquad \tau_i > 0,$$

with moments

$$\mu_n = \sum_{i=1}^{k} g_i \tau_i^{-n}, \qquad g_i = \frac{\eta_i}{\tau_i}, \qquad n \geq 1.$$

Let

$$g_{\max} = \max_{1\leq i\leq k}\{g_i\}, \quad g_{\min} = \min_{1\leq i\leq k}\{g_i\}, \quad \tau_{\max} = \max_{1\leq i\leq k}\{\tau_i\}, \quad \tau_{\min} = \min_{1\leq i\leq k}\{\tau_i\}.$$

Then

$$k g_{\min} \tau_{\max}^{-n} < \mu_n < k g_{\max} \tau_{\min}^{-n},$$

which implies that

$$(k g_{\max})^{-1/2n} \tau_{\min}^{1/2} < \mu_n^{-1/2n} < (k g_{\min})^{-1/2n} \tau_{\max}^{1/2}.$$

Thus, for all n, $\mu_n^{-1/2n}$ is bounded below by $(kg_{\max})^{-1/2}\tau_{\min}^{1/2}$ if $kg_{\max} \geq 1$, and by $\tau_{\min}^{1/2}$ if $kg_{\max} \leq 1$. Hence,

$$\sum_{n=1}^{\infty} \mu_n^{-1/2n} = \infty.$$

It is clear, in this case, that the S-fraction will terminate after a finite number of steps to give the exact result

$$\widehat{G}(s) = \sum_{i=1}^{k} \frac{g_i}{s + 1/\tau_i},$$

which is the Laplace transform of

$$G(t) = \sum_{i=1}^{k} g_i \exp\left(-\frac{t}{\tau_i}\right).$$

2.4 Connection with the Stieltjes moment problem

Let $\{\mu_n\}_{n\geq 0}$ be a sequence of real numbers. The Stieltjes moment problem consists of finding a non-negative measure $d\mu(s)$, $s \in [0, \infty)$, such that the μ_n are the moments of $\mu(s)$, i.e.,

$$\mu_n = \int_0^{\infty} s^n \, d\mu(s), \qquad n = 0, 1, 2, \ldots. \tag{2.25}$$

A necessary condition for the existence of a solution to the moment problem is

$$\Delta_k^{(0)} > 0 \qquad \text{and} \qquad \Delta_k^{(1)} > 0, \qquad k \geq 1,$$

where $\Delta_k^{(n)}$ is the Hankel determinant given by (2.8). A sufficient condition for the existence of a unique solution is the Carleman condition (2.24). For more details on this problem, see Henrici [15]. In this section, we relate the Stieltjes moment problem to two moment problems associated with the relaxation spectrum $H(\tau)$.

The negative moment problem of finding $H(\tau)$ from its moments (2.5), i.e.,

$$\mu_n = \int_0^\infty \tau^{-(n+1)} H(\tau)\, d\tau, \qquad n = 0, 1, 2, \ldots,$$

is equivalent to the Stieltjes moment problem (2.25) with solution

$$d\mu(s) = s^{-1} H(s^{-1})\, ds = \tau H(\tau)\, ds, \qquad s = \tau^{-1} > 0. \tag{2.26}$$

The positive moment problem of finding $H(\tau)$ from its moments

$$\eta_n = \int_0^\infty \tau^n H(\tau)\, d\tau, \qquad n = 0, 1, 2, \ldots, \tag{2.27}$$

is equivalent to the Stieltjes moment problem

$$\eta_n = \int_0^\infty s^n\, d\eta(s), \qquad n = 0, 1, 2, \ldots,$$

with solution

$$d\eta(s) = H(s)\, ds. \tag{2.28}$$

In what follows, we assume that the two sequences $\{\mu_n\}_{n\geq 0}$ and $\{\eta_n\}_{n\geq 0}$ satisfy the necessary and sufficient conditions for a unique solution of the related Stieltjes moment problem to exist.

2.4.1 The negative moment problem

Starting from (2.26), we may define a unique non-decreasing function

$$\mu(s) = \int_{s^{-1}}^\infty H(\tau)\, \frac{d\tau}{\tau}, \tag{2.29}$$

provided we stipulate that $\mu(s) = \mu(s^-)$ at a point of discontinuity. The function $\mu(s)$ may be constructed from the limit of the S-fraction associated with the formal

power series (2.3). In particular, the $2k$th approximant in (2.15) may be written as

$$\widehat{G}_{2k}(x) = \int_0^\infty \frac{d\mu^{[2k]}(s)}{x+s},$$

where $\mu^{[2k]}(s)$ is the step function given by

$$\mu^{[2k]}(s) = \begin{cases} 0, & s \le \tau_{2k,k}^{-1}, \\ g_{2k,k}, & \tau_{2k,k}^{-1} < s \le \tau_{2k,k-1}^{-1}, \\ g_{2k,k} + g_{2k,k-1}, & \tau_{2k,k-1}^{-1} < s \le \tau_{2k,k-2}^{-1}, \\ \vdots & \vdots \\ g_{2k,k} + g_{2k,k-1} + \ldots + g_{2k,1}, & \tau_{2k,1}^{-1} < s. \end{cases} \tag{2.30}$$

$\mu(s)$ is then obtained as the limit of a sequence of step functions

$$\mu(s) = \lim_{k\to\infty} \mu^{[2k]}(s).$$

Due to the uniqueness of the inverse Laplace transform, it follows from (1.9) that

$$G(t) = \lim_{k\to\infty} \int_0^\infty \exp(-st)\, d\mu^{[2k]}(s).$$

An alternative route to the limit is obtainable via the odd approximants $\widehat{G}_{2k+1}(x)$ in (2.16). In either case, if $\mu(s)$ is a continuously differentiable function of s, then $H(\tau)$ is a continuous function of τ, as seen from (2.29).

2.4.2 The positive moment problem

According to Bernstein's theorem, the function

$$F(t) = \int_0^\infty \exp(-\tau t) H(\tau)\, d\tau, \qquad H(\tau) \ge 0, \tag{2.31}$$

is completely monotonic on $[0,\infty)$. Then, as in the theorem of the appendix, assuming that there is a formal power series in t which is asymptotic to $F(t)$ as $t \to 0$, the moments (2.27) exist and have values

$$\eta_n = (-1)^n F^{(n)}(0), \qquad n = 0, 1, 2, \ldots.$$

Furthermore, the Laplace transform of (2.31) has a formal power series

$$\widehat{F}(s) = \sum_{n=0}^{\infty} (-1)^n \frac{\eta_n}{s^{n+1}}. \tag{2.32}$$

Starting from (2.28), we may define a unique non-decreasing function

$$\eta(s) = \int_0^s H(\tau)\, d\tau, \tag{2.33}$$

provided we stipulate that $\eta(s) = \eta(s^-)$ at a point of discontinuity. If

$$\widehat{F}_{2k}(x) = \frac{P^*_{2k}(s)}{Q^*_{2k}(s)} = \int_0^\infty \frac{d\eta^{[2k]}(s)}{x+s} = \sum_{i=1}^{k} \frac{\eta^*_{2k,i}}{x+\tau^*_{2k,i}},$$

denotes the $2k$th approximant of the S-fraction associated with (2.32), then $\eta^{[2k]}(s)$ is the step function

$$\eta^{[2k]}(s) = \begin{cases} 0, & s < \tau^*_{2k,1}, \\ \eta^*_{2k,1}, & \tau^*_{2k,1} \le s < \tau^*_{2k,2}, \\ \eta^*_{2k,1} + \eta^*_{2k,2}, & \tau^*_{2k,2} \le s < \tau^*_{2k,3}, \\ \quad\vdots & \quad\vdots \\ \eta^*_{2k,1} + \eta^*_{2k,2} + \ldots + \eta^*_{2k,k}, & \tau^*_{2k,k} \le s. \end{cases} \tag{2.34}$$

Again, $\eta(s)$ is obtained as the limit

$$\eta(s) = \lim_{k\to\infty} \eta^{[2k]}(s).$$

Due to the uniqueness of the inverse Laplace transform, it follows from (2.2) and (2.28) that

$$G(t) = \lim_{k\to\infty} \int_0^\infty \exp\left(-\frac{t}{s}\right) \frac{1}{s}\, d\eta^{[2k]}(s).$$

The $2k$th approximant (2.34) gives rise to an approximate Dirichlet series for $G(t)$ in the form

$$G^*_{2k}(t) = \sum_{i=1}^{k} g^*_{2k,i} \exp\left(-\frac{t}{\tau^*_{2k,i}}\right), \qquad g^*_{2k,i} = \frac{\eta^*_{2k,i}}{\tau^*_{2k,i}}, \tag{2.35}$$

with corresponding discrete relaxation spectrum

$$H^*_{2k}(\tau) = \sum_{i=1}^{k} \eta^*_{2k,i}\, \delta(\tau - \tau^*_{2k,i}). \tag{2.36}$$

We note that the relaxation times $\tau^*_{2k,i}$ are the negative zeros of $Q^*_{2k}(s)$. In a similar fashion, we can obtain the odd approximants of $G(t)$ in the form

$$G^*_{2k+1}(t) = \eta^*_{2k+1,0}\delta(t) + \sum_{i=1}^{k} g^*_{2k+1,i} \exp\left(-\frac{t}{\tau^*_{2k+1,i}}\right), \qquad g^*_{2k+1,i} = \frac{\eta^*_{2k+1,i}}{\tau^*_{2k+1,i}}, \tag{2.37}$$

with corresponding discrete relaxation spectrum

$$H^*_{2k+1}(\tau) = \eta^*_{2k+1,0}\delta(\tau) + \sum_{i=1}^{k} \eta^*_{2k+1,i}\, \delta(\tau - \tau^*_{2k+1,i}). \tag{2.38}$$

2.5 Solving the interconversion equation

Having constructed Dirichlet series approximations for the relaxation function, we proceed in this section to determine the corresponding approximations for the creep compliance function, $J(t)$. For this purpose, one has to consider the interconversion equation (1.20) derived in Chapter 1, i.e.,

$$\int_0^t G(t - t')J(t')\, dt' = t. \tag{2.39}$$

This equation allows us to find $J(t)$ from $G(t)$ through their Laplace transforms

$$\widehat{J}(s) = \frac{1}{s^2 \widehat{G}(s)}. \tag{2.40}$$

Indeed, since $\widehat{G}(s)$ has its approximants being rational functions, i.e.,

$$\widehat{G}_n(s) = \frac{P_n(s)}{Q_n(s)},$$

the approximants of $\widehat{J}(s)$ will also admit rational representations of the form

$$\widehat{J}_n(s) = \frac{Q_n(s)}{s^2 P_n(s)}.$$

We have shown in Section 2.2 that $\deg(P_n) = \deg(Q_n) - 1$ and all the zeros of $P_n(s)$ are real and negative. In particular, we may write

$$P_{2k}(s) = \prod_{i=1}^{k-1} \left(s + \frac{1}{\lambda_{2k,i}} \right), \quad 0 < \lambda_{2k,1} < \lambda_{2k,2} < \cdots < \lambda_{2k,k-1}, \quad k \geq 1,$$

and

$$P_{2k+1}(s) = \prod_{i=1}^{k} \left(s + \frac{1}{\lambda_{2k+1,i}} \right), \quad 0 < \lambda_{2k+1,1} < \lambda_{2k+1,2} < \cdots < \lambda_{2k+1,k}, \quad k \geq 1.$$

The reason for writing the zeros of $P_n(s)$ as reciprocals will become clear shortly. It then follows, since $P_n(s)$ and $Q_n(s)$ have no zeros in common, that the approximants $\widehat{J}_n(s)$ have two partial fractions of the form

$$\widehat{J}_{2k}(s) = \frac{j_{2k,0}}{s} + \frac{\beta_{2k}}{s^2} + \sum_{i=1}^{k-1} j_{2k,i} \left[\frac{1}{s} - \frac{1}{s + 1/\lambda_{2k,i}} \right], \qquad k \geq 1,$$

and

$$\widehat{J}_{2k+1}(s) = \frac{j_{2k+1,0}}{s} + \sum_{i=1}^{k} j_{2k+1,i} \left[\frac{1}{s} - \frac{1}{s + 1/\lambda_{2k+1,i}} \right], \qquad k \geq 1.$$

The desired approximations for $J(t)$ now follow by applying the inverse Laplace transform which gives

$$J_{2k}(t) = j_{2k,0} + \beta_{2k}t + \sum_{i=1}^{k-1} j_{2k,i}\left[1 - \exp\left(-\frac{t}{\lambda_{2k,i}}\right)\right], \qquad k \geq 1, \tag{2.41}$$

and

$$J_{2k+1}(t) = j_{2k+1,0} + \sum_{i=1}^{k} j_{2k+1,i}\left[1 - \exp\left(-\frac{t}{\lambda_{2k+1,i}}\right)\right], \qquad k \geq 1. \tag{2.42}$$

We note that the positive constants $\lambda_{n,i}$ represent the retardation times. Also

$$j_{2k,i} = -\lambda_{2k,i}^2 \frac{Q_{2k}(-1/\lambda_{2k,i})}{P'_{2k}(-1/\lambda_{2k,i})}, \qquad i = 1, 2, \ldots, k-1,$$

$$j_{2k+1,i} = -\lambda_{2k+1,i}^2 \frac{Q_{2k+1}(-1/\lambda_{2k+1,i})}{P'_{2k+1}(-1/\lambda_{2k+1,i})}, \qquad i = 1, 2, \ldots, k.$$

Furthermore, using (2.15) and (2.40), we obtain

$$\beta_{2k} = \lim_{s\to 0} s^2 \widehat{J}_{2k}(s) = \frac{1}{\sum_{i=1}^{k} \eta_{2k,i}}, \qquad \eta_{2k,i} = g_{2k,i}\tau_{2k,i}.$$

Finally, since (2.39) implies $J(0) = 1/G(0)$, it follows from (2.17) and (2.18) that

$$j_{2k,0} = \frac{1}{\sum_{i=1}^{k} g_{2k,i}}, \qquad \text{and} \qquad j_{2k+1,0} = \frac{1}{\sum_{i=0}^{k} g_{2k+1,i}}.$$

We now prove the following theorem regarding the signs of the above constants.

Theorem 2.8. *The constants in the formulae* (2.41) *and* (2.42) *are all positive.*

Proof. From Theorem 2.6 and the positivity of the relaxation times, it follows immediately that $j_{2k,0}$, $j_{2k+1,0}$ and β_{2k} are all positive. Also, the positivity of $Q_{2k}(0)$ and $P_{2k}(0)$ together with the interlacing property satisfied by the zeros of Q_{2k} and P_{2k} imply that Q_{2k} and P'_{2k} have different signs at the zeros of P_{2k}. Thus, $j_{2k,i} > 0$ for $i = 1, 2, \ldots, k-1$. Finally, since both $\widetilde{Q}_{2k+1}(0)$ defined by (2.14) and $P_{2k+1}(0)$

are positive, it follows from the interlacing property of the zeros of $Q_{2k+1}(s)$ and $P_{2k+1}(s)$ that Q_{2k+1} and P'_{2k+1} are of opposite signs at the zeros of P_{2k+1}. Thus, $j_{2k+1,i} > 0$ for $i = 1, 2, \ldots, k$. □

2.6 Interlacing properties of the relaxation and retardation times

It has been shown in Section 2.2 that the denominators of the approximants $\widehat{G}_n(s)$ give rise to two different sequences of polynomials, each of which is orthogonal. Because of these orthogonalities, we were able to show that their zeros as well as the zeros of the numerators are interlaced. Indeed, since the relaxation and retardation times are the negative reciprocals of these zeros, they must satisfy some interlacing properties. Such properties are presented in this short section.

Our first interlacing properties follow from Theorem 2.4 and the observation that the negative zeros of $Q_n(s)$ represent the negative reciprocals of the relaxation times.

Theorem 2.9. *The following interlacing properties hold:*

$$\tau_{2k+2,1} < \tau_{2k,1} < \tau_{2k+2,2} < \cdots < \tau_{2k+2,k} < \tau_{2k,k} < \tau_{2k+2,k+1}, \qquad k \geq 1,$$

$$\tau_{2k+3,1} < \tau_{2k+1,1} < \tau_{2k+3,2} < \cdots < \tau_{2k+3,k} < \tau_{2k+1,k} < \tau_{2k+3,k+1}, \qquad k \geq 1.$$

Similarly, Theorem 2.5 implies the following interlacing properties of the retardation times which are the negative reciprocals of the zeros of $P_n(s)$.

Theorem 2.10. *The following interlacing properties hold:*

$$\lambda_{2k+2,1} < \lambda_{2k,1} < \lambda_{2k+2,2} < \cdots < \lambda_{2k+2,k-1} < \lambda_{2k,k-1} < \lambda_{2k+2,k}, \qquad k \geq 2,$$

$$\lambda_{2k+3,1} < \lambda_{2k+1,1} < \lambda_{2k+3,2} < \cdots < \lambda_{2k+3,k} < \lambda_{2k+1,k} < \lambda_{2k+3,k+1}, \qquad k \geq 1.$$

As a final theorem, we present two more interlacing properties satisfied by a mixture of the relaxation and retardation times. This theorem is also a direct consequence of Theorem 2.5.

Theorem 2.11. *The following interlacing properties hold:*

$$\tau_{2k,1} < \lambda_{2k,1} < \tau_{2k,2} < \cdots < \tau_{2k,k-1} < \lambda_{2k,k-1} < \tau_{2k,k}, \qquad k \geq 2,$$

$$\tau_{2k+1,1} < \lambda_{2k+1,1} < \tau_{2k+1,2} < \cdots < \lambda_{2k+1,k-1} < \tau_{2k+1,k} < \lambda_{2k+1,k}, \qquad k \geq 1.$$

Remark 2.5. We believe that Theorems 2.9 and 2.10 and the second inequality of Theorem 2.11 are new to this thesis. The first inequality of Theorem 2.11 was proved by Mead [22] using a different approach.

2.7 Numerical examples

In this section, the S-fraction method proposed earlier is applied to construct Dirichlet series approximations for the relaxation function in which $H(\tau)$ is chosen to be the box relaxation spectrum

$$H(\tau) = \begin{cases} 1, & \frac{1}{2} \leq \tau \leq \frac{3}{2}, \\ 0, & \text{otherwise.} \end{cases} \tag{2.43}$$

It then follows from (2.2) that

$$G(t) = \mathrm{Ei}\left(\frac{2t}{3}\right) - \mathrm{Ei}(2t), \tag{2.44}$$

where Ei is the exponential integral defined by (1.15). Note that since $G(t) \to 0$ as $t \to \infty$, then (2.43) and (2.44) represent the relaxation spectrum and relaxation function for a viscoelastic fluid.

We first approximate $G(t)$ using the moments of negative order of $H(\tau)$. The results are then compared with those obtained from the moments of positive order. Furthermore, using these approximations as input functions for the interconversion equation, we obtain the corresponding approximations for $J(t)$. Finally, we close this section by discussing the ill-posedness inherent in the S-fraction method.

2.7.1 Approximating $G(t)$ using negative moments

From (2.5), we find that the moments of negative order of (2.43) are given by

$$\mu_0 = \ln(3), \qquad \mu_n = \frac{2^n}{n}\left(1 - \frac{1}{3^n}\right), \qquad n = 1, 2, \ldots. \tag{2.45}$$

These moments are the coefficients in the formal power series of the Laplace transform of (2.44), i.e.,

$$\widehat{G}(s) = \frac{1}{s}\ln\left(\frac{2+3s}{2+s}\right). \tag{2.46}$$

The coefficients α_n of the corresponding S-fraction are given in Table 2.1 for $n = 1, 2, \ldots, 21$. We note that the even and odd coefficients converge to different limits. Here, we quote a theorem due to Van Deun [26]:

Theorem 2.12. *If $H(s^{-1}) > 0$ has compact support $[a, b]$ with $0 \leq a < b < \infty$, then the coefficients in the S-fraction expansion of the Stieltjes transform* (2.21) *satisfy*

$$\lim_{k\to\infty} \alpha_{2k} = \frac{\left(\sqrt{b} + \sqrt{a}\right)^2}{4} \qquad \textit{and} \qquad \lim_{k\to\infty} \alpha_{2k+1} = \frac{\left(\sqrt{b} - \sqrt{a}\right)^2}{4}.$$

If we return to (2.43), we then find that

$$\lim_{k\to\infty} \alpha_{2k} \approx 1.24402 \qquad \text{and} \qquad \lim_{k\to\infty} \alpha_{2k+1} \approx 0.08932.$$

Table 2.1 shows the first few terms of the sequences leading to these limits.

k	α_{2k}	α_{2k+1}
0	-	1.09861
1	1.21365	0.11968
2	1.23786	0.09548
3	1.24136	0.09198
4	1.24253	0.09080
5	1.24307	0.09027
6	1.24336	0.08998
7	1.24353	0.08980
8	1.24365	0.08969
9	1.24372	0.08961
10	1.24378	0.08955

Table 2.1: The coefficients in the S-fraction expansion of $\widehat{G}(s)$.

The S-fraction method, using the negative moments (2.45), produces two different Dirichlet series approximations for $G(t)$. These are $G_{2k}(t)$ and $G_{2k+1}(t)$ given, respectively, by (2.17) and (2.18). We have computed these approximations for $k = 1, 2, \ldots, 10$. The coefficients in (2.17) are listed in Table 2.2, while Table 2.3 shows those in (2.18). These tables contain discrete relaxation spectra representations for the viscoelastic fluid whose true relaxation spectrum is given by (2.43). We note that the numerical values in these tables verify the interlacing properties between the relaxation times proved in Theorem 2.9. The numerical values also show that all the relaxation times satisfy

$$\frac{1}{2} \leq \tau_{n,i} \leq \frac{3}{2}.$$

This is a consequence of part (iii) of Theorem 2.4 and the fact that the relaxation times are the negative reciprocals of the negative zeros of $Q_n(s)$.

k	$g_{2k,1}$	$g_{2k,2}$	$g_{2k,3}$	$g_{2k,4}$	$g_{2k,5}$	$g_{2k,6}$	$g_{2k,7}$	$g_{2k,8}$	$g_{2k,9}$	$g_{2k,10}$
1	1.09861	-	-	-	-	-	-	-	-	-
2	0.44741	0.65120	-	-	-	-	-	-	-	-
3	0.22432	0.46734	0.40696	-	-	-	-	-	-	-
4	0.13321	0.29772	0.39348	0.27421	-	-	-	-	-	-
5	0.08795	0.20086	0.29413	0.31972	0.19595	-	-	-	-	-
6	0.06232	0.14358	0.21788	0.26872	0.25963	0.14648	-	-	-	-
7	0.04644	0.10744	0.16556	0.21428	0.23871	0.21277	0.11340	-	-	-
8	0.03594	0.08332	0.12936	0.17115	0.20219	0.20995	0.17643	0.09027	-	-
9	0.02863	0.06646	0.10361	0.13864	0.16846	0.18700	0.18424	0.14808	0.07349	-
10	0.02334	0.05423	0.08475	0.11412	0.14076	0.16158	0.17123	0.16193	0.12570	0.06096
k	$\tau_{2k,1}$	$\tau_{2k,2}$	$\tau_{2k,3}$	$\tau_{2k,4}$	$\tau_{2k,5}$	$\tau_{2k,6}$	$\tau_{2k,7}$	$\tau_{2k,8}$	$\tau_{2k,9}$	$\tau_{2k,10}$
1	0.82396	-	-	-	-	-	-	-	-	-
2	0.59757	1.11390	-	-	-	-	-	-	-	-
3	0.54599	0.77965	1.25966	-	-	-	-	-	-	-
4	0.52672	0.65481	0.93487	1.33839	-	-	-	-	-	-
5	0.51746	0.59823	0.76850	1.05390	1.38469	-	-	-	-	-
6	0.51230	0.56798	0.68120	0.87155	1.14312	1.41391	-	-	-	-
7	0.50914	0.54991	0.63060	0.76344	0.96034	1.21014	1.43341	-	-	-
8	0.50705	0.53823	0.59874	0.69620	0.84018	1.03518	1.26106	1.44703	-	-
9	0.50561	0.53024	0.57736	0.65188	0.76055	0.90966	1.09770	1.30030	1.45690	-
10	0.50457	0.52453	0.56230	0.62118	0.70584	0.82158	0.97152	1.14985	1.33100	1.46427

Table 2.2: The coefficients of $G_{2k}(t)$.

k	$g_{2k+1,0}$
1	9.8E-02
2	7.7E-03
3	5.7E-04
4	4.1E-05
5	3.0E-06
6	2.2E-07
7	1.5E-08
8	1.1E-09
9	8.2E-11
10	5.9E-12

Table 2.3: The coefficients of $G_{2k+1}(t)$.

k	$g_{2k+1,1}$	$g_{2k+1,2}$	$g_{2k+1,3}$	$g_{2k+1,4}$	$g_{2k+1,5}$	$g_{2k+1,6}$	$g_{2k+1,7}$	$g_{2k+1,8}$	$g_{2k+1,9}$	$g_{2k+1,10}$
1	1.00000	-	-	-	-	-	-	-	-	-
2	0.38800	0.70291	-	-	-	-	-	-	-	-
3	0.20023	0.44444	0.45337	-	-	-	-	-	-	-
4	0.12158	0.27870	0.39285	0.30544	-	-	-	-	-	-
5	0.08153	0.18855	0.28444	0.32748	0.21660	-	-	-	-	-
6	0.05842	0.13556	0.20902	0.26565	0.26947	0.16049	-	-	-	-
7	0.04391	0.10203	0.15871	0.20898	0.23952	0.22226	0.12321	-	-	-
8	0.03420	0.07952	0.12421	0.16611	0.19965	0.21276	0.18480	0.09736	-	-
9	0.02738	0.06370	0.09972	0.13439	0.16512	0.18639	0.18795	0.15520	0.07877	-
10	0.02242	0.05216	0.08177	0.11065	0.13753	0.15965	0.17188	0.16590	0.13168	0.06498

k	$\tau_{2k+1,1}$	$\tau_{2k+1,2}$	$\tau_{2k+1,3}$	$\tau_{2k+1,4}$	$\tau_{2k+1,5}$	$\tau_{2k+1,6}$	$\tau_{2k+1,7}$	$\tau_{2k+1,8}$	$\tau_{2k+1,9}$	$\tau_{2k+1,10}$
1	0.75000	-	-	-	-	-	-	-	-	-
2	0.58199	1.05437	-	-	-	-	-	-	-	-
3	0.54062	0.75000	1.22409	-	-	-	-	-	-	-
4	0.52427	0.64103	0.90360	1.31710	-	-	-	-	-	-
5	0.51614	0.59091	0.75000	1.02632	1.37134	-	-	-	-	-
6	0.51151	0.56365	0.67006	0.85160	1.12041	1.40511	-	-	-	-
7	0.50863	0.54714	0.62348	0.75000	0.94094	1.19192	1.42736	-	-	-
8	0.50671	0.53635	0.59393	0.68699	0.82573	1.01732	1.24654	1.44271	-	-
9	0.50536	0.52891	0.57397	0.64537	0.75000	0.89512	1.08176	1.28869	1.45371	-
10	0.50439	0.52355	0.55982	0.61642	0.69804	0.81032	0.95748	1.13586	1.32166	1.46186

Since we have a viscoelastic fluid, we will also consider the approximations

$$\widetilde{G}_{2k+1}(t) = \sum_{i=1}^{k} g_{2k+1,i} \exp\left(-\frac{t}{\tau_{2k+1,i}}\right), \qquad k \geq 1, \tag{2.47}$$

obtained from $G_{2k+1}(t)$ by ignoring the constant term. The question now arises as to which of the formulae (2.17), (2.18) and (2.47) are best approximations for $G(t)$. To answer the question, we present in Table 2.4 a comparison between the maximum absolute errors of these approximations for $k = 1, 2, \ldots, 10$. Also, Figure 2.1 shows the absolute errors of $G_{20}(t)$, $G_{21}(t)$ and $\widetilde{G}_{21}(t)$. The results suggest that the best approximations are obtained from the even approximants $G_{2k}(t)$ in (2.17).

k	$\lvert G(t) - G_{2k}(t)\rvert$	$\lvert G(t) - G_{2k+1}(t)\rvert$	$\lvert G(t) - \widetilde{G}_{2k+1}(t)\rvert$
1	2.9E-02	9.8E-02	9.8E-02
2	1.6E-03	7.7E-03	7.7E-03
3	9.5E-05	5.7E-04	5.7E-04
4	5.9E-06	4.1E-05	4.1E-05
5	3.9E-07	3.0E-06	3.0E-06
6	2.5E-08	2.2E-07	2.2E-07
7	1.7E-09	1.5E-08	1.5E-08
8	1.2E-10	1.1E-09	1.1E-09
9	7.8E-12	8.2E-11	8.2E-11
10	5.3E-13	5.9E-12	5.9E-12

Table 2.4: The maximum absolute errors of $G_{2k}(t)$, $G_{2k+1}(t)$ and $\widetilde{G}_{2k+1}(t)$.

Finally, we plot schematically in Figure 2.2 the discrete relaxation spectrum $H_{2k}(\tau)$ given by (2.19) for $k = 9, 10$. Also, Figure 2.3 shows the function

$$\mu(s) = \begin{cases} 0, & s \leq \frac{2}{3}, \\ \ln(s) - \ln\left(\frac{2}{3}\right), & \frac{2}{3} < s \leq 2, \\ \ln(3), & 2 < s, \end{cases}$$

obtained from (2.29) and (2.43), along with its approximant $\mu^{[20]}(s)$ given by (2.30).

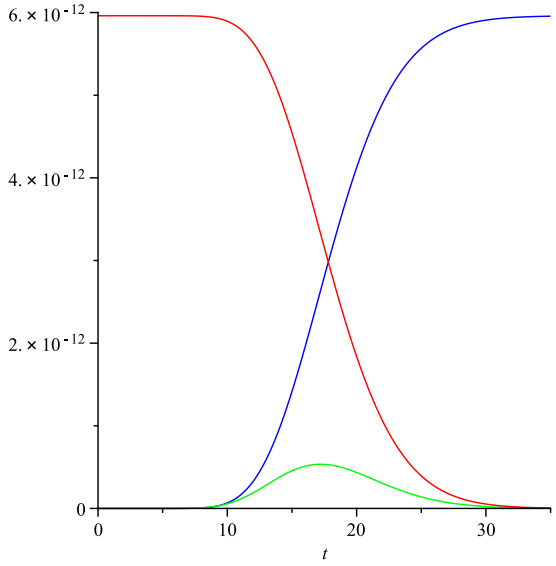

Figure 2.1: The absolute errors of $G_{20}(t)$ (green), $G_{21}(t)$ (blue) and $\widetilde{G}_{21}(t)$ (red).

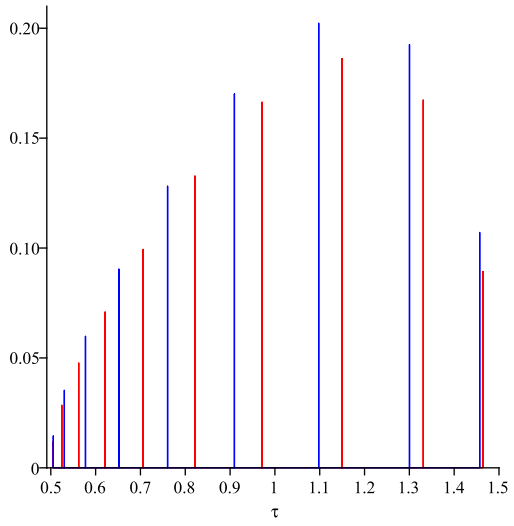

Figure 2.2: The discrete relaxation spectra $H_{18}(\tau)$ (blue) and $H_{20}(\tau)$ (red).

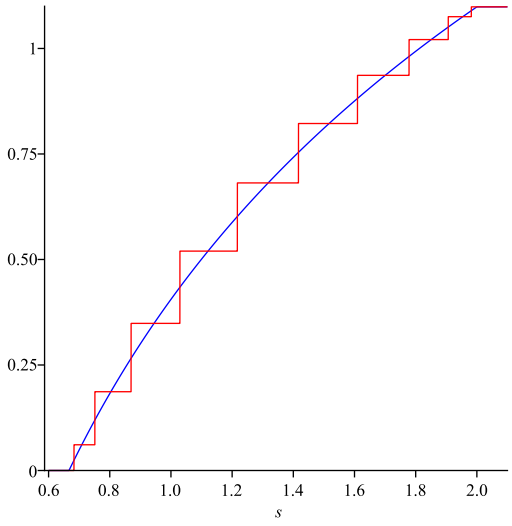

Figure 2.3: The functions $\mu(s)$ (blue) and $\mu^{[20]}(s)$ (red).

2.7.2 Approximating $G(t)$ using positive moments

From (2.27), we find that the moments of positive order of (2.43) are given by

$$\eta_n = \frac{3^{n+1}-1}{(n+1)2^{n+1}}, \qquad n = 0, 1, 2, \ldots. \tag{2.48}$$

These moments are the coefficients in the formal power series of the function

$$F(t) = \frac{1}{t}\left[\exp\left(-\frac{t}{2}\right) - \exp\left(-\frac{3t}{2}\right)\right],$$

obtained from (2.31) and (2.43). If α_n^* denote the coefficients in the S-fraction expansion of the Laplace transform $\widehat{F}(s)$ of $F(t)$, then it follows by Theorem 2.12 that

$$\lim_{k\to\infty} \alpha_{2k}^* \approx 0.93301 \qquad \text{and} \qquad \lim_{k\to\infty} \alpha_{2k+1}^* \approx 0.06699,$$

as shown in Table 2.5.

k	α_{2k}^*	α_{2k+1}^*
0	-	1.00000
1	1.00000	0.08333
2	0.91667	0.07273
3	0.92727	0.06933
4	0.93067	0.06822
5	0.93178	0.06775
6	0.93225	0.06751
7	0.93249	0.06737
8	0.93263	0.06728
9	0.93272	0.06722
10	0.93278	0.06717

Table 2.5: The coefficients in the S-fraction expansion of $\widehat{F}(s)$.

Starting from the positive moments (2.48), the S-fraction method generates two other Dirichlet series approximations for $G(t)$ in (2.44). These are $G_{2k}^*(t)$ and $G_{2k+1}^*(t)$ given, respectively, by (2.35) and (2.37). We have computed these approximations

for $k = 1, 2, \ldots, 10$. In Tables 2.6 and 2.7, we present the coefficients in these approximations, respectively. These tables contain other discrete representations for the box spectrum (2.43) different from those shown in Tables 2.2 and 2.3 of the previous subsection. We note that the interlacing properties of the relaxation times proved in Theorem 2.9 are satisfied by the numerical values in these tables. This follows from Theorem 2.4 and the fact that the relaxation times are the negative zeros of $Q_n^*(s)$. We also note that

$$\frac{1}{2} \leq \tau_{n,i}^* \leq \frac{3}{2},$$

since the relaxation times lie in the support of $H(\tau)$.

k	$g_{2k,1}^*$	$g_{2k,2}^*$	$g_{2k,3}^*$	$g_{2k,4}^*$	$g_{2k,5}^*$	$g_{2k,6}^*$	$g_{2k,7}^*$	$g_{2k,8}^*$	$g_{2k,9}^*$	$g_{2k,10}^*$
1	1.00000	-	-	-	-	-	-	-	-	-
2	0.70291	0.38800	-	-	-	-	-	-	-	-
3	0.45337	0.44444	0.20023	-	-	-	-	-	-	-
4	0.30544	0.39285	0.27870	0.12158	-	-	-	-	-	-
5	0.21660	0.32748	0.28444	0.18855	0.08153	-	-	-	-	-
6	0.16049	0.26947	0.26565	0.20902	0.13556	0.05842	-	-	-	-
7	0.12321	0.22226	0.23952	0.20898	0.15871	0.10203	0.04391	-	-	-
8	0.09736	0.18480	0.21276	0.19965	0.16611	0.12421	0.07952	0.03420	-	-
9	0.07877	0.15520	0.18795	0.18639	0.16512	0.13439	0.09972	0.06370	0.02738	-
10	0.06498	0.13168	0.16590	0.17188	0.15965	0.13753	0.11065	0.08177	0.05216	0.02242
k	$\tau_{2k,1}^*$	$\tau_{2k,2}^*$	$\tau_{2k,3}^*$	$\tau_{2k,4}^*$	$\tau_{2k,5}^*$	$\tau_{2k,6}^*$	$\tau_{2k,7}^*$	$\tau_{2k,8}^*$	$\tau_{2k,9}^*$	$\tau_{2k,10}^*$
1	1.00000	-	-	-	-	-	-	-	-	-
2	0.71132	1.28868	-	-	-	-	-	-	-	-
3	0.61270	1.00000	1.38730	-	-	-	-	-	-	-
4	0.56943	0.83001	1.16999	1.43057	-	-	-	-	-	-
5	0.54691	0.73077	1.00000	1.26923	1.45309	-	-	-	-	-
6	0.53377	0.66940	0.88069	1.11931	1.33060	1.46623	-	-	-	-
7	0.52545	0.62923	0.79708	1.00000	1.20292	1.37077	1.47455	-	-	-
8	0.51986	0.60167	0.73723	0.90828	1.09172	1.26277	1.39833	1.48014	-	-
9	0.51592	0.58198	0.69331	0.83787	1.00000	1.16213	1.30669	1.41802	1.48408	-
10	0.51305	0.56747	0.66030	0.78330	0.92556	1.07444	1.21670	1.33970	1.43253	1.48695

Table 2.6: The coefficients of $G_{2k}^*(t)$.

k	$\eta^*_{2k+1,0}$
1	7.6E-02
2	6.0E-03
3	4.5E-04
4	3.3E-05
5	2.4E-06
6	1.7E-07
7	1.2E-08
8	9.2E-10
9	6.6E-11
10	4.7E-12

Table 2.7: The coefficients of $G^*_{2k+1}(t)$.

k	$g^*_{2k+1,1}$	$g^*_{2k+1,2}$	$g^*_{2k+1,3}$	$g^*_{2k+1,4}$	$g^*_{2k+1,5}$	$g^*_{2k+1,6}$	$g^*_{2k+1,7}$	$g^*_{2k+1,8}$	$g^*_{2k+1,9}$	$g^*_{2k+1,10}$
1	0.85207	-	-	-	-	-	-	-	-	-
2	0.72824	0.33671	-	-	-	-	-	-	-	-
3	0.49786	0.41773	0.17943	-	-	-	-	-	-	-
4	0.33900	0.38769	0.26026	0.11132	-	-	-	-	-	-
5	0.23950	0.33256	0.27377	0.17699	0.07576	-	-	-	-	-
6	0.17611	0.27808	0.26131	0.20016	0.12808	0.05487	-	-	-	-
7	0.13414	0.23134	0.23927	0.20329	0.15206	0.09696	0.04157	-	-	-
8	0.10522	0.19315	0.21483	0.19661	0.16101	0.11927	0.07594	0.03257	-	-
9	0.08457	0.16247	0.19118	0.18531	0.16159	0.13018	0.09600	0.06109	0.02621	-
10	0.06937	0.13786	0.16960	0.17213	0.15747	0.13424	0.10727	0.07891	0.05021	0.02155

k	$\tau^*_{2k+1,1}$	$\tau^*_{2k+1,2}$	$\tau^*_{2k+1,3}$	$\tau^*_{2k+1,4}$	$\tau^*_{2k+1,5}$	$\tau^*_{2k+1,6}$	$\tau^*_{2k+1,7}$	$\tau^*_{2k+1,8}$	$\tau^*_{2k+1,9}$	$\tau^*_{2k+1,10}$
1	1.08333	-	-	-	-	-	-	-	-	-
2	0.75602	1.31671	-	-	-	-	-	-	-	-
3	0.63369	1.03665	1.39899	-	-	-	-	-	-	-
4	0.58030	0.85867	1.19283	1.43642	-	-	-	-	-	-
5	0.55312	0.75115	1.02350	1.28358	1.45641	-	-	-	-	-
6	0.53761	0.68376	0.90101	1.13684	1.34000	1.46829	-	-	-	-
7	0.52798	0.63952	0.81363	1.01729	1.21584	1.37720	1.47591	-	-	-
8	0.52161	0.60920	0.75047	0.92391	1.10573	1.27239	1.40290	1.48109	-	-
9	0.51718	0.58762	0.70386	0.85144	1.01368	1.17334	1.31398	1.42137	1.48476	-
10	0.51398	0.57177	0.66875	0.79487	0.93822	1.08606	1.22567	1.34533	1.43506	1.48746

Instead of $G^*_{2k+1}(t)$, we will consider the approximations

$$\widetilde{G}^*_{2k+1}(t) = \sum_{i=1}^{k} g^*_{2k+1,i} \exp\left(-\frac{t}{\tau^*_{2k+1,i}}\right), \qquad k \geq 1. \tag{2.49}$$

The maximum absolute errors of (2.49) are compared in Table 2.8 with those of $G^*_{2k}(t)$ for $k = 1, 2, \ldots, 10$. Also, shown in Figure 2.4 are the errors $G(t) - G^*_{20}(t)$ and $G(t) - \widetilde{G}^*_{21}(t)$. From these results, we find that the approximants $G^*_{2k}(t)$ are better than those given by (2.49).

k	$\left\lvert G(t) - G^*_{2k}(t)\right\rvert$	$\left\lvert G(t) - \widetilde{G}^*_{2k+1}(t)\right\rvert$
1	9.8E-02	2.4E-01
2	7.7E-03	3.3E-02
3	5.7E-04	3.5E-03
4	4.1E-05	3.4E-04
5	3.0E-06	3.0E-05
6	2.2E-07	2.6E-06
7	1.5E-08	2.1E-07
8	1.1E-09	1.7E-08
9	8.2E-11	1.4E-09
10	5.9E-12	1.1E-10

Table 2.8: The maximum absolute errors of $G^*_{2k}(t)$ and $\widetilde{G}^*_{2k+1}(t)$.

Similar to the previous example, we plot schematically in Figure 2.5 the discrete relaxation spectrum $H^*_{2k}(\tau)$ given by (2.36) for $k = 9, 10$. Also, the function

$$\eta(s) = \begin{cases} 0, & s \leq \frac{1}{2}, \\ s - \frac{1}{2}, & \frac{1}{2} < s \leq \frac{3}{2}, \\ 1, & \frac{3}{2} < s, \end{cases}$$

obtained from (2.33) and (2.43) is plotted in Figure 2.6 along with its approximant $\eta^{[20]}(s)$ given by (2.34).

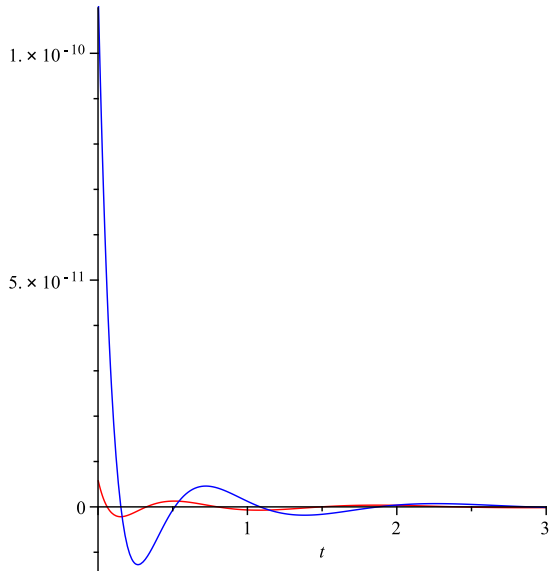

Figure 2.4: The errors of $G^*_{20}(t)$ (red) and $\widetilde{G}^*_{21}(t)$ (blue).

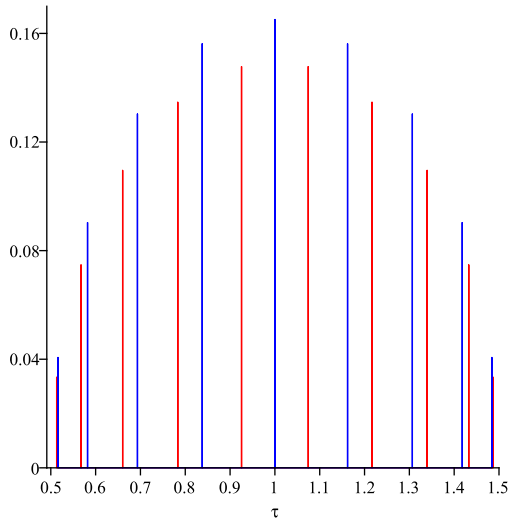

Figure 2.5: The discrete relaxation spectra $H^*_{18}(\tau)$ (blue) and $H^*_{20}(\tau)$ (red).

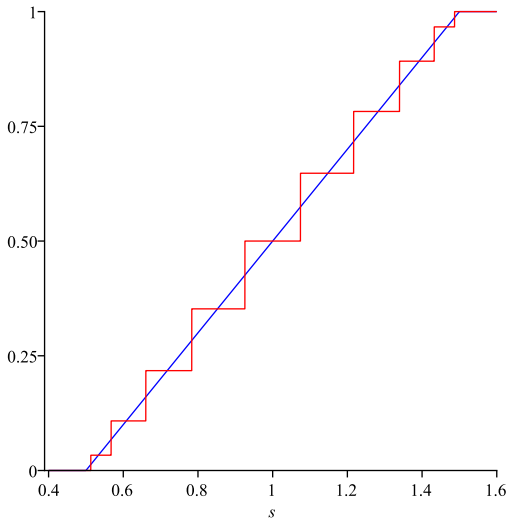

Figure 2.6: The functions $\eta(s)$ (blue) and $\eta^{[20]}(s)$ (red).

Finally, we compare the two best approximations for $G(t)$ obtained from the negative and positive moments of $H(\tau)$. As we have shown in previous and this subsections, the best approximations obtained from the moments of negative order are the series $G_{2k}(t)$ given by (2.17), while the best approximations obtained from the moments of positive order are the series $G^*_{2k}(t)$ given by (2.35). According to the first column of Tables 2.4 and 2.8, the approximants $G_{2k}(t)$ are the most accurate. However, Figure 2.7 below shows that over the range $8 \leq t \leq 30$, the series $G^*_{20}(t)$ gives better approximation than $G_{20}(t)$.

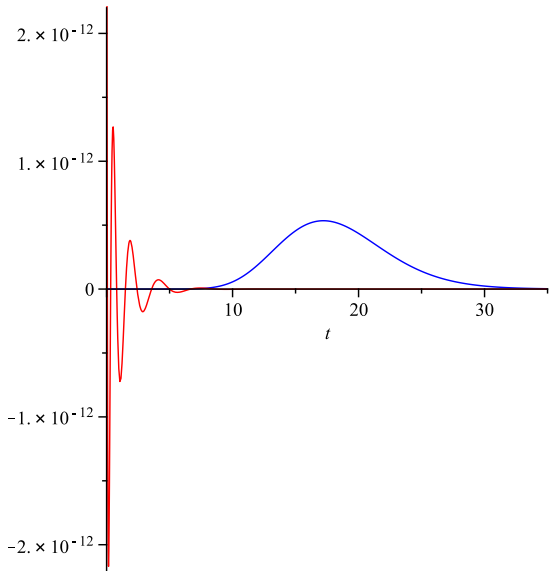

Figure 2.7: The errors of $G_{20}(t)$ (blue) and $G^*_{20}(t)$ (red).

2.7.3 Approximate solutions of the interconversion equation

Here, we consider solving for $J(t)$ the interconversion equation (2.39) in which $G(t)$ is given by (2.44). The laplace transform of $J(t)$ may be found from (2.40) and (2.46) in the form

$$\widehat{J}(s) = \frac{1}{s \ln\left(\frac{2+3s}{2+s}\right)}, \qquad s > 0.$$

This shows that $J(t)$ does not exist in closed-form. It can be shown from the above equation that

$$J(t) \sim 1 + t \qquad \text{as} \qquad t \to \infty. \tag{2.50}$$

In Section 2.5, we have shown how to obtain an approximation $J_n(t)$ to $J(t)$ by replacing $G(t)$ by its Dirichlet series approximant $G_n(t)$. Here, we restrict our attention only to the approximations $G_{2k}(t)$ and $G_{2k+1}(t)$ generated from the negative moments (2.45). The corresponding approximations for $J(t)$ therefore take two different forms, namely, $J_{2k}(t)$ and $J_{2k+1}(t)$ given, respectively, by (2.41) and (2.42). Table 2.9 lists the coefficients in (2.41), while those in (2.42) are shown in Table 2.10. The true retardation spectrum corresponding to the box spectrum (2.43) cannot be expressed in closed-form, but Tables 2.9 and 2.10 contain its discrete representations. We note that the numerical values in these tables verify the interlacing properties between the retardation times proved in Theorem 2.10. We also note that the retardation times shown in Tables 2.9 and 2.10 interlace, respectively, with the relaxation times shown in Tables 2.2 and 2.3 verifying the interlacing properties proved in Theorem 2.11.

k	$j_{2k,0}$	β_{2k}
1	0.91024	1.10471
2	0.91024	1.00732
3	0.91024	1.00054
4	0.91024	1.00004
5	0.91024	1.00000
6	0.91024	1.00000
7	0.91024	1.00000
8	0.91024	1.00000
9	0.91024	1.00000
10	0.91024	1.00000

Table 2.9: The coefficients of $J_{2k}(t)$.

k	$j_{2k,1}$	$j_{2k,2}$	$j_{2k,3}$	$j_{2k,4}$	$j_{2k,5}$	$j_{2k,6}$	$j_{2k,7}$	$j_{2k,8}$	$j_{2k,9}$
1	-	-	-	-	-	-	-	-	-
2	0.07174	-	-	-	-	-	-	-	-
3	0.02381	0.06370	-	-	-	-	-	-	-
4	0.01070	0.03582	0.04302	-	-	-	-	-	-
5	0.00578	0.01995	0.03579	0.02822	-	-	-	-	-
6	0.00351	0.01214	0.02383	0.03133	0.01896	-	-	-	-
7	0.00231	0.00795	0.01603	0.02426	0.02602	0.01319	-	-	-
8	0.00162	0.00551	0.01121	0.01784	0.02289	0.02120	0.00949	-	-
9	0.00118	0.00400	0.00814	0.01323	0.01823	0.02074	0.01719	0.00705	-
10	0.00089	0.00300	0.00610	0.01002	0.01426	0.01773	0.01839	0.01399	0.00537

k	$\lambda_{2k,1}$	$\lambda_{2k,2}$	$\lambda_{2k,3}$	$\lambda_{2k,4}$	$\lambda_{2k,5}$	$\lambda_{2k,6}$	$\lambda_{2k,7}$	$\lambda_{2k,8}$	$\lambda_{2k,9}$
1	-	-	-	-	-	-	-	-	-
2	0.73663	-	-	-	-	-	-	-	-
3	0.59132	0.99676	-	-	-	-	-	-	-
4	0.54833	0.74304	1.16370	-	-	-	-	-	-
5	0.52987	0.64376	0.88325	1.26591	-	-	-	-	-
6	0.52027	0.59530	0.74533	0.99903	1.33014	-	-	-	-
7	0.51464	0.56795	0.67063	0.84073	1.09085	1.37218	-	-	-
8	0.51106	0.55096	0.62582	0.74649	0.92575	1.16274	1.40083	-	-
9	0.50865	0.53966	0.59678	0.68675	0.81868	0.99954	1.21905	1.42109	-
10	0.50694	0.53176	0.57685	0.64659	0.74719	0.88530	1.06271	1.26342	1.43586

k	$j_{2k+1,0}$
1	0.91024
2	0.91024
3	0.91024
4	0.91024
5	0.91024
6	0.91024
7	0.91024
8	0.91024
9	0.91024
10	0.91024

Table 2.10: The coefficients of $J_{2k+1}(t)$.

k	$j_{2k+1,1}$	$j_{2k+1,2}$	$j_{2k+1,3}$	$j_{2k+1,4}$	$j_{2k+1,5}$	$j_{2k+1,6}$	$j_{2k+1,7}$	$j_{2k+1,8}$	$j_{2k+1,9}$	$j_{2k+1,10}$
1	9.23048	-	-	-	-	-	-	-	-	-
2	0.05945	1.28E02	-	-	-	-	-	-	-	-
3	0.02013	0.06386	1.74E03	-	-	-	-	-	-	-
4	0.00936	0.03289	0.04670	2.38E04	-	-	-	-	-	-
5	0.00518	0.01824	0.03477	0.03147	3.28E05	-	-	-	-	-
6	0.00321	0.01118	0.02256	0.03156	0.02125	4.53E06	-	-	-	-
7	0.00214	0.00738	0.01511	0.02358	0.02681	0.01473	6.27E07	-	-	-
8	0.00151	0.00516	0.01058	0.01714	0.02270	0.02213	0.01054	8.70E08	-	-
9	0.00111	0.00377	0.00771	0.01267	0.01778	0.02087	0.01809	0.00777	1.20E10	-
10	0.00084	0.00284	0.00580	0.00959	0.01381	0.01751	0.01870	0.01477	0.00588	1.67E11

k	$\lambda_{2k+1,1}$	$\lambda_{2k+1,2}$	$\lambda_{2k+1,3}$	$\lambda_{2k+1,4}$	$\lambda_{2k+1,5}$	$\lambda_{2k+1,6}$	$\lambda_{2k+1,7}$	$\lambda_{2k+1,8}$	$\lambda_{2k+1,9}$	$\lambda_{2k+1,10}$
1	8.35554	-	-	-	-	-	-	-	-	-
2	0.69199	1.26E02	-	-	-	-	-	-	-	-
3	0.57912	0.94428	1.74E03	-	-	-	-	-	-	-
4	0.54338	0.71954	1.12418	2.38E04	-	-	-	-	-	-
5	0.52740	0.63214	0.85621	1.23909	3.28E05	-	-	-	-	-
6	0.51886	0.58878	0.72942	0.97323	1.31208	4.53E06	-	-	-	-
7	0.51376	0.56393	0.66080	0.82293	1.06826	1.35978	6.27E07	-	-	-
8	0.51048	0.54831	0.61937	0.73447	0.90779	1.14377	1.39209	8.70E08	-	-
9	0.50824	0.53782	0.59233	0.67840	0.80550	0.98247	1.20339	1.41475	1.20E10	-
10	0.50665	0.53043	0.57366	0.64060	0.73753	0.87176	1.04704	1.25058	1.43115	1.67E11

We note with interest that the coefficients $j_{2k+1,k}$ and $\lambda_{2k+1,k}$ in Table 2.10 appear to grow without bound as k increases. Both (2.41) and (2.42) are valid approximations but have different forms. Formula (2.41) contains a linear term $\beta_{2k}t$, and all coefficients remain finite as $k \to \infty$, while formula (2.42) has no linear term. Table 2.9 suggests that

$$\lim_{k\to\infty} \beta_{2k} = 1.$$

In addition, the unbounded growth of the coefficients $j_{2k+1,k}$ and $\lambda_{2k+1,k}$ suggests that the contribution

$$j_{2k+1,k}\left[1 - \exp\left(-\frac{t}{\lambda_{2k+1,k}}\right)\right],$$

to the expression in (2.42) is attempting to play the role of its linear approximation

$$\frac{j_{2k+1,k}}{\lambda_{2k+1,k}}\, t, \tag{2.51}$$

as shown in Table 2.11.

k	$\frac{j_{2k+1,k}}{\lambda_{2k+1,k}}$
1	1.10471
2	1.01880
3	1.00233
4	1.00024
5	1.00002
6	1.00000
7	1.00000
8	1.00000
9	1.00000
10	1.00000

Table 2.11: The coefficients of (2.51).

Table 2.12 presents the numerical results of $J_{2k}(t)$ and $J_{2k+1}(t)$ with $k = 2, 6, 10$ for different values of t. The results show that $J_{2k}(t)$ and $J_{2k+1}(t)$ satisfy the relation (2.50).

	$J_{2k}(t)$			$J_{2k+1}(t)$		
t	$k=2$	$k=6$	$k=10$	$k=2$	$k=6$	$k=10$
0	0.91024	0.91024	0.91024	0.91024	0.91024	0.91024
10	11.05520	10.99999	10.99999	10.76530	10.99999	10.99999
20	21.12842	21.00000	21.00000	19.81619	20.99999	21.00000

Table 2.12: The numerical values of $J_{2k}(t)$ and $J_{2k+1}(t)$.

Finally, in Figure 2.8 below, we plot the approximations of $G(t)$ and $J(t)$ obtained from the even approximants $G_{2k}(t)$ and $J_{2k}(t)$ given by (2.17) and (2.41) for $k = 1, 2, 3$.

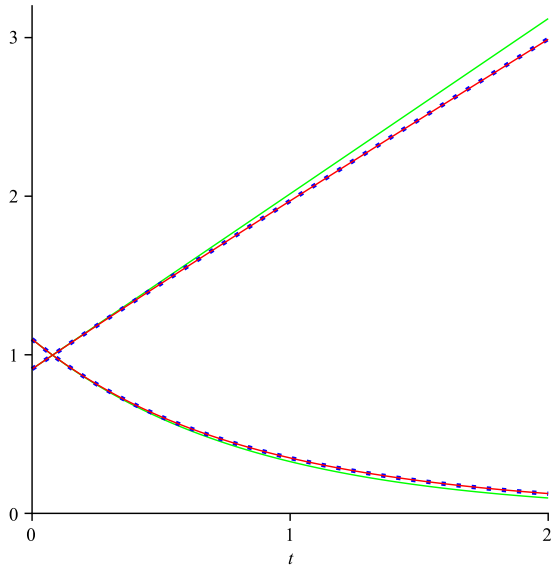

Figure 2.8: The approximants $G_{2k}(t)$ (decreasing) and $J_{2k}(t)$ (increasing) for $k = 1$ (green), $k = 2$ (blue) and $k = 3$ (red).

2.7.4 Ill-posedness and the S-fraction method

It is to be expected that the S-fraction method will be subject to the ill-posedness of recovering a discrete relaxation spectrum from $G(t)$. To demonstrate this, we add some noise to $G(t)$ in (2.44), in particular,

$$G^{\epsilon}(t) = G(t) + \frac{\ln(3)}{1000}\sin(2t), \tag{2.52}$$

which has noise of order 10^{-3}. The S-fraction method is used to construct the Dirichlet series approximations for (2.52), and the results are then compared with those obtained in Subsection 2.7.1.

In Table 2.13, we present the moments μ_n^ϵ obtained from $G^\epsilon(t)$ together with the exact moments μ_n obtained from $G(t)$ in (2.44). Also, shown in Table 2.14 are the coefficients in the S-fraction expansions of the Laplace transforms of $G^\epsilon(t)$ and $G(t)$. We note that, as a result of the noise in (2.52), the coefficients α_n^ϵ become negative, and then unstable, once $n > 4$.

n	μ_n	μ_n^ϵ
0	1.09861	1.09861
1	1.33333	1.33114
2	1.77778	1.77778
3	2.56790	2.57669
4	3.95062	3.95062
5	6.37366	6.33851
6	10.65203	10.65203

Table 2.13: The moments obtained from $G(t)$ and $G^\epsilon(t)$.

n	α_n	α_n^ϵ
1	1.09861	1.09861
2	1.21365	1.21165
3	0.11968	0.12388
4	1.23786	1.22743
5	0.09548	-0.04645
6	1.24136	-7.33674
7	0.09198	9.62523

Table 2.14: The coefficients in the S-fraction expansions of $\widehat{G}(s)$ and $\widehat{G}^\epsilon(s)$.

Using the S-fraction method, we generate the Dirichlet series approximations for (2.52). These approximations, according to Subsection 2.3.1, take the form

$$G_{2k}^\epsilon(t) = \sum_{i=1}^{k} g_{2k,i}^\epsilon \exp\left(-\frac{t}{\tau_{2k,i}^\epsilon}\right), \qquad k \geq 1,$$

and

$$G_{2k+1}^\epsilon(t) = g_{2k+1,0}^\epsilon + \sum_{i=1}^{k} g_{2k+1,i}^\epsilon \exp\left(-\frac{t}{\tau_{2k+1,i}^\epsilon}\right), \qquad k \geq 1.$$

The coefficients in the above formulae are shown, respectively, in Tables 2.15 and 2.17. The tables show that it is only possible to recover $G_n^\epsilon(t)$ for $n = 2, 3$ and 4. For the sake of comparison, we also reproduce in Tables 2.16 and 2.18, respectively, the coefficients in the Dirichlet series approximations $G_{2k}(t)$ and $G_{2k+1}(t)$ for $G(t)$ obtained in Subsection 2.7.1.

k	$g^{\epsilon}_{2k,1}$	$g^{\epsilon}_{2k,2}$	$g^{\epsilon}_{2k,3}$	$\tau^{\epsilon}_{2k,1}$	$\tau^{\epsilon}_{2k,2}$	$\tau^{\epsilon}_{2k,3}$
1	1.09861	-	-	0.82532	-	-
2	0.45187	0.64674	-	0.59696	1.12637	-
3	-0.2E-05	0.45632	0.64229	-0.13556	0.59828	1.13000

Table 2.15: The coefficients of $G^{\epsilon}_{2k}(t)$.

k	$g_{2k,1}$	$g_{2k,2}$	$g_{2k,3}$	$\tau_{2k,1}$	$\tau_{2k,2}$	$\tau_{2k,3}$
1	1.09861	-	-	0.82396	-	-
2	0.44741	0.65120	-	0.59757	1.11390	-
3	0.22432	0.46734	0.40696	0.54599	0.77965	1.25966

Table 2.16: The coefficients of $G_{2k}(t)$.

k	$g^{\epsilon}_{2k+1,0}$	$g^{\epsilon}_{2k+1,1}$	$g^{\epsilon}_{2k+1,2}$	$g^{\epsilon}_{2k+1,3}$	$\tau^{\epsilon}_{2k+1,1}$	$\tau^{\epsilon}_{2k+1,2}$	$\tau^{\epsilon}_{2k+1,3}$
1	0.10191	0.99671	-	-	0.74876	-	-
2	-0.00444	0.48011	0.62294	-	0.60394	1.16181	-
3	-0.02168	0.00921	0.63017	0.48091	0.39062	0.65483	1.39308

Table 2.17: The coefficients of $G^{\epsilon}_{2k+1}(t)$.

k	$g_{2k+1,0}$	$g_{2k+1,1}$	$g_{2k+1,2}$	$g_{2k+1,3}$	$\tau_{2k+1,1}$	$\tau_{2k+1,2}$	$\tau_{2k+1,3}$
1	9.8E-02	1.00000	-	-	0.75000	-	-
2	7.7E-03	0.38800	0.70291	-	0.58199	1.05437	-
3	5.7E-04	0.20023	0.44444	0.45337	0.54062	0.75000	1.22409

Table 2.18: The coefficients of $G_{2k+1}(t)$.

Finally, in Figure 2.9, we plot the errors $G(t) - G_4(t)$ and $G(t) - G_4^\epsilon(t)$. Also, Figure 2.10 shows the errors $G(t) - \widetilde{G}_5(t)$ and $G(t) - \widetilde{G}_5^\epsilon(t)$, where $\widetilde{G}_5(t)$ is obtained from (2.47) and $\widetilde{G}_5^\epsilon(t)$ is obtained from

$$\widetilde{G}_{2k+1}^\epsilon(t) = \sum_{i=1}^{k} g_{2k+1,i}^\epsilon \exp\left(-\frac{t}{\tau_{2k+1,i}^\epsilon}\right), \qquad k \geq 1.$$

The figures show that the maximum error in $G_4^\epsilon(t)$ is of order 10^{-3} (the same level as the noise in the data), whereas the maximum error in $\widetilde{G}_5^\epsilon(t)$ is of order 5×10^{-3}.

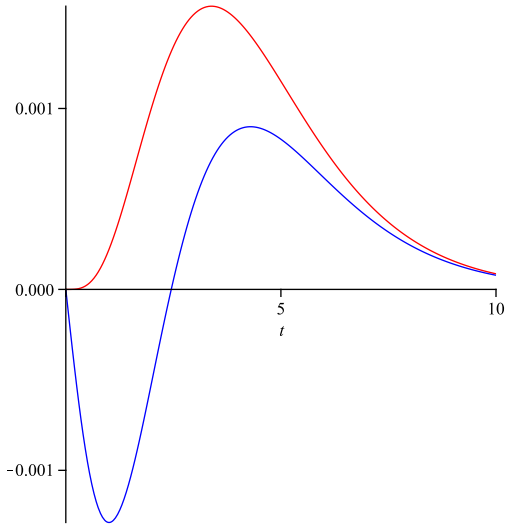

Figure 2.9: The errors of $G_4(t)$ (red) and $G_4^\epsilon(t)$ (blue).

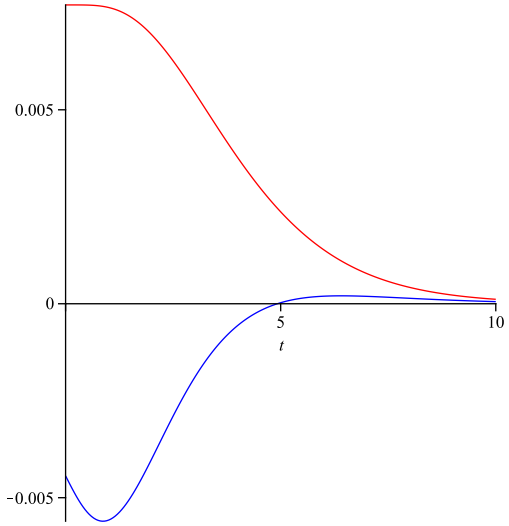

Figure 2.10: The errors of $\widetilde{G}_5(t)$ (red) and $\widetilde{G}_5^\epsilon(t)$ (blue).

3

LINEAR VISCOELASTICITY AND SPECTRAL THEORY

In this chapter, two important topics from the spectral theory, particularly the spectral and Weyl-Titchmarsh functions, are related to the theory of linear viscoelasticity. Through these relations, several inverse spectral problems in linear viscoelasticity are formulated and then explicitly solved.

The chapter is organized as follows. We recall, in Section 3.1, the definition and some important facts of the Weyl-Titschmarsh function, $m(z)$. In particular, we give the Herglotz integral formula which expresses $m(z)$ in terms of the spectral function.

In Section 3.2, we derive a condition on the relaxation spectrum $H(\tau)$ which is sufficient for the existence of a Sturm-Liouville problem whose spectral function is determined by $H(\tau)$. The $m(z)$ associated with this problem is given in Section 3.3 explicitly in terms of $H(\tau)$ and the Laplace transform of the relaxation function.

The spectral function for discrete $H(\tau)$ is used in Section 3.4 to formulate an inverse spectral problem for a Sturm-Liouville operator. In solving such a problem, we use the well-known Gelfand-Levitan method. We show there that, fortunately, the Gelfand-Levitan equation can be solved explicitly leading to an explicit solution of the inverse problem. We consider in more detail the cases where $H(\tau)$ corresponds to the Newtonian, Maxwell and Oldroyd-B models.

3.1 Spectral and Weyl-Titchmarsh functions

This section introduces the Weyl-Titchmarsh function and reviews some of its basic properties including its relation to the spectral function. Most of the material given here is collected from [8] and [17].

Consider the Sturm-Liouville operator

$$-\frac{d^2}{dx^2} + q(x), \qquad x \geq 0, \tag{3.1}$$

in which the potential function $q(x)$ is real-valued. We will assume throughout

that (3.1) is in the limit-point case at infinity. This means that for every complex z with $\mathrm{Im}(z) > 0$, exactly one solution (up to a multiplicative constant) $u(x,z)$ of

$$-y''(x,z) + q(x)y(x,z) = zy(x,z), \qquad x \geq 0, \tag{3.2}$$

is square-integrable on $(0,\infty)$, i.e.,

$$\int_0^\infty |u(x,z)|^2\, dx < \infty, \qquad \mathrm{Im}(z) > 0.$$

If $u_1(x,z)$ and $u_2(x,z)$ solve equation (3.2) with

$$u_1(0,z) = 1 = u_2'(0,z), \qquad u_2(0,z) = 0 = u_1'(0,z),$$

then $u(x,z)$ may be written in the form

$$u(x,z) = u_1(x,z) + m(z)u_2(x,z).$$

The function $m(z)$ in this equation is unique and is called the Weyl-Titchmarsh function or just the m-function. In consequence of the initial condition $u_2(0,z) = 0$, this m-function may be associated with the Sturm-Liouville problem

$$\begin{cases} -y''(x,z) + q(x)y(x,z) = zy(x,z), \qquad x \geq 0, \\ y(0,z) = 0, \end{cases} \tag{3.3}$$

for which $u_2(x,z)$ is a solution. An important property of the m-function is that it is a Herglotz function, i.e., analytic in the upper half-plane and satisfies

$$\mathrm{Im}(m(z)) > 0, \qquad \text{for} \qquad \mathrm{Im}(z) > 0.$$

This property allows $m(z)$ to be written as

$$m(z) = \mathrm{Re}(m(i)) + \int_{-\infty}^{\infty} \left[\frac{1}{\tau - z} - \frac{\tau}{1+\tau^2} \right] d\rho(\tau), \qquad \mathrm{Im}(z) > 0, \tag{3.4}$$

where $\rho(\tau)$ is a monotone non-decreasing function satisfying

$$\int_{-\infty}^{\infty} \frac{d\rho(\tau)}{1+\tau^2} < \infty.$$

The function $\rho(\tau)$ is called the spectral function associated with the Sturm-Liouville problem (3.3) and is uniquely determined from $m(z)$ by using the Stieltjes inversion formula

$$\rho(\tau) = \lim_{\epsilon \to 0^+} \frac{1}{\pi} \int_0^{\tau} \mathrm{Im}(m(\nu + i\epsilon))\, d\nu. \tag{3.5}$$

In the special case where $q(x) = 0$ in the Sturm-Liouville problem (3.3), the m-function takes the form

$$m_0(z) = iz^{1/2}, \qquad \mathrm{Im}(z) > 0, \tag{3.6}$$

which, according to (3.4), has the representation

$$m_0(z) = \mathrm{Re}(m_0(i)) + \int_{-\infty}^{\infty} \left[\frac{1}{\tau - z} - \frac{\tau}{1+\tau^2} \right] d\rho_0(\tau), \qquad \mathrm{Im}(z) > 0, \tag{3.7}$$

with the spectral function

$$\rho_0(\tau) = \frac{2}{3\pi}\tau^{3/2}, \quad \tau \geq 0; \qquad \rho_0(\tau) = 0, \quad \tau < 0. \tag{3.8}$$

The integral on the right-hand side of equation (3.7) cannot be written as the difference of the two integrals, since the improper integrals obtained by taking each integrand separately are both divergent. Writing $z = x + iy$ with $y > 0$, equation (3.6) gives

$$m_0(z) = -\sqrt{\frac{\sqrt{x^2+y^2} - x}{2}} + i\sqrt{\frac{\sqrt{x^2+y^2} + x}{2}}.$$

It then follows by equating the real and imaginary parts of (3.7) that the following two remarkable identities hold:

$$\frac{1}{\pi}\int_0^\infty \frac{\sqrt{\tau}\big[(\tau-x)(1+\tau x)-\tau y^2\big]}{(1+\tau^2)\big[(\tau-x)^2+y^2\big]}\,d\tau = \frac{1-\sqrt{\sqrt{x^2+y^2}-x}}{\sqrt{2}}, \qquad y\neq 0,$$

and

$$\frac{1}{\pi}\int_0^\infty \frac{y\sqrt{\tau}}{(\tau-x)^2+y^2}\,d\tau = \sqrt{\frac{\sqrt{x^2+y^2}+x}{2}}, \qquad y>0.$$

3.2 A sufficient condition for a spectral function

In this section, we provide a sufficient condition for the function

$$\rho(\tau) = \int_0^\tau H(\tau')\,d\tau' + \rho_0(\tau), \qquad \tau\geq 0, \tag{3.9}$$

to be the spectral function associated with a Sturm-Liouville problem of the form (3.3). In (3.9), $H(\tau)$ is a viscoelastic relaxation spectrum and $\rho_0(\tau)$ is given by (3.8). We also show that $\rho(\tau)$ is a spectral function in the case where $H(\tau)$ is in a discrete form.

In his book on inverse Sturm-Liouville problems, Levitan [17, § 2.9] gives two necessary and sufficient conditions in order for a monotone non-decreasing function to be the spectral function associated with a problem of the form (3.3). In terms of (3.9), these conditions may by stated as follows:

(i) The sequence of functions

$$\Phi_N(x) = \int_0^N \frac{\cos(\sqrt{\tau}x)-1}{\tau}H(\tau)\,d\tau, \tag{3.10}$$

converges boundedly as $N\to\infty$.

(ii) Let

$$E(\tau) = \int_0^\infty f(x) \frac{\sin(\sqrt{\tau}x)}{\sqrt{\tau}}\, dx,$$

where $f(x)$ is a smooth function of bounded support. Then the equality

$$\int_0^\infty E^2(\tau)\, d\rho(\tau) = 0, \tag{3.11}$$

implies that $f(x) \equiv 0$.

We now state and prove a simpler condition on $H(\tau)$ which is sufficient to make $\rho(\tau)$ in (3.9) a spectral function.

Theorem 3.1. *If the cosine transform*

$$C(x) = \int_0^\infty \cos(\sqrt{\tau}x)\tau^{-1}H(\tau)\, d\tau, \tag{3.12}$$

is bounded and continuous for all $x \geq 0$, then the function $\rho(\tau)$ given by (3.9) *is a spectral function of a certain Sturm-Liouville problem of the form* (3.3).

Proof. We will show that conditions (i) and (ii) are satisfied. Clearly, (3.12) implies that condition (i) is satisfied, since

$$\Phi_N(x) \to C(x) - C(0) \qquad \text{as} \qquad N \to \infty.$$

Condition (ii) does not depend on (3.12), but on the fact that $d\rho(\tau)$ is a positive measure on $(0, \infty)$. Since $f(x)$ is a smooth function of bounded support, $E(\tau)$ is a continuous function of τ on $(0, \infty)$. Consequently, (3.11) implies that $E(\tau) \equiv 0$ on $(0, \infty)$. Using the Fourier sine formula, we may write

$$\begin{aligned} f(x) &= \frac{1}{\pi} \int_0^\infty \sin(\sqrt{\tau}x)\, d\tau \int_0^\infty f(t) \frac{\sin(\sqrt{\tau}t)}{\sqrt{\tau}}\, dt \\ &= \frac{1}{\pi} \int_0^\infty E(\tau) \sin(\sqrt{\tau}x)\, d\tau. \end{aligned}$$

Hence, $f(x) \equiv 0$. □

In what follows, we will consider the case where $H(\tau)$ is discrete. Let

$$H(\tau) = \sum_{j=1}^{n} \eta_j \delta(\tau - \tau_j), \tag{3.13}$$

where $\eta_j > 0$ and

$$\begin{cases} \tau_j \geq 0, & n \leq 2, \\ \tau_j > 0, & n > 2. \end{cases}$$

This spectrum contains all the relaxation spectra for the viscoelastic models listed in Table 1.1 of Section 1.2. More precisely,

(i) if $n = 1$ and $\tau_1 = 0$, then (3.13) corresponds to the Newtonian model,

(ii) if $n = 1$ and $\tau_1 > 0$, then (3.13) corresponds to the Maxwell model,

(iii) if $n = 2$, $\tau_1 = 0$ and $\tau_2 > 0$, then (3.13) corresponds to the Oldroyd-B model,

(iv) if $n \geq 2$ and $\tau_j > 0$ for all j, then (3.13) corresponds to the multi-mode Maxwell model.

Substituting (3.13) into (3.9) and then using the well-known relation

$$\int_0^{\tau} \delta(\tau' - \tau_j)\, d\tau' = U(\tau - \tau_j),$$

where $U(\tau - \tau_j)$ is the Heaviside step function defined by

$$U(\tau - \tau_j) = \begin{cases} 0, & \tau \leq \tau_j, \\ 1, & \tau > \tau_j, \end{cases}$$

we obtain

$$\rho(\tau) = \sum_{j=1}^{n} \eta_j U(\tau - \tau_j) + \rho_0(\tau). \tag{3.14}$$

If $\tau_j > 0$ for all j, then the above function is a spectral function of a Sturm-Liouville problem of the form (3.3), since in this case, the discrete relaxation spectrum (3.13)

satisfies the condition (3.12). The condition is not satisfied if at least one τ_j is zero. However, it can be shown in this case that Levitan's two conditions stated above are satisfied and consequently (3.14) is again a spectral function. Thus, we may state the following theorem.

Theorem 3.2. *The function $\rho(\tau)$ in* (3.14) *is a spectral function of a certain Sturm-Liouville problem of the form* (3.3).

Remark 3.1. That Theorem 3.2 is true is not surprising. Eastham and Kalf [8] and Levitan [17] give explicit constructions for potentials which embed a finite number of eigenvalues into a continuous spectrum. These constructions are for Sturm-Liouville problems with different initial conditions from the zero boundary condition given in (3.3).

Theorem 3.2 will serve later as the basis of Section 3.4 in which we formulate and solve an inverse spectral problem for the Sturm-Liouville operator (3.1).

3.3 The m-function in linear viscoelasticity

In the previous section we have established that, given a linear viscoelastic material whose relaxation spectrum satisfies the condition of Theorem 3.1, then there exists a Sturm-Liouville problem of the form (3.3) for which $\rho(\tau)$ in (3.9) is its spectral function. Our purpose in this section is to determine the m-function associated with this problem.

The desired m-function is the function $m(z)$ that satisfies the representation (3.4) with $\rho(\tau)$ given by (3.9). So, starting with the integral term of (3.4) and taking (3.7) into account, we find

$$\int_0^\infty \left[\frac{1}{\tau - z} - \frac{\tau}{1+\tau^2}\right] \left[H(\tau)d\tau + d\rho_0(\tau)\right] = \int_0^\infty \left[\frac{1}{\tau - z} - \frac{\tau}{1+\tau^2}\right] H(\tau)d\tau$$
$$+ m_0(z) - \mathrm{Re}(m_0(i)).$$

The above equation, upon writing

$$g(z) = \int_0^\infty \frac{H(\tau)}{\tau - z}\, d\tau, \qquad \mathrm{Im}(z) > 0,$$

and then rearranging the terms, becomes

$$g(z) + m_0(z) = \mathrm{Re}(g(i) + m_0(i)) + \int_0^\infty \left[\frac{1}{\tau - z} - \frac{\tau}{1+\tau^2}\right]\big[H(\tau)d\tau + d\rho_0(\tau)\big].$$

Thus, we have arrived at the following theorem which presents the m-function explicitly in terms of $H(\tau)$.

Theorem 3.3. *If $\rho(\tau)$ in* (3.9) *is a spectral function of a certain Sturm-Liouville problem of the form* (3.3)*, then the associated m-function is*

$$m(z) = \int_0^\infty \frac{H(\tau)}{\tau - z}\, d\tau + m_0(z), \qquad \mathrm{Im}(z) > 0. \tag{3.15}$$

In Table 3.1 below, we collect the spectral functions and m-functions for the viscoelastic models introduced in Chapter 1.

Model	$m(z)$	$\rho(\tau)$
Newtonian	$-\frac{\eta_1}{z} + m_0(z)$	$\eta_1 U(\tau) + \rho_0(\tau)$
Maxwell	$\frac{\eta_1}{\tau_1 - z} + m_0(z)$	$\eta_1 U(\tau - \tau_1) + \rho_0(\tau)$
Oldroyd-B	$-\frac{\eta_1}{z} + \frac{\eta_2}{\tau_2 - z} + m_0(z)$	$\eta_1 U(\tau) + \eta_2 U(\tau - \tau_2) + \rho_0(\tau)$
Multi-mode Maxwell	$\sum_{j=1}^{n} \frac{\eta_j}{\tau_j - z} + m_0(z)$	$\sum_{j=1}^{n} \eta_j U(\tau - \tau_j) + \rho_0(\tau)$

Table 3.1: Spectral functions and m-functions for four well-known models.

The next theorem gives the m-function in terms of the Laplace transform of the relaxation function.

Theorem 3.4. *The following relation holds:*

$$m(z) = -z^{-1}\widehat{G}(-z^{-1}) + m_0(z), \qquad \mathrm{Im}(z) > 0.$$

Proof. The result follows from (3.15) and the analytic continuation of

$$-z^{-1}\widehat{G}(-z^{-1}) = \int_0^\infty \frac{H(\tau)}{\tau - z}\, d\tau,$$

to the upper half-plane (see Section 1.5). □

3.4 Inverse spectral problems in linear viscoelasticity

We have shown in Theorem 3.2 that the function $\rho(\tau)$ in (3.14), which is determined by the discrete relaxation spectrum (3.13), is a spectral function of a Sturm-Liouville problem of the form (3.3). In this section, we proceed to determine the potential function $q(x)$ of the Sturm-Liouville operator associated with this problem. This process, i.e., recovering $q(x)$ from $\rho(\tau)$, is called the inverse spectral problem for the Sturm-Liouville operator. Thus, we may state our inverse problem as follows.

Problem 3.1. *Given $\rho(\tau)$ by* (3.14)*, reconstruct $q(x)$.*

In the literature, several methods exist for solving inverse spectral problems. In this thesis, we consider two possible methods. One method is due to Simon [24] where the inverse problem is reduced to a problem of solving a particular nonlinear integro-differential equation, the A-equation. This method, however, will be postponed until the next chapter. Here, we will use the other method produced by Gelfand and Levitan [17]. Such a method allows one to reconstruct the potential from a given spectral function by solving a particular linear integral equation, the Gelfand-Levitan equation.

3.4.1 Gelfand-Levitan method

In this subsection, we first briefly describe the Gelfand-Levitan method [17]. We then show that using this method, Problem 3.1 can be solved explicitly.

In the Gelfand-Levitan method [17], the potential $q(x)$ is reconstructed by the formula

$$q(x) = 2\frac{d}{dx}K(x,x), \tag{3.16}$$

where $K(x,t)$ is the unique solution of the Gelfand-Levitan equation

$$K(x,t) + F(x,t) + \int_0^x K(x,s)F(s,t)\,ds = 0, \qquad 0 \le t \le x, \tag{3.17}$$

in which the input function $F(x,t)$ is given by

$$F(x,t) = \int_0^\infty \frac{\sin(\sqrt{\tau}x)\sin(\sqrt{\tau}t)}{\tau}\big[d\rho(\tau) - d\rho_0(\tau)\big]. \tag{3.18}$$

Thus, given a spectral function $\rho(\tau)$, one can use (3.18) to calculate $F(x,t)$, which in turn uniquely determines $K(x,t)$ by solving (3.17). Once $K(x,t)$ is obtained, the potential $q(x)$ can be found by (3.16). Clearly, $\rho(\tau)$ determines $q(x)$ uniquely.

$$\rho(\tau) \Longrightarrow F(x,t) \Longrightarrow K(x,t) \Longrightarrow q(x).$$

Let us now return to our problem, Problem 3.1, and consider solving it using the above method. Substituting (3.14) into (3.18), we obtain

$$F(x,t) = \sum_{j=1}^{n} \eta_j u_0(x,\tau_j)u_0(t,\tau_j), \tag{3.19}$$

where

$$u_0(x,\tau_j) = \begin{cases} x, & \tau_j = 0, \\ \dfrac{\sin(\sqrt{\tau_j}x)}{\sqrt{\tau_j}}, & \tau_j > 0. \end{cases}$$

We look for a solution of the Gelfand-Levitan equation in the form

$$K(x,t) = \sum_{j=1}^{n} K_j(x) u_0(t,\tau_j), \tag{3.20}$$

where $K_j(x)$, $j = 1,2,\ldots,n$, are the unknown functions to be determined. These unknowns, upon substituting (3.19) and (3.20) into (3.17), satisfy the following system of equations

$$K_j(x) + \sum_{l=1}^{n} y_{jl}(x) K_l(x) = -\eta_j u_0(x,\tau_j),$$

where

$$y_{jl}(x) = \eta_j \int_0^x u_0(y,\tau_j) u_0(y,\tau_l)\, dy.$$

If $T(x)$ is the $n \times n$ matrix defined by

$$T(x) = I_n + Y(x), \tag{3.21}$$

where I_n is the identity matrix and $Y(x)$ is the matrix

$$Y(x) = \begin{bmatrix} y_{11}(x) & y_{12}(x) & \ldots & y_{1n}(x) \\ y_{21}(x) & y_{22}(x) & \ldots & y_{2n}(x) \\ \vdots & \vdots & \ddots & \vdots \\ y_{n1}(x) & y_{n2}(x) & \ldots & y_{nn}(x) \end{bmatrix},$$

then we obtain

$$K_j(x) = \frac{\det T^{(j)}(x)}{\det T(x)}, \tag{3.22}$$

where the new matrix $T^{(j)}(x)$ is constructed by substituting the jth column of the matrix $T(x)$ with the new column $-\eta_j u_0(x,\tau_j)$, $j = 1,2,\ldots,n$. It now follows from (3.20) and (3.22) that the Gelfand-Levitan equation has the explicit solution

$$K(x,t) = \frac{1}{\det T(x)} \sum_{j=1}^{n} u_0(t,\tau_j) \det T^{(j)}(x), \tag{3.23}$$

which on substitution into (3.16) gives

$$q(x) = -2\frac{d^2}{dx^2} \ln \det T(x). \tag{3.24}$$

Hence, with $\rho(\tau)$ given by (3.14), the potential $q(x)$ is obtained explicitly.

Remark 3.2. The method shown above for solving Problem 3.1 is a modification of the method used in [17] which was developed for a non-zero initial condition in problem (3.3).

3.4.2 Inverse problem for the Newtonian model

In the previous subsection, we have shown that Problem 3.1 can be explicitly solved using the Gelfand-Levitan method. This follows because we managed to obtain an explicit solution of the Gelfand-Levitan equation. In this and the following two subsections, we will consider three special cases of Problem 3.1 in more detail. In particular, we will consider the inverse problems in which the spectral functions are those for the Newtonian, Maxwell and Oldroyd-B models. For each problem, we will give the explicit solution of the Gelfand-Levitan equation and most importantly the explicit solution of the problem itself.

Let us first consider the simplest case, where $n = 1$ and $\tau_1 = 0$ in (3.14). Then

$$\rho(\tau) = \eta_1 U(\tau) + \rho_0(\tau),$$

which is the spectral function for the Newtonian model. In this case, equation (3.19) reduces to

$$F(x,t) = \eta_1 xt. \tag{3.25}$$

The solution of the Gelfand-Levitan equation corresponding to (3.25) is given by the following theorem.

Theorem 3.5. *The function*

$$K(x,t) = -\frac{3\eta_1 xt}{\eta_1 x^3 + 3},$$

solves the Gelfand-Levitan equation (3.17) *with* $F(x,t)$ *given by* (3.25).

Proof. With $F(x,t)$ given as above, the matrix (3.21) has only one element

$$T(x) = \left[\frac{\eta_1 x^3 + 3}{3}\right]. \tag{3.26}$$

The desired result now follows from (3.23) and (3.26). □

The next theorem is the main result of this subsection.

Theorem 3.6. *For the Newtonian model, the potential takes the form*

$$q(x) = \frac{6\eta_1 x(\eta_1 x^3 - 6)}{(\eta_1 x^3 + 3)^2}. \tag{3.27}$$

Proof. The result follows immediately from (3.24) and (3.26). □

We note that $q(x)$ has no poles on $[0,\infty)$ and has only two zeros: $x = 0$ and $x = \sqrt[3]{6/\eta_1}$. Furthermore, $q'(0) = -4\eta_1$ and $q(x) \sim 6/x^2$ as $x \to \infty$. In Figure 3.1 below, we plot $q(x)$ with $\eta_1 = 1$.

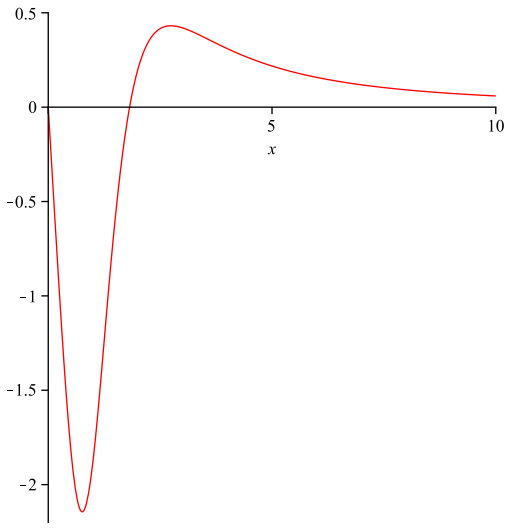

Figure 3.1: $q(x)$ for the Newtonian model with $\eta_1 = 1$.

3.4.3 Inverse problem for the Maxwell model

For the Maxwell model, the spectral function takes the form

$$\rho(\tau) = \eta_1 U(\tau - \tau_1) + \rho_0(\tau),$$

which is the special case of (3.14) with $n = 1$ and $\tau_1 > 0$. It then follows from (3.19) that

$$F(x,t) = \frac{\eta_1 \sin(\sqrt{\tau_1}x)\sin(\sqrt{\tau_1}t)}{\tau_1}. \tag{3.28}$$

The next theorem presents the solution of the Gelfand-Levitan equation in which the input function is (3.28).

Theorem 3.7. *The function*

$$K(x,t) = -\frac{4\eta_1\sqrt{\tau_1}\sin(\sqrt{\tau_1}x)\sin(\sqrt{\tau_1}t)}{2\sqrt{\tau_1}(\eta_1 x + 2\tau_1) - \eta_1\sin(2\sqrt{\tau_1}x)}, \tag{3.29}$$

solves the Gelfand-Levitan equation (3.17) *with* $F(x,t)$ *given by* (3.28).

Proof. With $F(x,t)$ given as above, the matrix (3.21) reduces to

$$T(x) = \left[\frac{2\sqrt{\tau_1}(\eta_1 x + 2\tau_1) - \eta_1\sin(2\sqrt{\tau_1}x)}{4\tau_1\sqrt{\tau_1}}\right]. \tag{3.30}$$

The desired result now follows from (3.23) and (3.30). □

The main result for this subsection is given by the following theorem.

Theorem 3.8. *For the Maxwell model, the potential takes the form*

$$q(x) = \frac{16\eta_1\tau_1\left[\eta_1\left(1-\cos(2\sqrt{\tau_1}x)\right) - \sqrt{\tau_1}(\eta_1 x + 2\tau_1)\sin(2\sqrt{\tau_1}x)\right]}{\left[2\sqrt{\tau_1}(\eta_1 x + 2\tau_1) - \eta_1\sin(2\sqrt{\tau_1}x)\right]^2}. \tag{3.31}$$

Proof. The result follows immediately from (3.24) and (3.30). □

It can be easily shown that $q(x)$ has no poles on $[0,\infty)$ and has an infinite number of zeros

$$x_{2n} = \frac{n\pi}{\sqrt{\tau_1}} \qquad \text{and} \qquad \frac{n\pi}{\sqrt{\tau_1}} < x_{2n+1} < \frac{(2n+1)\pi}{2\sqrt{\tau_1}}, \qquad n \geq 0. \tag{3.32}$$

Furthermore, $q'(0) = -4\eta_1$ and

$$q(x) \sim -\frac{4\sqrt{\tau_1}\sin(2\sqrt{\tau_1}x)}{x} \qquad \text{as} \qquad x \to \infty. \tag{3.33}$$

Figure 3.2 shows $q(x)$ with $\eta_1 = \tau_1 = 1$.

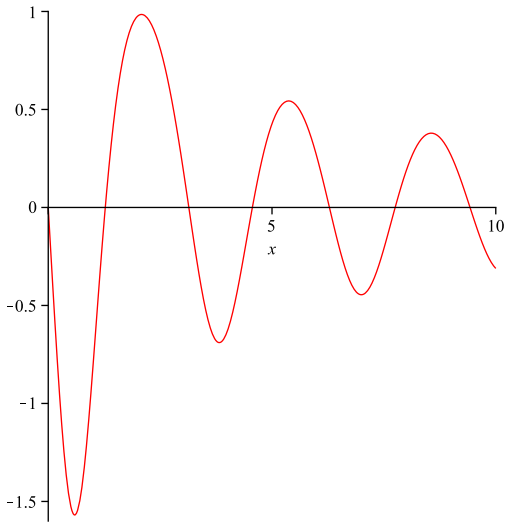

Figure 3.2: $q(x)$ for the Maxwell model with $\eta_1 = \tau_1 = 1$.

3.4.4 Inverse problem for the Oldroyd-B model

As a final case, we consider (3.14) with $n = 2$, $\tau_1 = 0$ and $\tau_2 > 0$. Then

$$\rho(\tau) = \eta_1 U(\tau) + \eta_2 U(\tau - \tau_2) + \rho_0(\tau), \tag{3.34}$$

which is the spectral function for the Oldroyd-B model. Equation (3.19) now gives

$$F(x,t) = \eta_1 xt + \frac{\eta_2 \sin(\sqrt{\tau_2}x)\sin(\sqrt{\tau_2}t)}{\tau_2}. \tag{3.35}$$

In the next theorem, we present the solution of the Gelfand-Levitan equation when $F(x,t)$ is given by (3.35).

Theorem 3.9. *The solution of the Gelfand-Levitan equation* (3.17) *corresponding to* (3.35) *takes the form*

$$K(x,t) = \frac{1}{\det T(x)}\left[t \det T^{(1)}(x) + \frac{\sin(\sqrt{\tau_2}t)}{\sqrt{\tau_2}} \det T^{(2)}(x)\right], \tag{3.36}$$

where

$$\det T^{(1)}(x) = \frac{\eta_1}{4\tau_2^2}\Big[2\eta_2(1-\tau_2x^2) - 4\tau_2^2x - \eta_2\big(\sqrt{\tau_2}x\sin(2\sqrt{\tau_2}x) + 2\cos(2\sqrt{\tau_2}x)\big)\Big],$$

$$\det T^{(2)}(x) = \frac{\eta_2}{3\tau_2\sqrt{\tau_2}}\Big[\big(\eta_1x(3-\tau_2x^2) - 3\tau_2\big)\sin(\sqrt{\tau_2}x) - 3\eta_1\sqrt{\tau_2}x^2\cos(\sqrt{\tau_2}x)\Big],$$

and

$$\begin{aligned}\det T(x) = \frac{1}{12\tau_2^3}\Big[&2\tau_2^2(\eta_1x^3+3)(\eta_2x+2\tau_2) - 6\eta_1\eta_2(\tau_2x^2+1)\\ &+ \eta_2\sqrt{\tau_2}\big(\eta_1x(12-\tau_2x^2) - 3\tau_2\big)\sin(2\sqrt{\tau_2}x)\\ &+ 6\eta_1\eta_2(1-\tau_2x^2)\cos(2\sqrt{\tau_2}x)\Big].\end{aligned} \tag{3.37}$$

Proof. With $F(x,t)$ given as above, the matrix (3.21) reads

$$T(x) = \begin{bmatrix} \frac{\eta_1x^3+3}{3} & \frac{\eta_1\left(\sin(\sqrt{\tau_2}x) - \sqrt{\tau_2}x\cos(\sqrt{\tau_2}x)\right)}{\tau_2\sqrt{\tau_2}} \\ \frac{\eta_2\left(\sin(\sqrt{\tau_2}x) - \sqrt{\tau_2}x\cos(\sqrt{\tau_2}x)\right)}{\tau_2\sqrt{\tau_2}} & \frac{2\sqrt{\tau_2}(\eta_2x+2\tau_2) - \eta_2\sin(2\sqrt{\tau_2}x)}{4\tau_2\sqrt{\tau_2}} \end{bmatrix}. \tag{3.38}$$

The desired result now follows from (3.23) and (3.38). □

We now state our main result for this subsection.

Theorem 3.10. *For the Oldroyd-B model, the potential takes the form*

$$q(x) = -2\frac{d^2}{dx^2}\ln\det T(x), \tag{3.39}$$

where $\det T(x)$ *is given by* (3.37).

Proof. The result follows immediately from (3.24) and (3.38). □

Direct calculation shows that $q(x)$ has the following structure

$$q(x) = \frac{p(x)}{\big[\det T(x)\big]^2},$$

where

$$\begin{aligned} p(x) = {} & p_0(x) + p_1(x)\sin(2\sqrt{\tau_2}x) + p_2(x)\cos(2\sqrt{\tau_2}x) + p_3(x)\sin(4\sqrt{\tau_2}x) \\ & + p_4(x)\cos(4\sqrt{\tau_2}x), \end{aligned}$$

and $p_i(x)$ are polynomials in x. From (3.37), we obtain

$$\det T(x) \sim 1 + \frac{1}{3}(\eta_1+\eta_2)x^3 - \frac{1}{15}\eta_2\tau_2 x^5 \qquad \text{as} \qquad x \to 0,$$

which implies that

$$q(x) \sim -4(\eta_1+\eta_2)x + \frac{8}{3}\eta_2\tau_2 x^3 \qquad \text{as} \qquad x \to 0. \tag{3.40}$$

On the other side, since (3.36) gives

$$K(x,x) \sim -\frac{3+2\sin^2(\sqrt{\tau_2}x)}{x} \qquad \text{as} \qquad x \to \infty,$$

then it follows from (3.16) that $q(x)$ for the Oldroyd-B model has the same asymptotic behaviour (3.33) as $q(x)$ for the Maxwell model, with τ_1 replaced by τ_2, and

consequently has infinitely many zeros. Regarding the poles of $q(x)$, equation (3.21) with $n = 2$ gives

$$\det T(x) = (1 + \lambda_1)(1 + \lambda_2),$$

where λ_1 and λ_2 are the eigenvalues of the matrix $Y(x)$. These eigenvalues, upon writing

$$Y(x) = \begin{bmatrix} \eta_1 I_{11} & \eta_1 I_{12} \\ \eta_2 I_{12} & \eta_2 I_{22} \end{bmatrix}, \qquad I_{jl} = \int_0^x u_0(y, \tau_j) u_0(y, \tau_l)\, dy,$$

take the form

$$\lambda = \frac{b \pm \sqrt{b^2 - 4c}}{2},$$

where

$$b = \eta_1 I_{11} + \eta_2 I_{22} \geq 0 \qquad \text{and} \qquad c = \eta_1 \eta_2 (I_{11} I_{22} - I_{12}^2).$$

The Cauchy-Schwarz inequality implies that $c \geq 0$. Now, since

$$b^2 - 4c = (\eta_1 I_{11} - \eta_2 I_{22})^2 + 4\eta_1 \eta_2 I_{12}^2 \geq 0,$$

it follows that λ_1 and λ_2 are both non-negative. Hence, $q(x)$ has no poles on $[0, \infty)$. Finally, in Figure 3.3 below, we plot $q(x)$ with $\eta_1 = \eta_2 = \tau_2 = 1$.

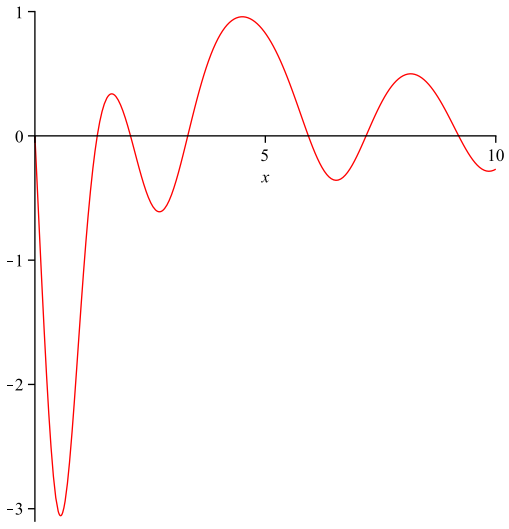

Figure 3.3: $q(x)$ for the Oldroyd-B model with $\eta_1 = \eta_2 = \tau_2 = 1$.

3.5 Concluding remarks

The connection between Weyl-Titchmarsh theory and linear viscoelasticity, to our knowledge, has never before been explored. Furthermore, the idea of identifying a potential $q(x)$ with a linear viscoelastic material is new to this thesis. There are two questions one can ask about these connections:

Q1. *What are the properties of $q(x)$?*

Q2. *Does $q(x)$ have a physical meaning?*

We have gone some way towards answering the first question, at least for the simple viscoelastic models of Newtonian, Maxwell and Oldroyd-B types. Here $q(x)$ gives rise to a finite number of non-negative eigenvalues embedded in the continuous spectrum of the operator and these eigenvalues are the relaxation times of the viscoelastic model. Thus if $q(x)$ were known, the relaxation times could be found by solving the direct Sturm-Liouville problem (3.3). Moreover, Eastham and Kalf [8, p109] argue that the asymptotic behaviour of $q(x)$ when $y(0) \neq 0$ and

$$\rho(\tau) = \sum_{j=1}^{n} \eta_j U(\tau - \tau_j) + \frac{2}{\pi}\sqrt{\tau}, \qquad \tau_j > 0,$$

is

$$q(x) \sim \frac{4}{x} \sum_{j=1}^{n} \sqrt{\tau_j} \sin(2\sqrt{\tau_j}x) \qquad \text{as} \qquad x \to \infty.$$

(The change in sign, compared to (3.33), is due to the different initial condition). Hence one could, in principle, determine the eigenvalues from a sinusoidal decomposition of $xq(x)$ as $x \to \infty$. Unfortunately, we do not know the form of the asymptotics of $q(x)$ when the relaxation spectrum is itself a continuous function.

The viscoelastic part of the m-function in (3.15), i.e.,

$$g(z) = \int_0^\infty \frac{H(\tau)}{\tau - z}\, d\tau, \qquad \mathrm{Im}(z) > 0,$$

has a physical interpretation. The real and imaginary parts of the complex shear modulus

$$G^*(\omega) = \int_0^\infty \frac{i\omega}{1+i\omega\tau} H(\tau)\, d\tau,$$

are called the storage and loss moduli of the material, respectively. These can be measured for a range of discrete frequencies, ω, in an oscillatory shear rheometer [25, 27]. The complex shear modulus is just the viscoelastic part of the m-function along the imaginary z-axis, $z = i\omega^{-1}$. This observation gives a physical meaning to the m-function, but there appears to be no obvious way of attributing a physical meaning to the potential $q(x)$.

4

A NEW FAMILY OF EXACT SOLUTIONS TO THE *A*-EQUATION

4.1 Simon method

In 1999, Simon [24] proposed a new method for reconstructing the potential $q(x)$ in the Sturm-Liouville problem

$$\begin{cases} -y''(x,z) + q(x)y(x,z) = zy(x,z), \qquad x \geq 0, \\ y(0,z) = 0, \end{cases} \tag{4.1}$$

from its spectral function $\rho(\tau)$. He showed that $q(x)$ can be reconstructed by the formula

$$q(x) = \lim_{t \to 0} A(t,x), \tag{4.2}$$

where $A(t,x)$ is the unique solution of the nonlinear integro-differential equation

$$\frac{\partial A(t,x)}{\partial x} = \frac{\partial A(t,x)}{\partial t} + \int_0^t A(s,x)A(t-s,x)\,ds, \tag{4.3}$$

in the domain

$$\big\{(x,t) : 0 \leq x \leq a,\ 0 \leq t \leq a - x\big\},$$

with the initial condition [13]

$$A(t,0) = A(t) = -2\lim_{\varepsilon \to 0} \int_0^\infty e^{-\varepsilon\tau}\, \frac{\sin(2\sqrt{\tau}t)}{\sqrt{\tau}}\, d\rho(\tau). \tag{4.4}$$

Equation (4.3) is called the A-equation and the initial function $A(t)$ is called the A-amplitude. Thus, given $\rho(\tau)$, one can use (4.4) to calculate $A(t)$, which in turn uniquely determines $A(t,x)$ by solving (4.3) with $A(t,0) = A(t)$. Once the solution $A(t,x)$ is obtained, the potential $q(x)$ can be found by (4.2).

$$\rho(\tau) \Longrightarrow A(t) \Longrightarrow A(t,x) \Longrightarrow q(x).$$

Simon [24] also proved the uniqueness theorem: $q(x)$ in the interval $x \in [0,a]$ is uniquely determined by $A(t)$ in the interval $t \in [0,a]$ and vice versa. In prov-

ing this, he also proved that for a given $A(t)$ in $[0, a]$, equation (4.3) has a unique solution $A(t, x)$ in the sector $0 \leq x + t \leq a$.

In this chapter, after relating the A-amplitude to the theory of linear viscoelasticity in Section 4.2, we derive a new family of exact solutions to the A-equation (4.3). Our first exact solution is obtained in Section 4.3 by means of the Laplace transform. The form of this solution is then generalized in Section 4.4 leading to a further exact solution. The zero-level curves of these solutions are discussed in Section 4.5. Using the generalized solution as a point of departure, we arrive at a larger family of new exact solutions by means of complexification. This family is presented in Section 4.6, together with a conjecture.

4.2 The A-amplitude in linear viscoelasticity

Assume that we have a linear viscoelastic material for which its relaxation spectrum $H(\tau)$ satisfies the condition (3.12) derived in the previous chapter. Then the function

$$\rho(\tau) = \int_0^\tau H(\tau')\, d\tau' + \rho_0(\tau), \qquad \tau \geq 0, \tag{4.5}$$

is a spectral function of a Sturm-Liouville problem of the form (4.1). The main purpose of this section is to look at the A-amplitude associated with (4.5).

In the case where $q(x) = 0$ in the problem (4.1), Gesztesy and Simon [13] have shown that $A(t) = 0$. Taking this into account, one easily arrives at the following theorem which gives an explicit representation for $A(t)$ in terms of $H(\tau)$.

Theorem 4.1. *If $\rho(\tau)$ in* (4.5) *is a spectral function of a certain Sturm-Liouville problem of the form* (4.1)*, then the associated A-amplitude is*

$$A(t) = -2 \int_0^\infty \frac{\sin(2\sqrt{\tau}t)}{\sqrt{\tau}} H(\tau)\, d\tau. \tag{4.6}$$

Remark 4.1. Using exactly the same argument as we have used in Section 1.3, it is easy to show that the recovery of $H(\tau)$ from $A(t)$ in (4.6) is ill-posed.

In Table 4.1, we list $A(t)$ for the viscoelastic models introduced in Chapter 1.

Model	$A(t)$
Newtonian	$-4\eta_1 t$
Maxwell	$-\frac{2\eta_1}{\sqrt{\tau_1}}\sin(2\sqrt{\tau_1}t)$
Oldroyd-B	$-4\eta_1 t - \frac{2\eta_2}{\sqrt{\tau_2}}\sin(2\sqrt{\tau_2}t)$
Multi-mode Maxwell	$-2\sum_{j=1}^{n}\frac{\eta_j}{\sqrt{\tau_j}}\sin(2\sqrt{\tau_j}t)$

Table 4.1: A-amplitudes for four well-known models.

The representation (4.6) allows us to establish the following relationship between the Laplace transform of $A(t)$ and that of the relaxation function, $G(t)$.

Theorem 4.2. *The following relation holds:*

$$\widehat{A}\big(-2iz^{1/2}\big) = z^{-1}\widehat{G}\big(-z^{-1}\big), \qquad \mathrm{Im}(z) > 0.$$

Proof. The Laplace transform of (4.6) reads

$$\widehat{A}(s) = -\int_0^\infty \frac{4}{4\tau + s^2} H(\tau)\, d\tau, \qquad \mathrm{Re}(s) > 0,$$

which, upon writing $s = -2iz^{1/2}$, becomes

$$\widehat{A}\big(-2iz^{1/2}\big) = -\int_0^\infty \frac{H(\tau)}{\tau - z}\, d\tau.$$

The desired result now follows from the analytic continuation of

$$-z^{-1}\widehat{G}\big(-z^{-1}\big) = \int_0^\infty \frac{H(\tau)}{\tau - z}\, d\tau,$$

to the upper half-plane (see Section 1.5). □

We close this section with an interesting property satisfied by the zeros of $A(t)$ and $q(x)$ associated with the Maxwell model. For this model, $A(t)$ takes the form

$$A(t) = -\frac{2\eta_1}{\sqrt{\tau_1}} \sin(2\sqrt{\tau_1}t), \tag{4.7}$$

which has infinitely many zeros given by

$$t_{2n} = \frac{n\pi}{\sqrt{\tau_1}} \qquad \text{and} \qquad t_{2n+1} = \frac{(2n+1)\pi}{2\sqrt{\tau_1}}, \qquad n \geq 0.$$

Taking (3.32) into account, we easily obtain the following result.

Theorem 4.3. *For the Maxwell model, the zeros of $A(t)$ partially interlace with those of $q(x)$, i.e.,*

$$x_{2n} = t_{2n} \qquad \textit{and} \qquad x_{2n+1} < t_{2n+1}, \qquad n \geq 0.$$

4.3 A new exact solution to the A-equation

In this section, after presenting the existing exact solutions to the A-equation (4.3), we derive a new exact solution. Such a solution is derived from the Laplace transform of the A-equation.

In the literature, only a few exact solutions to the A-equation have been derived, since it is a quite new equation in inverse spectral theory. Using two properties of Bessel functions $J_n(t)$, Zhang [29] shows that for all $x \geq 0$, the function

$$A(t,x) = \frac{q_0^{1/2}}{t} J_1(2tq_0^{1/2}), \qquad q_0 > 0, \tag{4.8}$$

solves the A-equation (4.3) with $q(x) = q_0$. This solution was first found by Gesztesy and Simon [13] who proved it for the case $x = 0$ only. Zhang [29] also suggests the following form of solution

$$A(t,x) = q(x)e^{tf(x)}, \tag{4.9}$$

which on substitution into the A-equation (4.3) gives a system of two differential equations in two unknowns $f(x)$ and $q(x)$. By solving such a system, she has three possibilities for (4.9):

(i)

$$A(t,x) = \frac{2}{(x+a)^2} e^{-\frac{2t}{x+a}}, \tag{4.10}$$

with

$$q(x) = \frac{2}{(x+a)^2}, \qquad a > 0.$$

(ii)

$$A(t,x) = -\frac{8b^2\beta e^{-2bx}}{\left(1+\beta e^{-2bx}\right)^2} e^{-2bt\frac{1-\beta e^{-2bx}}{1+\beta e^{-2bx}}}, \tag{4.11}$$

with the Bargmann potential [5]

$$q(x) = -\frac{8b^2\beta e^{-2bx}}{\left(1+\beta e^{-2bx}\right)^2}, \qquad \beta = \frac{b-a}{b+a}, \qquad a \geq 0, \qquad b > 0.$$

(iii)

$$A(t,x) = a\sec^2\left[\sqrt{\frac{a}{2}}(x+b)\right] e^{\sqrt{2a}\tan\left[\sqrt{\frac{a}{2}}(x+b)\right]t}, \tag{4.12}$$

with

$$q(x) = a\sec^2\left[\sqrt{\frac{a}{2}}(x+b)\right], \qquad a > 0.$$

Our method for deriving new exact solutions to the A-equation is based on using the Laplace transform. The Laplace transform, with respect to t, reduces the A-equation (4.3) to

$$\frac{\partial \widehat{A}(u,x)}{\partial x} = -q(x) + u\widehat{A}(u,x) + \widehat{A}^2(u,x), \tag{4.13a}$$

which is a differential equation of Riccati type. To this equation, we attach the

Laplace transform of $A(t)$ as an initial condition

$$\widehat{A}(u,0) = \widehat{A}(u). \tag{4.13b}$$

Thus if we are given $A(t)$ and $q(x)$, we can solve the initial value problem (4.13) for $\widehat{A}(u,x)$ and then take the inverse Laplace transform to obtain the desired solution $A(t,x)$ of the A-equation.

In Sections 4.2 and 3.4, respectively, we have found $A(t)$ and $q(x)$ for some well-known viscoelastic models. For the simplest one which is of the Newtonian type, these functions read

$$A(t) = -4\eta_1 t \qquad \text{and} \qquad q(x) = \frac{6\eta_1 x(\eta_1 x^3 - 6)}{(\eta_1 x^3 + 3)^2}.$$

In this case, with the help of Maple, the solution of the Riccati problem (4.13) is

$$\widehat{A}(u,x) = \frac{6\eta_1\big[ux(\eta_1 x^3 - 6) + 2(2\eta_1 x^3 - 3)\big]}{(\eta_1 x^3 + 3)\big[u^2(\eta_1 x^3 + 3) + 6\eta_1 x(ux + 2)\big]},$$

which may be written in the form

$$\widehat{A}(u,x) = \frac{\big[u - f(x)\big]q(x) + r(x)}{\big[u - f(x)\big]^2 + k^2(x)}, \tag{4.14}$$

where

$$f(x) = -\frac{3\eta_1 x^2}{\eta_1 x^3 + 3}, \tag{4.15a}$$

$$k^2(x) = \frac{3\eta_1 x(\eta_1 x^3 + 12)}{(\eta_1 x^3 + 3)^2}, \tag{4.15b}$$

$$r(x) = \frac{6\eta_1(\eta_1^2 x^6 + 24\eta_1 x^3 - 18)}{(\eta_1 x^3 + 3)^3}. \tag{4.15c}$$

Equation (4.14) can be conveniently transformed to the time domain to give

$$A(t,x) = e^{tf(x)}\Big\{q(x)\cos\big[tk(x)\big] + p(x)\sin\big[tk(x)\big]\Big\}, \tag{4.16}$$

where

$$p(x) = \frac{r(x)}{k(x)}.$$

We have therefore proved the following theorem.

Theorem 4.4. *The function $A(t,x)$ given by* (4.16) *with $f(x)$, $k(x)$ and $r(x)$ given by* (4.15) *solves the A-equation* (4.3) *with $A(0,x)$ the Newtonian potential.*

4.4 Further exact solutions

In the previous section, we have derived a new exact solution to the A-equation (4.3) through its Laplace transform. In this section, we will use the ansatz (4.16) and derive new exact solutions directly from the A-equation.

The following theorem gives all possible solutions of the form

$$A(t,x) = e^{tf(x)}\Big\{q(x)\cos\big[tk(x)\big] + p(x)\sin\big[tk(x)\big]\Big\}. \tag{4.17}$$

We note that if $p(x) \equiv q(x) \equiv 0$, then (4.17) reduces to $A(t,x) \equiv 0$, so we will ignore this case. We will also ignore the case where $k(x) \equiv 0$, since this leads to Zhang's solution (4.9).

Theorem 4.5. *If $A(t,x)$ is of the form* (4.17) *and solves the A-equation* (4.3)*, then*

$$q(x) = 2f'(x), \tag{4.18}$$

$$p(x) = -2k'(x), \tag{4.19}$$

and $f(x)$ and $k(x)$ satisfy the system of differential equations

$$f''(x) = f(x)f'(x) - k(x)k'(x), \tag{4.20a}$$

$$k''(x) = \big[f(x)k(x)\big]' - \frac{\big[f'(x)\big]^2 + \big[k'(x)\big]^2}{k(x)}. \tag{4.20b}$$

Conversely, if $f(x)$ and $k(x)$ satisfy (4.20)*, then the function*

$$A(t,x) = 2e^{tf(x)}\Big\{f'(x)\cos\big[tk(x)\big] - k'(x)\sin\big[tk(x)\big]\Big\}, \tag{4.21}$$

solves the A-equation (4.3)*.*

Proof. From (4.17), we find

$$\frac{\partial A}{\partial x}(t,x) = e^{tf(x)}\Bigg\{\bigg[p'(x) + \Big(f'(x)p(x) - k'(x)q(x)\Big)t\bigg]\sin\big[tk(x)\big] + \bigg[q'(x) + \Big(f'(x)q(x) + k'(x)p(x)\Big)t\bigg]\cos\big[tk(x)\big]\Bigg\},$$

$$\frac{\partial A}{\partial t}(t,x) = e^{tf(x)}\Bigg\{\Big[f(x)p(x) - k(x)q(x)\Big]\sin\big[tk(x)\big] + \Big[f(x)q(x) + k(x)p(x)\Big]\cos\big[tk(x)\big]\Bigg\},$$

and

$$\int_0^t A(s,x)A(t-s,x)\,ds = e^{tf(x)}\Bigg\{\bigg[\frac{p^2(x)+q^2(x)}{2k(x)} + p(x)q(x)t\bigg]\sin\big[tk(x)\big] + \frac{t}{2}\Big[q^2(x) - p^2(x)\Big]\cos\big[tk(x)\big]\Bigg\}.$$

If $A(t,x)$ in (4.17) solves the A-equation (4.3), then the above equalities imply that $f(x)$, $k(x)$, $p(x)$ and $q(x)$ satisfy the following system of differential equations

$$q'(x) - f(x)q(x) - k(x)p(x) = 0, \tag{4.22a}$$

$$f'(x)p(x) - k'(x)q(x) - p(x)q(x) = 0, \tag{4.22b}$$

$$2f'(x)q(x) + 2k'(x)p(x) + p^2(x) - q^2(x) = 0, \tag{4.22c}$$

$$2k(x)p'(x) - 2f(x)k(x)p(x) + 2k^2(x)q(x) - p^2(x) - q^2(x) = 0. \tag{4.22d}$$

Equations (4.22b) and (4.22c) may be rewritten in the form

$$(p + k')(q - f') = -f'k',$$
$$(p + k')^2 - (q - f')^2 = (k')^2 - (f')^2.$$

(We have dropped the x-dependence for convenience). The above two equations represent two rectangular hyperbolas in the pq-plane. There are exactly two points of intersection, namely,

$$(p,q) = (0,0) \qquad \text{and} \qquad (p,q) = (-2k', 2f').$$

We have therefore established (4.18) and (4.19), since the trivial case $p \equiv q \equiv 0$ is excluded. Finally, the system (4.20) follows by substituting (4.18) and (4.19) into the system (4.22).

Conversely, if $f(x)$ and $k(x)$ satisfy (4.20), then direct calculation shows that $A(t,x)$ in (4.21) is indeed a solution of the A-equation. □

Remark 4.2. We note that the set of solutions of the form (4.17) is non-empty, since, according to Theorem 4.4, the Newtonian solution is of this form. We also note that Theorem 4.5 implies that the Newtonian solution has the form (4.21).

Using (4.18), it is possible to eliminate $f(x)$ and $k(x)$ from the system (4.20) and obtain a single differential equation for $q(x)$. To this end, we eliminate $k(x)k'(x)$ from (4.20) by differentiation and obtain

$$k^2(x) = \frac{\big[f^2(x)\big]'' - f^2(x)f'(x) - f'''(x)}{f'(x)}, \tag{4.23}$$

which, upon differentiating and then using (4.20a), gives

$$F'(x) - 2f(x)F(x) = 0, \tag{4.24}$$

where

$$F(x) = f'(x)f'''(x) - \big[f''(x)\big]^2 - 2\big[f'(x)\big]^3.$$

Differentiating (4.24) and then using (4.18), we obtain the nonlinear differential equation

$$Q(x)Q''(x) - \big[Q'(x)\big]^2 - q(x)Q^2(x) = 0, \tag{4.25}$$

where

$$Q(x) = q(x)q''(x) - \big[q'(x)\big]^2 - q^3(x).$$

Thus, we have proved the following result.

Corollary 4.1. *If $A(t,x)$ is of the form* (4.17) *and solves the A-equation* (4.3)*, then $q(x)$ satisfies* (4.25)*.*

If $q(0) = 0$, then there is a solution of the A-equation of the form (4.17) with

$$A(t) = p(0)e^{tf(0)}\sin\big[tk(0)\big].$$

In addition, if we choose

$$p(0) = -\frac{2\eta_1}{\sqrt{\tau_1}}, \qquad f(0) = 0 \qquad \text{and} \qquad k(0) = 2\sqrt{\tau_1},$$

then we obtain the A-amplitude (4.7) for the Maxwell model. The potential for this

model is given by $q(x)$ in (3.31) for which $q(0) = 0$. This tells us that there exists a solution of the A-equation of the form (4.17) which has the Maxwell A-amplitude for $x = 0$ and the Maxwell potential for $t = 0$. Such a solution is given by the following Theorem.

Theorem 4.6. *The function $A(t,x)$ given by* (4.21) *with*

$$f(x) = -\frac{2\eta_1\sqrt{\tau_1}\big(1-\cos(2\sqrt{\tau_1}x)\big)}{2\sqrt{\tau_1}\big(\eta_1 x+2\tau_1\big)-\eta_1\sin(2\sqrt{\tau_1}x)}, \tag{4.26a}$$

$$k^2(x) = \frac{8\tau_1\Big[2\tau_1\big(\eta_1 x+2\tau_1\big)^2-\eta_1^2\big(1-\cos(2\sqrt{\tau_1}x)\big)\Big]}{\Big[2\sqrt{\tau_1}(\eta_1 x+2\tau_1)-\eta_1\sin(2\sqrt{\tau_1}x)\Big]^2}, \tag{4.26b}$$

solves the A-equation (4.3) *with $A(0,x)$ the Maxwell potential.*

Proof. From (3.16) and (4.18), we immediately obtain

$$f(x) = K(x,x) + c,$$

where c is an arbitrary constant and $K(x,t)$ is the solution of the Gelfand-Levitan equation. For the Maxwell model, $K(x,t)$ is given by (3.29), which on substitution into the above equation gives (4.26a). Equation (4.26b) follows by substituting (4.26a) into (4.23). Now, direct calculation shows that (4.26) satisfy the system

$$2f'(x) = f^2(x) - k^2(x) + k^2(0),$$

$$\big[k^2(x)\big]'' = f(x)\big[k^2(x)\big]' + 2f'(x)\big[k^2(x) - f'(x)\big],$$

which is equivalent to the system (4.20). Consequently, by Theorem 4.5, the function $A(t,x)$ solves the A-equation. □

We close this section with the following lemma, which will be needed later.

Lemma 4.1. *For the Maxwell models, the function $k'(x)$ has infinitely many simple zeros. Moreover, they do not coincide with those of $f'(x)$.*

Proof. We have shown in Subsection 3.4.3 that the Maxwell potential $q(x)$ has infinitely many zeros all of which are simple. Let x_n denote a zero of $q(x)$. It then follows from (4.18) and (4.20a) that

$$f'(x_n) = 0 \qquad \text{and} \qquad q'(x_n) = -2k(x_n)k'(x_n). \tag{4.27}$$

If x_n and x_{n+1} are adjacent zeros of $q(x)$, then $q'(x_n)$ and $q'(x_{n+1})$ have different signs. Consequently, from (4.27), $k(x)k'(x)$ will change sign infinitely many times. Since $k(x) > 0$, $k'(x)$ will have infinitely many zeros none of which coincide with those of $f'(x)$. □

4.5 Zero-level curves

In this section, we look at the zero-level curves of certain functions $A(t, x)$ which solve the A-equation (4.3), i.e., we look at the curves in the xt-plane for which $A(t, x) = 0$. The zero-level curves (if they exist) cross the t-axis at the zeros of $A(t)$ and cross the x-axis at the zeros of $q(x)$. Our principal motivation is to discuss whether there exist continuous zero-level curves which connect the zeros of $A(t)$ to those of $q(x)$.

We first answer this question for the existing exact solutions presented in Section 4.3. In the case (4.8) in which $q(x) = q_0 > 0$, the zero-level curves are the horizontal straight lines which intersect the t-axis at the zeros of $J_1(2tq_0^{1/2})$. With $q_0 = 1/4$, these are shown in Figure 4.1. We note that $A(t, x)$ changes sign at these curves. Therefore, if we use black and white colours to fill, respectively, the regions where $A(t, x)$ takes negative and positive values, then we obtain black and white horizontal stripes as shown in Figure 4.2.

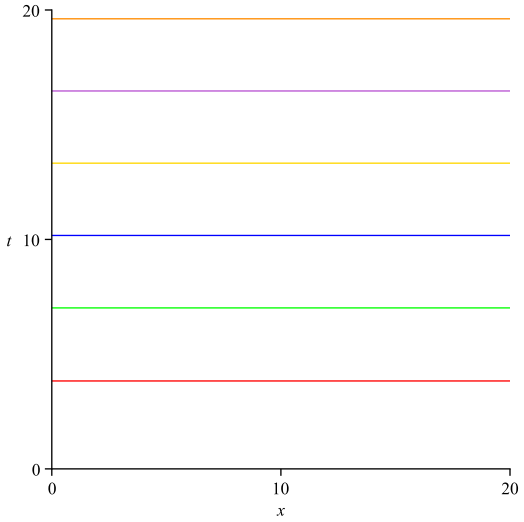

Figure 4.1: The zero level curves of (4.8) with $q_0 = 1/4$.

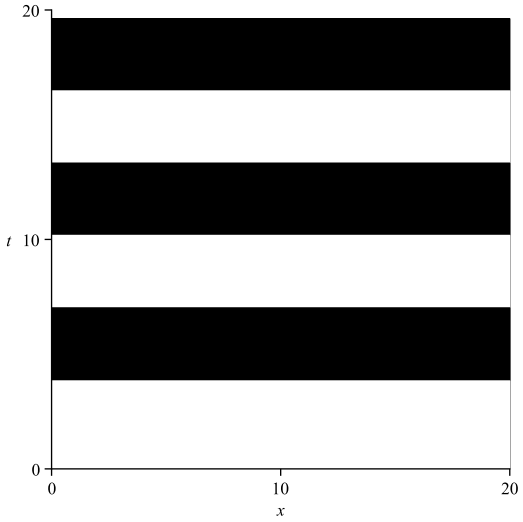

Figure 4.2: Black and white horizontal stripes for (4.8) with $q_0 = 1/4$.

In the cases (4.10), (4.11) and (4.12) which are of the form (4.9), any zero-level curves would correspond to zeros of $q(x)$. Since $q(x)$ has no zeros in each of these cases, there are no zero-level curves.

We now look at the solution

$$A(t,x) = 2e^{tf(x)}\Big\{f'(x)\cos\big[tk(x)\big] - k'(x)\sin\big[tk(x)\big]\Big\}. \tag{4.28}$$

It is possible to derive closed-form expressions for the zero-level curves of (4.28) provided the zeros of $k'(x)$ are treated with care.

Let x_0 denote the zero of $k'(x)$. Then (4.28) may be rewritten in the form

$$A(t,x) = \begin{cases} -2\sqrt{\big[f'(x)\big]^2 + \big[k'(x)\big]^2}\,e^{tf(x)}\sin\Big[tk(x) - \arctan\Big(\frac{f'(x)}{k'(x)}\Big)\Big], & x \neq x_0, \\ 2f'(x_0)e^{tf(x_0)}\cos\big[tk(x_0)\big], & x = x_0. \end{cases}$$

It is clear from the above expression that $A(t,x)$ has infinitely many zero-level curves given by

$$t = \begin{cases} \frac{1}{k(x)}\left[\arctan\left(\frac{f'(x)}{k'(x)}\right) + n\pi\right], & x \neq x_0, \\ \\ \frac{1}{k(x_0)}\left(n+\frac{1}{2}\right)\pi, & x = x_0, \end{cases} \qquad n \geq 0. \tag{4.29}$$

The curves in (4.29) for each fixed value of n are disjoint, and have a jump discontinuity of $\pi/k(x_0)$ at $x = x_0$. Provided the zeros of $f'(x)$ and $k'(x)$ do not coincide, the ensemble of all such curves represents a set of continuous curves. To illustrate this, consider the case $k'(x) > 0$ when $x < x_0$, $k'(x) < 0$ when $x > x_0$, and $f'(x_0) < 0$ (the other cases can be shown similarly). Then

$$\lim_{x\to x_0^-} \frac{1}{k(x)}\left[\arctan\left(\frac{f'(x)}{k'(x)}\right) + n\pi\right] = \frac{(n-\frac{1}{2})\pi}{k(x_0)},$$

and

$$\lim_{x\to x_0^+} \frac{1}{k(x)}\left[\arctan\left(\frac{f'(x)}{k'(x)}\right) + n\pi\right] = \frac{(n+\frac{1}{2})\pi}{k(x_0)}.$$

Hence, the curve for $n = m+1$ in the interval $x < x_0$ joins continuously with the curve for $n = m$ in the interval $x > x_0$.

In what follows, we will look at the zero-level curves of the two special cases of (4.28) which correspond to the Newtonian and Maxwell models.

For the Newtonian model, the functions $f(x)$ and $k(x)$ are given by (4.15a) and (4.15b), respectively. The derivative $k'(x)$ has only one zero x_0 which does not coincide with those of $f'(x)$, as shown in Figure 4.3. Consequently, the ensemble of the zero-level curves represents a set of continuous curves given by

$$t = \begin{cases} \frac{1}{k(x)}\left[\arctan\left(\frac{f'(x)}{k'(x)}\right) + (n+1)\pi\right], & 0 \leq x < x_0, \\ \\ \frac{1}{k(x_0)}\left(n+\frac{1}{2}\right)\pi, & x = x_0, \\ \\ \frac{1}{k(x)}\left[\arctan\left(\frac{f'(x)}{k'(x)}\right) + n\pi\right], & x_0 < x. \end{cases} \tag{4.30}$$

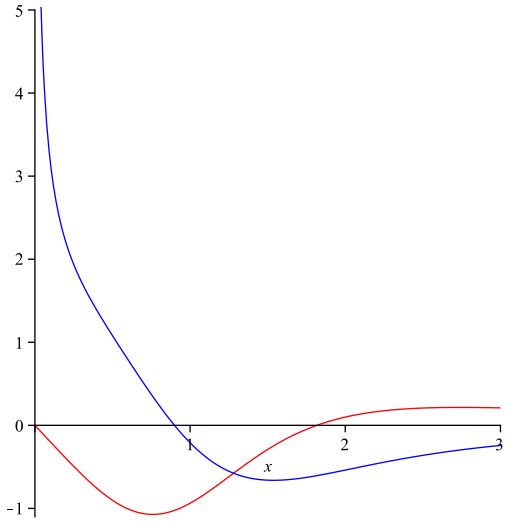

Figure 4.3: $f'(x)$ (red) and $k'(x)$ (blue) for the Newtonian model with $\eta_1 = 1$.

Figure 4.4 shows that the curves in (4.30) never intersect the t-axis, since $A(t)$ has no zeros in this case. On the other side, the curve for $n = 0$ is the only curve that intersects the x-axis which occurs at the zero of $q(x)$. These curves, using black and white colours as before, generate a pattern of zebroid stripes as shown in Figure 4.5.

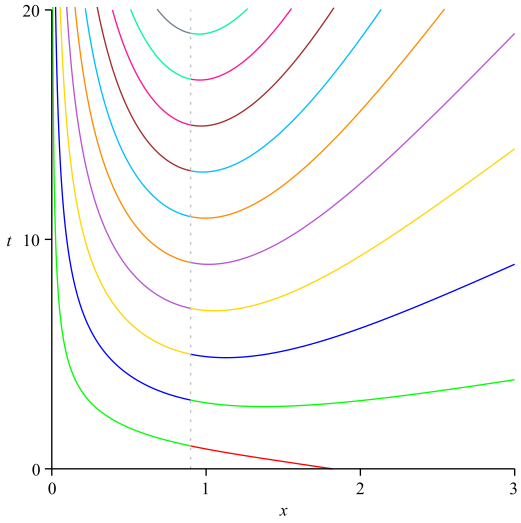

Figure 4.4: The zero-level curves for the Newtonian model with $\eta_1 = 1$.

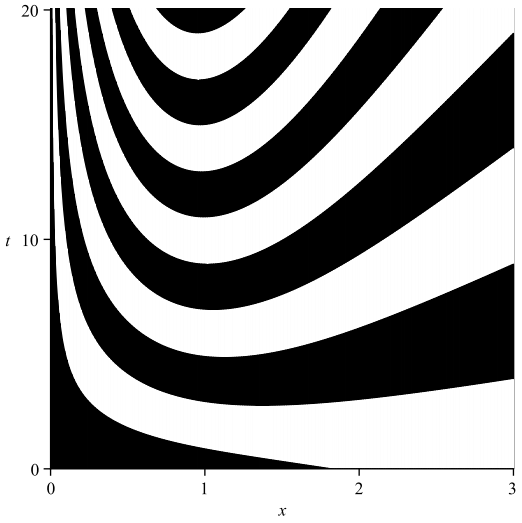

Figure 4.5: The zebroid stripes pattern for the Newtonian model with $\eta_1 = 1$.

Turning now to the Maxwell model, the functions $f(x)$ and $k(x)$ are given by (4.26). According to Lemma 4.1, the derivative $k'(x)$ has infinitely many zeros $x_0, x_1, \ldots$, which do not coincide with the zeros of $f'(x)$, as shown in Figure 4.6 below.

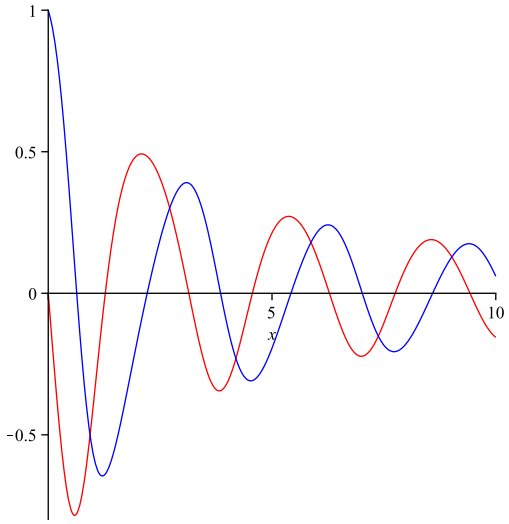

Figure 4.6: $f'(x)$ (red) and $k'(x)$ (blue) for the Maxwell model with $\eta_1 = \tau_1 = 1$.

Consequently, the ensemble of the zero-level curves represents a set of continuous curves given by

$$t = \begin{cases} \frac{1}{k(x)}\left[\arctan\left(\frac{f'(x)}{k'(x)}\right) + (n+1)\pi\right], & 0 \le x < x_0, \\ \frac{1}{k(x_0)}\left(n+\frac{1}{2}\right)\pi, & x = x_0, \\ \frac{1}{k(x)}\left[\arctan\left(\frac{f'(x)}{k'(x)}\right) + n\pi\right], & x_0 < x < x_1, \\ \vdots & \vdots \\ \frac{1}{k(x)}\left[\arctan\left(\frac{f'(x)}{k'(x)}\right) + \pi\right], & x_{n-1} < x < x_n, \\ \frac{1}{k(x_n)}\left(n+\frac{1}{2}\right)\pi, & x = x_n, \\ \frac{1}{k(x)}\left[\arctan\left(\frac{f'(x)}{k'(x)}\right)\right], & x_n < x. \end{cases}$$

As a result of these continuities, the above curves will connect the zeros of $A(t)$ to those of $q(x)$, as shown in Figure 4.7. Finally, Figure 4.8 shows the zebroid stripes pattern generated from these curves.

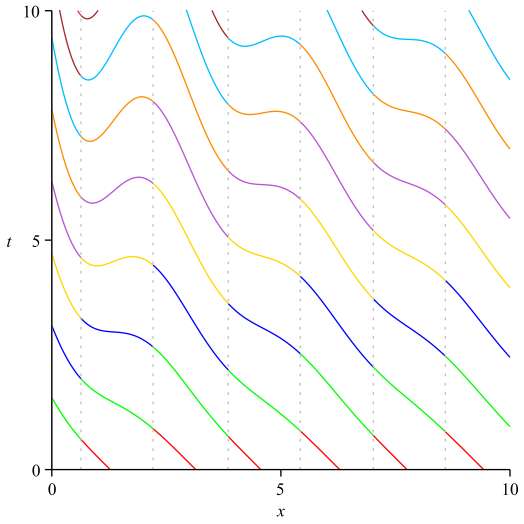

Figure 4.7: The zero-level curves for the Maxwell model with $\eta_1 = \tau_1 = 1$.

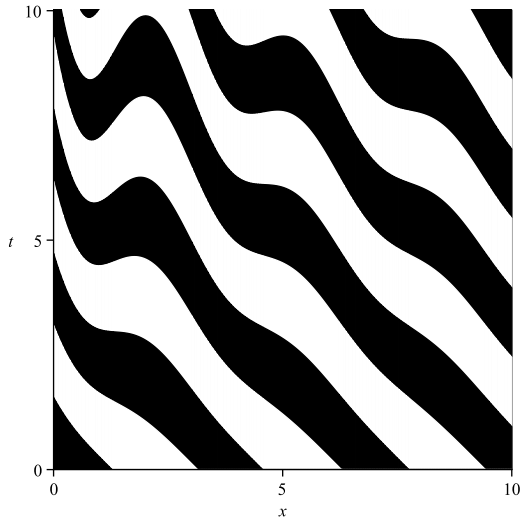

Figure 4.8: The zebroid stripes pattern for the Maxwell model with $\eta_1 = \tau_1 = 1$.

4.6 Complexification and a conjecture

In this section, we continue to derive new exact solutions to the A-equation (4.3) by generalizing the form of $A(t,x)$ in (4.21).

4.6.1 Complexification

In this subsection, we will show that the A-equation (4.3) possesses solutions of the form

$$A(t,x) = 2\sum_{j=1}^{n} e^{tf_j(x)}\Big\{f_j'(x)\cos\big[tk_j(x)\big] - k_j'(x)\sin\big[tk_j(x)\big]\Big\}, \tag{4.31}$$

by dealing with their complex analogues.

Writing the trigonometric functions in complex form

$$\cos\theta = \frac{e^{i\theta}+e^{-i\theta}}{2} \qquad \text{and} \qquad \sin\theta = \frac{e^{i\theta}-e^{-i\theta}}{2i},$$

equation (4.31) gives

$$A(t,x) = \sum_{j=1}^{n}\Big\{\big[f_j'(x)+ik_j'(x)\big]e^{t[f_j(x)+ik_j(x)]} + \big[f_j'(x)-ik_j'(x)\big]e^{t[f_j(x)-ik_j(x)]}\Big\}. \quad (4.32)$$

By defining

$$\gamma_j(x) = f_j(x) + ik_j(x), \qquad j = 1,2,\ldots,n, \quad (4.33)$$

with their complex conjugate $\bar{\gamma}_j(x)$, equation (4.32) can be more elegantly written as

$$\begin{aligned} A(t,x) &= \sum_{j=1}^{n}\Big[\gamma_j'(x)e^{t\gamma_j(x)} + \bar{\gamma}_j'(x)e^{t\bar{\gamma}_j(x)}\Big] \quad (4.34)\\ &= 2\,\mathrm{Re}\sum_{j=1}^{n}\gamma_j'(x)e^{t\gamma_j(x)}. \end{aligned}$$

We now state and prove the following theorem.

Theorem 4.7. *Let $A(t,x)$ be a function of the form* (4.34)*. Then $A(t,x)$ solves the A-equation* (4.3) *if and only if $\gamma_j(x)$ satisfy the following system of differential equations*

$$\gamma_j'' = \gamma_j\gamma_j' + \sum_{\substack{l=1\\ l\neq j}}^{n}\frac{2\gamma_j'\gamma_l'}{\gamma_j-\gamma_l} + \sum_{l=1}^{n}\frac{2\gamma_j'\bar{\gamma}_l'}{\gamma_j-\bar{\gamma}_l}, \qquad j = 1,2,\ldots,n. \quad (4.35)$$

Proof. Let

$$I_1 = \frac{\partial A}{\partial x}(t,x), \qquad I_2 = \frac{\partial A}{\partial t}(t,x) \qquad \text{and} \qquad I_3 = \int_0^t A(s,x)A(t-s,x)\,ds.$$

From (4.34), we find

$$I_1 = \sum_{j=1}^{n} \Big\{ \Big[\gamma_j''(x) + t\big(\gamma_j'(x)\big)^2 \Big] e^{t\gamma_j(x)} + \Big[\bar{\gamma}_j''(x) + t\big(\bar{\gamma}_j'(x)\big)^2 \Big] e^{t\bar{\gamma}_j(x)} \Big\},$$

$$I_2 = \sum_{j=1}^{n} \Big\{ \gamma_j(x)\gamma_j'(x) e^{t\gamma_j(x)} + \bar{\gamma}_j(x)\bar{\gamma}_j'(x) e^{t\bar{\gamma}_j(x)} \Big\},$$

and

$$I_3 = \sum_{j=1}^{n} \Bigg\{ \Bigg[\sum_{\substack{l=1 \\ l\neq j}}^{n} \frac{2\gamma_j'(x)\gamma_l'(x)}{\gamma_j(x) - \gamma_l(x)} + \sum_{l=1}^{n} \frac{2\gamma_j'(x)\bar{\gamma}_l'(x)}{\gamma_j(x) - \bar{\gamma}_l(x)} + t\big(\gamma_j'(x)\big)^2 \Bigg] e^{t\gamma_j(x)}$$
$$+ \Bigg[\sum_{\substack{l=1 \\ l\neq j}}^{n} \frac{2\bar{\gamma}_j'(x)\bar{\gamma}_l'(x)}{\bar{\gamma}_j(x) - \bar{\gamma}_l(x)} + \sum_{l=1}^{n} \frac{2\bar{\gamma}_j'(x)\gamma_l'(x)}{\bar{\gamma}_j(x) - \gamma_l(x)} + t\big(\bar{\gamma}_j'(x)\big)^2 \Bigg] e^{t\bar{\gamma}_j(x)} \Bigg\}.$$

If $A(t,x)$ solves the A-equation (4.3), then the system (4.35) follows immediately from the above equalities.

Conversely, if $\gamma_j(x)$ satisfy (4.35), then direct calculation shows that the function $A(t,x)$ is indeed a solution of the A-equation. □

From (4.31), we immediately obtain

$$q(x) = 2\sum_{j=1}^{n} f_j'(x), \tag{4.36}$$

which, according to (4.34), takes the form

$$q(x) = \sum_{j=1}^{n} \Big[\gamma_j'(x) + \bar{\gamma}_j'(x) \Big]$$
$$= 2\,\mathrm{Re} \sum_{j=1}^{n} \gamma_j'(x).$$

4.6.2 A conjecture

The purpose of this subsection is to test the following conjecture.

Conjecture 4.1. *The exact solution of the A-equation* (4.3) *corresponding to the Oldroyd-B model is of the form*

$$A(t,x) = 2\sum_{j=1}^{2} e^{tf_j(x)}\Big\{f_j'(x)\cos\big[tk_j(x)\big] - k_j'(x)\sin\big[tk_j(x)\big]\Big\}. \tag{4.37}$$

With $n = 2$ and taking into account (4.33), the system (4.35) gives

$$\begin{aligned} f_1'' = {} & f_1 f_1' - k_1 k_1' + 2\frac{(f_1-f_2)(f_1'f_2' + k_1'k_2') + (k_1+k_2)(f_2'k_1' - f_1'k_2')}{(f_1-f_2)^2 + (k_1+k_2)^2} \\ & + 2\frac{(f_1-f_2)(f_1'f_2' - k_1'k_2') + (k_1-k_2)(f_1'k_2' + f_2'k_1')}{(f_1-f_2)^2 + (k_1-k_2)^2}, \end{aligned} \tag{4.38a}$$

$$\begin{aligned} f_2'' = {} & f_2 f_2' - k_2 k_2' + 2\frac{(f_2-f_1)(f_2'f_1' + k_2'k_1') + (k_2+k_1)(f_1'k_2' - f_2'k_1')}{(f_2-f_1)^2 + (k_2+k_1)^2} \\ & + 2\frac{(f_2-f_1)(f_2'f_1' - k_2'k_1') + (k_2-k_1)(f_2'k_1' + f_1'k_2')}{(f_2-f_1)^2 + (k_2-k_1)^2}, \end{aligned} \tag{4.38b}$$

$$\begin{aligned} k_1'' = {} & f_1' k_1 + f_1 k_1' + 2\frac{(f_1-f_2)(f_2'k_1' - f_1'k_2') - (k_1+k_2)(f_1'f_2' + k_1'k_2')}{(f_1-f_2)^2 + (k_1+k_2)^2} \\ & + 2\frac{(f_1-f_2)(f_1'k_2' + f_2'k_1') - (k_1-k_2)(f_1'f_2' - k_1'k_2')}{(f_1-f_2)^2 + (k_1-k_2)^2} - \frac{(f_1')^2 + (k_1')^2}{k_1}, \end{aligned} \tag{4.38c}$$

$$\begin{aligned} k_2'' = {} & f_2' k_2 + f_2 k_2' + 2\frac{(f_2-f_1)(f_1'k_2' - f_2'k_1') - (k_2+k_1)(f_2'f_1' + k_2'k_1')}{(f_2-f_1)^2 + (k_2+k_1)^2} \\ & + 2\frac{(f_2-f_1)(f_2'k_1' + f_1'k_2') - (k_2-k_1)(f_2'f_1' - k_2'k_1')}{(f_2-f_1)^2 + (k_2-k_1)^2} - \frac{(f_2')^2 + (k_2')^2}{k_2}. \end{aligned} \tag{4.38d}$$

In order that (4.37) at $x = 0$ agrees with the A-amplitude for the Oldroyd-B model, i.e.,

$$A(t) = -4\eta_1 t - \frac{2\eta_2}{\sqrt{\tau_2}} \sin(2\sqrt{\tau_2}t),$$

we must choose

$$f_1(0) = f_1'(0) = f_2(0) = f_2'(0) = 0, \qquad k_2(0) = 2\sqrt{\tau_2}, \qquad k_2'(0) = \frac{\eta_2}{\sqrt{\tau_2}}, \tag{4.39a}$$

$$\lim_{x\to 0} k_1'(x) \sin\big[tk_1(x)\big] = 2\eta_1 t. \tag{4.39b}$$

The reason why we state Conjecture 4.1 as a conjecture rather than a theorem is because we have been unable to find an explicit solution for the nonlinear system (4.38) and (4.39). Neither have we proved that this system admits a solution. Nevertheless, we are able to present strong evidence that the conjecture is true. We do this in two ways. Firstly, by showing that the system admits an asymptotic solution as $x \to 0$, and that the resulting asymptotic solution for $q(x)$ agrees with the Oldroyd-B potential derived in the previous chapter, up to and including the third order. Secondly, by solving the system numerically in the range $0 \leq x \leq 10$ and comparing the resulting $q(x)$ with the exact values obtained from the Oldroyd-B potential.

We note that (4.39b) is satisfied if $k_1(x) \to 0$ and

$$\frac{k_1'(x)}{2\eta_1} \sim \frac{1}{k_1(x)}, \qquad \text{as} \qquad x \to 0. \tag{4.40}$$

We anticipate the same singularity in $k_1'(x)$ as is found in the Newtonian case. From (4.15b), we note

$$k(x) = O(\sqrt{x}), \qquad \text{as} \qquad x \to 0.$$

Therefore, if we assume

$$k_1(x) \sim \alpha x^\beta, \qquad \text{as} \qquad x \to 0,$$

then it follows from (4.40) that

$$k_1(x) \sim 2\sqrt{\eta_1 x}, \qquad \text{as} \qquad x \to 0.$$

Hence, to eliminate the singularity of $k_1'(x)$ at the origin, we can use the following transformation

$$k_1(x) = \sqrt{x}\, y(x). \tag{4.41}$$

Having substituted (4.41) into system (4.38), we look for series expansions of the transformed system, i.e., we look for solutions expanded as follows

$$f_j(x) \sim \frac{f_j^{(2)}(0)}{2}x^2 + \frac{f_j^{(3)}(0)}{6}x^3 + \frac{f_j^{(4)}(0)}{24}x^4, \qquad j = 1, 2, \tag{4.42a}$$

$$k_2(x) \sim 2\sqrt{\tau_2} + \frac{\eta_2}{\sqrt{\tau_2}}x + \frac{k_2^{(2)}(0)}{2}x^2 + \frac{k_2^{(3)}(0)}{6}x^3, \tag{4.42b}$$

$$y(x) \sim 2\sqrt{\eta_1} + y^{(1)}(0)x + \frac{y^{(2)}(0)}{2}x^2 + \frac{y^{(3)}(0)}{6}x^3, \tag{4.42c}$$

as $x \to 0$. Substituting (4.42) into the transformed system, we obtain

$$f_1^{(2)}(0) = -2\eta_1, \qquad f_1^{(3)}(0) = \frac{12\eta_1\eta_2}{\tau_2}, \qquad f_1^{(4)}(0) = \frac{72\eta_1\eta_2(\eta_1 - \eta_2)}{\tau_2^2},$$

$$f_2^{(2)}(0) = -2\eta_2, \qquad f_2^{(3)}(0) = -\frac{12\eta_1\eta_2}{\tau_2}, \qquad f_2^{(4)}(0) = 8\eta_2\tau_2 - \frac{72\eta_1\eta_2(\eta_1 - \eta_2)}{\tau_2^2},$$

$$k_2^{(2)}(0) = \frac{\eta_2(4\eta_1 - \eta_2)}{2\tau_2\sqrt{\tau_2}}, \quad k_2^{(3)}(0) = \frac{\eta_2(24\eta_1^2 - 36\eta_1\eta_2 + 3\eta_2^2 - 16\tau_2^3)}{4\tau_2^2\sqrt{\tau_2}},$$

and

$$y^{(1)}(0) = -\frac{\eta_2\sqrt{\eta_1}}{\tau_2}, \qquad y^{(2)}(0) = \frac{\eta_2\sqrt{\eta_1}(3\eta_2 - 4\eta_1)}{2\tau_2^2},$$

$$y^{(3)}(0) = \frac{\sqrt{\eta_1}\left[2\tau_2^3(4\eta_2 - 7\eta_1) - 3\eta_2(8\eta_1^2 + 5\eta_2^2 - 20\eta_1\eta_2)\right]}{4\tau_2^3}.$$

Consequently, from (4.36), it follows that

$$\begin{aligned} q(x) &= 2\big[f_1'(x) + f_2'(x)\big] \\ &\sim -4(\eta_1+\eta_2)x + \frac{8}{3}\eta_2\tau_2 x^3, \qquad \text{as} \qquad x \to 0. \end{aligned}$$

This is the same asymptotic behaviour as that for the Oldroyd-B potential (see (3.40)), which is consistent with Conjecture 4.1.

We now turn to the second way of testing Conjecture 4.1. With $\eta_1 = \eta_2 = \tau_2 = 1$, the transformed system together with the initial conditions is solved numerically using a Fehlberg fourth-fifth order Runge-Kutta method in Maple 15. The resulting values for $q(x)$ are shown in Figure 4.9 and Table 4.2 together with the exact values obtained from the Oldroyd-B potential (3.39). The figure and the table show a very good agreement between these values, which again suggests that the Oldroyd-B solution is of the form (4.37).

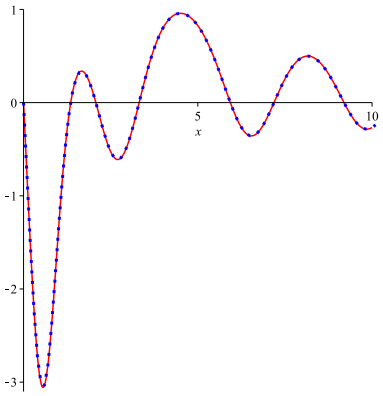

Figure 4.9: The numerical (dots) and exact (line) $q(x)$ for the Oldroyd-B model with $\eta_1 = \eta_2 = \tau_2 = 1$.

	$q(x)$	
x	Numerical	Exact
0	0.0000000	0.0000000
2	0.0972307	0.0972304
4	0.8009791	0.8009787
6	-0.0656150	-0.0656148
8	0.4856779	0.4856768
10	-0.2681532	-0.2681515

Table 4.2: The numerical and exact $q(x)$ for the Oldroyd-B model with $\eta_1 = \eta_2 = \tau_2 = 1$.

5

AN INVERSE SPECTRAL PROBLEM WITH CONTINUOUS SPECTRAL FUNCTION

In Chapter 3, we have considered inverse spectral problems with spectral functions of the form

$$\rho(\tau) = \int_0^\tau H(\tau')\,d\tau' + \rho_0(\tau), \qquad \tau \geq 0. \tag{5.1}$$

We were able to provide exact solutions to these problems in the case where the relaxation spectrum $H(\tau)$ is discrete. In this final chapter, we study an inverse spectral problem in which $H(\tau)$ in (5.1) is piecewise continuous. It is not possible to solve this problem exactly, and we look at two numerical approaches to solve the problem.

The first approach is based on approximating the solution of the A-equation

$$\frac{\partial A(t,x)}{\partial x} = \frac{\partial A(t,x)}{\partial t} + \int_0^t A(s,x)A(t-s,x)\,ds, \tag{5.2}$$

as an expansion in shifted Chebyshev polynomials. This approximation reduces (5.2) to a system of Riccati differential equations, which can be solved numerically resulting in an approximation for the potential $q(x)$. In the second approach, we approximate $\rho(\tau)$ in (5.1) by a stepwise spectral function, which corresponds to a multi-mode Maxwell model. The Gelfand-Levitan method is then used to calculate the corresponding potential which serves as an alternative approximation for $q(x)$.

5.1 Reducing the A-equation to a Riccati system

Let $\{\phi_n(t)\}_{n\geq 0}$ be a sequence of polynomials orthogonal on the interval Ω with respect to the weight function $w(t)$, i.e.,

$$\langle \phi_m, \phi_n \rangle = \int_\Omega \phi_m(t)\phi_n(t)w(t)\,dt = \begin{cases} 0, & m \neq n, \\ a_n, & m = n. \end{cases} \tag{5.3}$$

We look for an approximate solution of the A-equation (5.2) expanded as follows

$$A(t,x) \approx \sum_{n=0}^{N} \phi_n(t) C_n(x), \qquad t,x \in \Omega, \tag{5.4}$$

where $C_n(x)$ are unknown functions to be determined. Substituting (5.4) into (5.2) yields

$$\sum_{n=0}^{N} \phi_n(t) C_n'(x) = \sum_{n=0}^{N} \phi_n'(t) C_n(x) + \sum_{m=0}^{N} \sum_{n=0}^{N} I_{mn}(t) C_m(x) C_n(x),$$

where

$$I_{mn}(t) = \int_0^t \phi_m(s) \phi_n(t-s)\, ds.$$

Using (5.3), we obtain the following system of Riccati equations

$$C_k'(x) = \frac{1}{a_k} \sum_{n=0}^{N} \langle \phi_k, \phi_n' \rangle C_n(x) + \frac{1}{a_k} \sum_{m=0}^{N} \sum_{n=0}^{N} \langle \phi_k, I_{mn} \rangle C_m(x) C_n(x), \qquad k = 0,1,\ldots,N. \tag{5.5}$$

In addition, from (5.4), we find

$$A(t) \approx \sum_{n=0}^{N} \phi_n(t) C_n(0), \qquad t \in \Omega, \tag{5.6}$$

which, upon using (5.3), gives

$$C_k(0) = \frac{1}{a_k} \langle \phi_k, A \rangle, \qquad k = 0,1,\ldots,N. \tag{5.7}$$

Hence, it turns out that the suggested approximation (5.4) reduces the A-equation (5.2) to the system of $N+1$ Riccati equations (5.5). By solving this system, together with the initial conditions (5.7), one can find the unknown functions $C_k(x)$, and consequently obtain the following approximation for the solution of the inverse spectral problem

$$q(x) \approx \sum_{n=0}^{N} \phi_n(0) C_n(x), \qquad x \in \Omega. \tag{5.8}$$

In setting up the Riccati system (5.5), we must choose the interval Ω and a convenient sequence of orthogonal polynomials $\{\phi_n(t)\}_{n\geq 0}$. Ideally, the choice $\Omega = [0, \infty)$ would enable us to approximate the potential $q(x)$ over the entire half-line, $x \geq 0$. An essential requirement is that an accurate approximation is possible for the initial condition (5.6). In particular, we must allow for the fact that $A(t)$ is likely to be an oscillatory function (see equation (4.6) and Table 4.1). It is well known (see, for instance, Gottlieb and Orszag [14, p 42]) that orthogonal polynomials defined on $[0, \infty)$ require a larger number of terms per wavelength in approximating an oscillatory function than do orthogonal polynomials defined on a finite interval. For example, the expansion of $\sin t$ in terms of Chebyshev polynomials

$$T_n(t) = \cos(n \arccos t), \qquad t \in [-1, 1], \qquad n \geq 0,$$

is

$$\sin t = 2 \sum_{n=1}^{\infty} J_n(1) \sin\Big(\frac{n\pi}{2}\Big) T_n(t), \tag{5.9}$$

where J_n denotes the Bessel function of order n. The Laguerre expansion of $\sin t$ on the interval $[0, \infty)$ is

$$\sin t = \sum_{n=0}^{\infty} 2^{-\frac{n+1}{2}} \cos\left[\frac{(n+1)\pi}{4}\right] L_n(t). \tag{5.10}$$

The maximum error after N terms (N odd) in (5.9) is approximately $2J_{N+2}(1)$, while in (5.10), with $N \gg t > 0$, the error is roughly

$$\frac{e^{t/2}}{2^{N/2}(Nt)^{1/4}}.$$

Comparing (5.9) and (5.10), truncated to N terms, for values of t in the range $[0, 1]$, (5.9) requires $N = 7$ to give an error of $\approx 10^{-8}$, whereas (5.10) requires $N > 50$ to give an error of $\approx 10^{-8}$.

Another possibility in dealing with the interval $\Omega = [0, \infty)$ is the choice of rational Chebyshev functions, as studied by Boyd [4]. Here one maps the interval $0 \leq t < \infty$ onto the interval $-1 \leq y \leq 1$ using the map

$$t = \frac{L(1+y)}{1-y}, \qquad y = \frac{t-L}{t+L},$$

with a mapping constant L. Boyd [4, pp 457-458]) points out that rational Chebyshev approximations give poor results for oscillatory functions unless the function also decays exponentially at infinity. If we attempt to expand $\sin t$ in terms of the rational Chebyshev functions

$$R_n(t) = T_n\left(\frac{t-L}{t+L}\right),$$

in the form

$$\sin t = \sum_{n=0}^{\infty} c_n R_n(t),$$

then

$$c_n = \frac{2}{\pi}\int_0^{\pi} \cos(n\theta)\sin\left[L\cot^2\left(\frac{\theta}{2}\right)\right] d\theta, \qquad n \geq 1.$$

The function $\cot^2(\theta/2)$ and its derivatives are all singular at $\theta = 0$ which rules out a rapid rate of decay in the coefficients. For this reason, we restrict attention to finite intervals, and the use of shifted Chebyshev polynomials.

5.2 Shifted Chebyshev polynomials

The facts given in this section can be found in [12].

The shifted Chebyshev polynomials, denoted by $S_n(t)$, are defined on the finite interval $[0, a]$ by

$$S_n(t) = T_n\left(\frac{2t-a}{a}\right).$$

Such polynomials can also be generated using the three-term recurrence relation

$$\begin{cases} S_n(t) = 2\left(\frac{2t-a}{a}\right)S_{n-1}(t) - S_{n-2}(t), & n \geq 2, \\ S_0(t) = 1 \qquad S_1(t) = \frac{2t-a}{a}. \end{cases}$$

Two important properties of the shifted Chebyshev polynomials are the orthogonality relation

$$\langle S_m, S_n \rangle = \int_0^a \frac{S_m(t)S_n(t)}{\sqrt{t(a-t)}}\, dt = \begin{cases} \pi, & m = n = 0, \\ 0, & m \neq n, \\ \frac{\pi}{2}, & m = n > 0, \end{cases}$$

and

$$S_n(0) = (-1)^n, \qquad n \geq 0. \tag{5.11}$$

The shifted Chebyshev expansion, truncated after $N+1$ terms, of a function $f(t)$ continuous on $[0, a]$ serves as an approximation for $f(t)$

$$f(t) \approx \sum_{n=0}^{N} b_n S_n(t), \qquad t \in [0, a],$$

where

$$b_0 = \frac{1}{\pi}\langle S_0, f \rangle \qquad \text{and} \qquad b_n = \frac{2}{\pi}\langle S_n, f \rangle, \quad n = 1, 2, \ldots, N.$$

The error bound for the above approximation is given by

$$\left| f(t) - \sum_{n=0}^{N} b_n S_n(t) \right| \leq \sum_{n=N+1}^{\infty} |b_n|.$$

Furthermore, if the function $f(t)$ is sufficiently smooth, then the coefficients b_n decay exponentially fast as n increases, guaranteeing an accurate approximation with relatively few terms.

5.3 Numerical examples for inverse spectral problems

In this section, we will attempt to recover the potential $q(x)$ from a continuous spectral function of the form (5.1) by solving the A-equation numerically. We shall do this for the spectral function which corresponds to a viscoelastic box spectrum. Before attempting the calculations for a box spectrum, for which $q(x)$ is unknown, we will first test our numerical method using two examples from Chapter 3 for which $q(x)$ is known exactly.

In the following three examples, the solution $A(t,x)$ of the A-equation (5.2) is approximated in the domain

$$0 \leq x \leq 6, \qquad \text{and} \qquad 0 \leq x+t \leq 6,$$

using the shifted Chebyshev method, i.e., the method presented in Section 5.1 with the shifted Chebyshev polynomials as basis polynomials. The resulting Riccati system is solved numerically using a Fehlberg fourth-fifth order Runge-Kutta method in Maple 15. The desired approximation for $q(x)$ is then obtained using

$$q(x) \approx \sum_{n=0}^{N} (-1)^n C_n(x), \qquad x \in [0,6],$$

which follows from (5.8) and the property (5.11).

5.3.1 The Newtonian potential

For the Newtonian model, the A-amplitude with $\eta_1 = 1$ takes the form

$$A(t) = -4t, \tag{5.12}$$

and the corresponding exact potential, according to Theorem 3.6, is

$$q(x) = \frac{6x(x^3-6)}{(x^3+3)^2}. \tag{5.13}$$

The coefficients in the shifted Chebyshev expansion of (5.12) have the following values

$$C_k(0) = \begin{cases} -12, & k \leq 1, \\ 0, & k > 1. \end{cases}$$

The numerical results of $q(x)$ obtained using the shifted Chebyshev method with $N = 10$ and $N = 15$ are shown in Table 5.1 together with the exact results obtained from (5.13) for different values of x. The table shows that the numerical results converge to the exact results in the interval $[0, 6]$.

	$q(x)$		
x	$N = 10$	$N = 15$	Exact
0	0.00000	0.00000	0.00000
1	-1.87513	-1.87500	-1.87500
2	0.19806	0.19835	0.19835
3	0.42024	0.42000	0.42000
4	0.30993	0.31009	0.31009
5	0.21797	0.21790	0.21790
6	0.15728	0.15763	0.15763

Table 5.1: The numerical and exact Newtonian potential with $\eta_1 = 1$.

Figure 5.1 shows (5.13) along with its approximation obtained with $N = 15$.

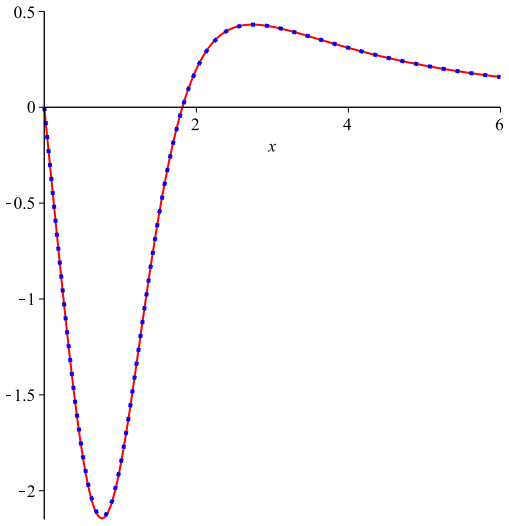

Figure 5.1: The Newtonian potential with $\eta_1 = 1$ (line) and its approximation with $N = 15$ (dots).

5.3.2 The Maxwell potential

For the Maxwell model, the A-amplitude with $\eta_1 = \tau_1 = 1$ takes the form

$$A(t) = -2\sin(2t), \tag{5.14}$$

and the corresponding exact potential, according to Theorem 3.8, is

$$q(x) = \frac{16\big[\big(1-\cos(2x)\big) - (x+2)\sin(2x)\big]}{\big[2(x+2) - \sin(2x)\big]^2}. \tag{5.15}$$

The coefficients in the shifted Chebyshev expansion of (5.14) are shown in Table 5.2 for $n = 0, 1, \ldots, 20$. The table indicates that 21 shifted Chebyshev polynomials produce a good approximation for $A(t)$.

n	$C_n(0)$	n	$C_n(0)$	n	$C_n(0)$
0	0.08419	7	0.49770	14	-0.00003
1	1.06266	8	0.06318	15	0.00002
2	0.27145	9	-0.08129	16	1.3E-06
3	0.44079	10	-0.00778	17	-8.4E-07
4	0.39972	11	0.00787	18	-4.2E-08
5	-1.39066	12	0.00061	19	2.3E-08
6	-0.27476	13	-0.00051	20	1.0E-09

Table 5.2: The coefficients in the shifted Chebyshev expansion of (5.14).

The numerical results of $q(x)$ obtained using the shifted Chebyshev method with $N = 15$ and $N = 20$ are shown in Table 5.3 together with the exact results obtained from (5.15) for different values of x. As can be seen, the numerical results converge to the exact results in the interval $[0, 6]$. Finally, we plot in Figure 5.2 the exact $q(x)$ in (5.15) along with its approximation obtained with $N = 20$.

	$q(x)$		
x	$N = 15$	$N = 20$	Exact
0	0.00000	0.00000	0.00000
1	-0.80983	-0.80987	-0.80987
2	0.97670	0.97668	0.97668
3	0.21760	0.21758	0.21758
4	-0.63222	-0.63225	-0.63225
5	0.42795	0.42716	0.42716
6	0.67877	0.26029	0.26029

Table 5.3: The numerical and exact Maxwell potential with $\eta_1 = \tau_1 = 1$.

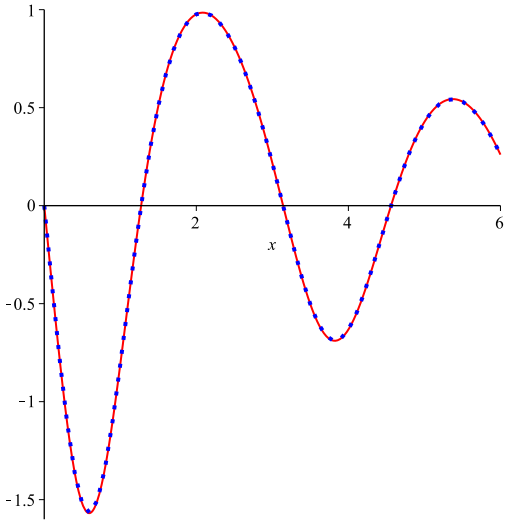

Figure 5.2: The Maxwell potential with $\eta_1 = \tau_1 = 1$ (line) and its approximation with $N = 20$ (dots).

5.3.3 The box potential

Having tested our numerical method, we now proceed to recover the potential $q(x)$ from the spectral function (5.1) in which $H(\tau)$ is chosen to be the box relaxation spectrum

$$H(\tau) = \begin{cases} 1, & \frac{1}{2} \leq \tau \leq \frac{3}{2}, \\ 0, & \text{otherwise.} \end{cases} \tag{5.16}$$

It then follows from (5.1) that

$$\rho(\tau) = \rho_0(\tau) + \begin{cases} 0, & 0 < \tau \leq \frac{1}{2}, \\ \tau - \frac{1}{2}, & \frac{1}{2} < \tau \leq \frac{3}{2}, \\ 1, & \frac{3}{2} < \tau. \end{cases} \tag{5.17}$$

Remark 5.1. We note that the box spectrum (5.16) satisfies the condition of Theorem 3.1 for $\rho(\tau)$ in (5.17) to be a spectral function.

From (4.6) and (5.16), we find that the A-amplitude for the box spectrum takes the form

$$A(t) = -\frac{2}{t}\Big[\cos\big(\sqrt{2}t\big) - \cos\big(\sqrt{6}t\big)\Big]. \tag{5.18}$$

Table 5.4 shows the first twenty six coefficients in the shifted Chebyshev expansion of (5.18). The table indicates that with $N = 25$, we get a very good approximation for $A(t)$.

n	$C_n(0)$	n	$C_n(0)$	n	$C_n(0)$
0	-0.25145	9	-0.07792	18	3.7E-07
1	0.46270	10	0.01222	19	8.5E-08
2	-0.28206	11	0.00958	20	-1.3E-08
3	0.07444	12	-0.00161	21	-2.6E-09
4	0.61463	13	-0.00080	22	3.9E-10
5	-0.83847	14	0.00014	23	6.1E-11
6	-0.03766	15	0.00005	24	-8.7E-12
7	0.38031	16	-8.2E-06	25	-2.8E-12
8	-0.04431	17	-2.3E-06		

Table 5.4: The coefficients in the shifted Chebyshev expansion of (5.18).

The numerical results for $q(x)$ obtained using the shifted Chebyshev method with $N = 15$, $N = 20$ and $N = 25$ are shown in Table 5.5 for different values of x. These results demonstrate numerical convergence as N increases.

	$q(x)$		
x	$N = 15$	$N = 20$	$N = 25$
0	0.00000	0.00000	0.00000
1	-0.83208	-0.83214	-0.83214
2	0.78042	0.78040	0.78040
3	0.03767	0.03763	0.03763
4	-0.04715	-0.04721	-0.04721
5	0.00023	-0.00274	-0.00274
6	2.34840	-0.18767	-0.18762

Table 5.5: The numerical results of the box potential.

For later convenience, we denote by $q_{sc}(x)$ the approximation of the box potential obtained using the shifted Chebyshev method with $N = 25$, i.e.,

$$q_{sc}(x) = \sum_{n=0}^{25} (-1)^n C_n(x), \qquad x \in [0,6]. \tag{5.19}$$

This is shown in Figure 5.3 below.

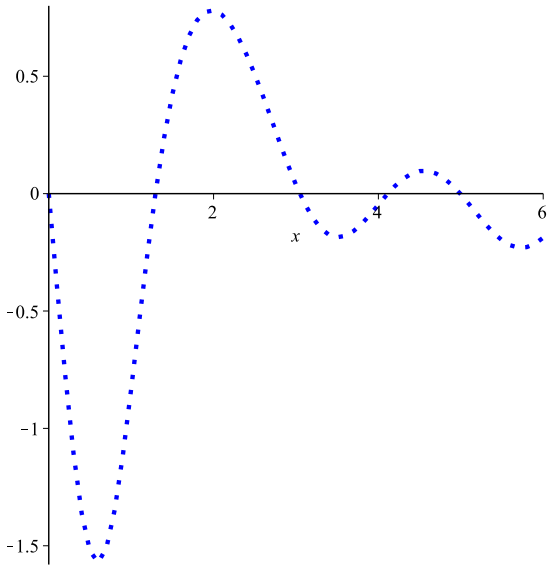

Figure 5.3: The approximation $q_{sc}(x)$ of the box potential.

Remark 5.2. In the above three examples, the calculations are run on a PC with a 2.70 GHz Pentium(R) Dual-Core processor. The CPU time taken (in minutes) for setting up and solving the Riccati system (5.5) is shown in Table 5.6.

N	Time (min)
10	2
15	11
20	35
25	94

Table 5.6: The CPU time.

5.4 Alternative approximations to the box potential

In the previous section, we have shown that it is possible to recover $q(x)$ numerically for a viscoelastic box spectrum by solving a Riccati system reduced from the A-equation, at least for a finite interval in x. If we attempt to increase the size of the finite interval, then the value of N required to reach numerical convergence also increases, making the CPU time for the calculations prohibitive. In this section, we adopt a different approach to recovering $q(x)$ for the box spectrum. The approach consists of two main steps:

(i) We approximate the box spectral function (5.17) by stepwise approximations

$$\rho_{2m}(\tau) = \sum_{k=1}^{m} \eta_{2m,k} U(\tau - \tau_{2m,k}) + \rho_0(\tau), \qquad \eta_{2m,k} = g_{2m,k}\tau_{2m,k}. \tag{5.20}$$

These are the spectral functions associated with the m-mode Maxwell model. The coefficients $g_{2m,k}$ and $\tau_{2m,k}$ are taken from the Dirichlet series approximations (2.17) derived in Chapter 2 for the box relaxation function (2.44) using the S-fraction method. These coefficients are to be found in Table 2.2 for various values of m.

(ii) The Gelfand-Levitan method of Chapter 3 is then used to calculate the corresponding potentials $q_{2m}(x)$. The elements of the matrix $T(x)$ in (3.21) are evaluated explicitly using Maple, and the differentiation (3.24) is also performed explicitly in Maple. It is not necessary to record the resulting expressions explicitly. They are easily evaluated and plotted numerically over any interval.

Using the data from Table 2.2, we plot $\rho_{2m}(\tau)$ versus the box spectral function (5.17) in Figures 5.4, 5.5, 5.6 with $m = 2, 4, 6$, respectively. These figures show that as m increases, $\rho_{2m}(\tau)$ gets closer to the box spectral function.

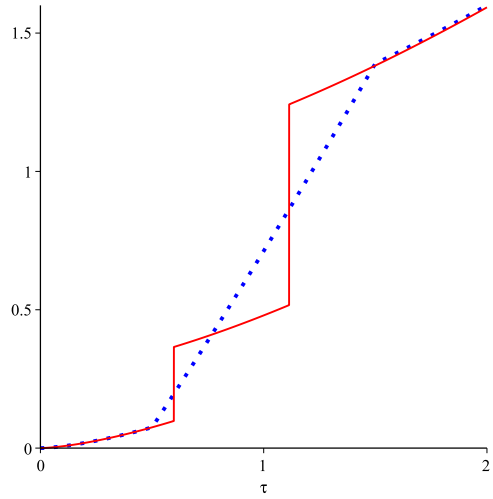

Figure 5.4: The box spectral function (dots) and $\rho_4(\tau)$ (line).

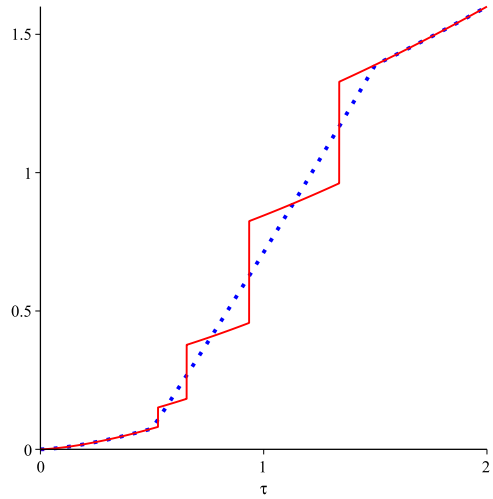

Figure 5.5: The box spectral function (dots) and $\rho_8(\tau)$ (line).

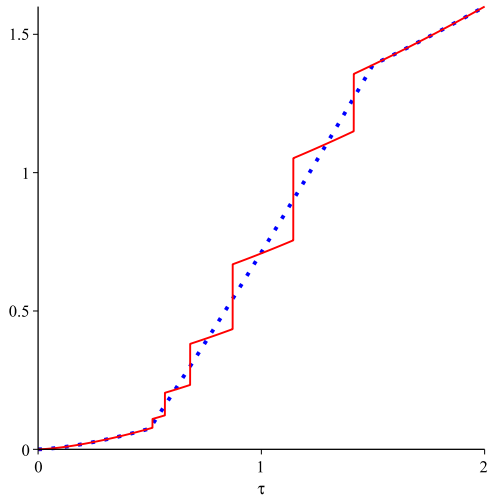

Figure 5.6: The box spectral function (dots) and $\rho_{12}(\tau)$ (line).

Using the Gelfand-Levitan method, we calculate the potentials $q_{2m}(x)$ for $m = 2, 4$ and 6. These are shown in Figure 5.7. The figure shows that, as m increases, $q_{2m}(x)$ demonstrates numerical convergence in the interval $0 \leq x \leq 6$.

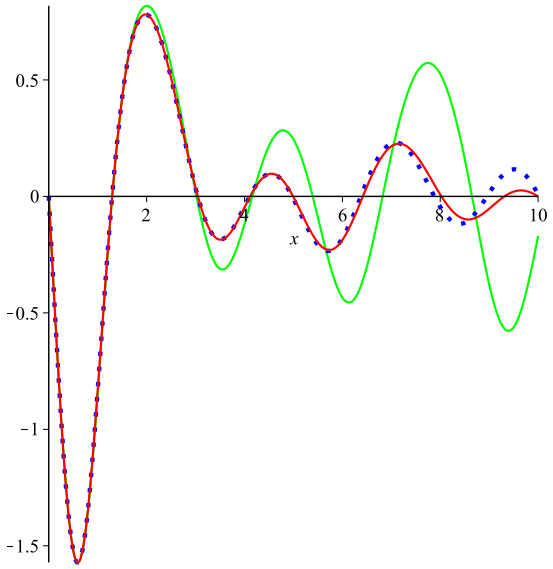

Figure 5.7: $q_{2m}(x)$ for $m = 2$ (green), $m = 4$ (blue) and $m = 6$ (red).

In Table 5.7, we show the numerical results of $q_{2m}(x)$ with $m = 2, 4, 6$ for different values of x. The table also shows the numerical results of $q_{sc}(x)$ in (5.19). We note that as we increase m, the values of $q_{2m}(x)$ approach those of $q_{sc}(x)$.

x	$q_4(x)$	$q_8(x)$	$q_{12}(x)$	$q_{sc}(x)$
0	0.00000	0.00000	0.00000	0.00000
1	-0.84625	-0.83221	-0.83214	-0.83214
2	0.81819	0.78064	0.78040	0.78040
3	0.01788	0.03623	0.03764	0.03763
4	-0.11878	-0.04330	-0.04722	-0.04721
5	0.24517	-0.01028	-0.00278	-0.00274
6	-0.43457	-0.18049	-0.18738	-0.18762

Table 5.7: $q_{2m}(x)$ with $m = 2, 4, 6$ and $q_{sc}(x)$ for different values of x.

Finally, in Figure 5.8, we plot $q_{12}(x)$ against $q_{sc}(x)$. The values of $q_{sc}(x)$ are available only in the interval $[0,6]$, whereas $q_{12}(x)$ is available for all $x \geq 0$ and is plotted in the interval $[0,10]$ for information.

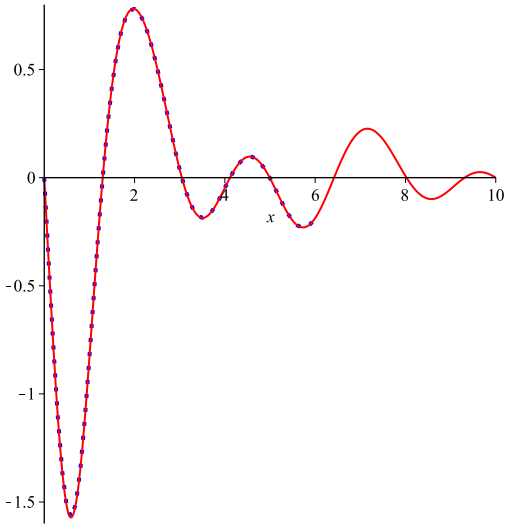

Figure 5.8: $q_{12}(x)$ (line) and $q_{sc}(x)$ (dots).

5.5 Discussion of results

Simon's uniqueness theorem [24] (see Section 4.1) tells us that $A(t)$ on the interval $0 \leq t \leq a$ determines $q(x)$ uniquely on the interval $0 \leq x \leq a$, and vice versa. If the process of calculating $q(x)$ from $A(t)$ is stable, then small perturbations in $A(t)$ will result in small perturbations in $q(x)$ on the interval $[0,a]$. In the shifted Chebyshev method with $a = 6$ and $N = 25$, the approximation of $A(t)$ in (5.18) by

$$A_{sc}(t) = \sum_{n=0}^{25} C_n(0) S_n(t), \qquad t \in [0,6],$$

is accurate to $\approx 10^{-12}$ (see Table 5.4). Furthermore, the numerical convergence of the potentials in Table 5.5 as N increases from 15 to 25 shows no evidence of instability. It would be reasonable to expect that the potential $q_{sc}(x)$ in (5.19) should be an accurate representation of the box potential on that interval.

Next, we consider the potentials $q_{2m}(x)$ derived from the stepwise spectral functions $\rho_{2m}(\tau)$. We see from Figures 5.4-5.6 that the perturbation $\|\rho(\tau) - \rho_{2m}(\tau)\|_\infty$ is not small. Nevertheless, as Figure 5.7 shows, the potentials $q_4(x)$, $q_8(x)$ and $q_{12}(x)$ change very little in the interval $0 \leq x \leq 2$, while $q_8(x)$ and $q_{12}(x)$ are in good agreement in the interval $0 \leq x \leq 6$. We also note from Figure 5.8 that $q_{12}(x)$ and $q_{sc}(x)$ are in excellent agreement in the interval $0 \leq x \leq 6$.

It is of interest to consider the A-amplitudes corresponding to the stepwise spectral functions $\rho_{2m}(\tau)$. These are given by

$$A_{2m}(t) = -2\sum_{k=1}^{m} \frac{\eta_{2m,k}}{\sqrt{\tau_{2m,k}}} \sin(2\sqrt{\tau_{2m,k}}t), \qquad \eta_{2m,k} = g_{2m,k}\tau_{2m,k}, \tag{5.21}$$

and are compared with the exact A-amplitude (5.18) in Figures 5.9, 5.10, 5.11 with $m = 2, 4, 6$, respectively. We note that $A_4(t)$ approximates $A(t)$ well in the interval $0 \leq t \leq 2$, $A_8(t)$ is accurate in the interval $0 \leq t \leq 6$, while $A_{12}(t)$ is accurate in the interval $0 \leq t \leq 10$. This would suggest that $q_{12}(x)$ is an accurate representation of the true box potential in the interval $0 \leq x \leq 10$.

As $t \to \infty$, the asymptotic behaviour of $A_{2m}(t)$ in (5.21) cannot reproduce the asymptotic behaviour of the exact $A(t)$ in (5.18). This means that while $q_{2m}(x)$ may provide a good approximation to the box potential $q(x)$ on a finite interval which increases in size with m, it must differ from $q(x)$ as $x \to \infty$.

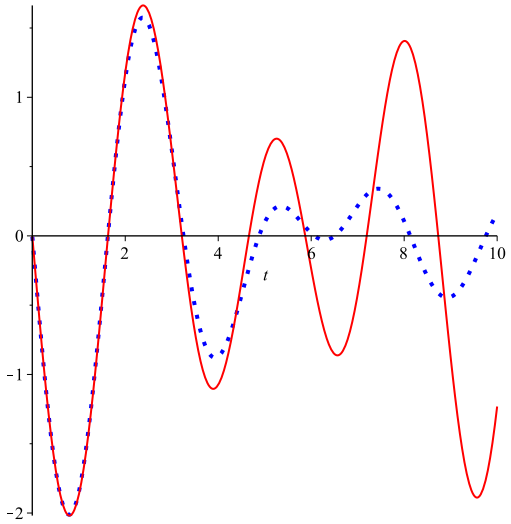

Figure 5.9: The box A-amplitude (dots) and $A_4(t)$ (line).

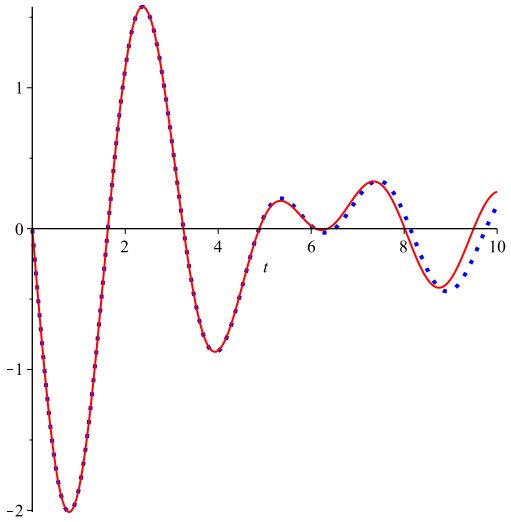

Figure 5.10: The box A-amplitude (dots) and $A_8(t)$ (line).

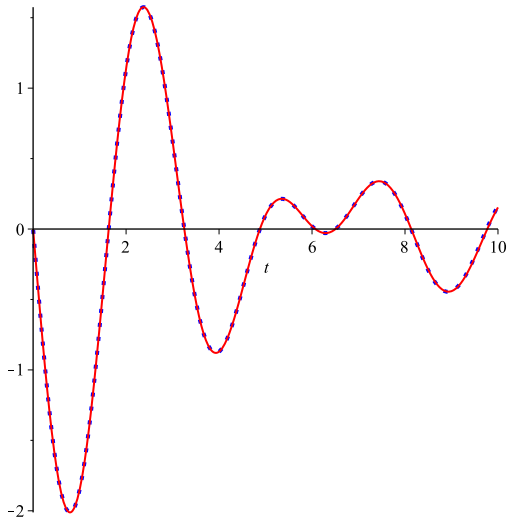

Figure 5.11: The box A-amplitude (dots) and $A_{12}(t)$ (line).

APPENDIX

In this appendix, we prove the following theorem.

Theorem. *Let*

$$G(t) = \int_0^\infty \exp(-st)\, d\mu(s), \tag{A.1}$$

where

(i) $d\mu(s)$ *is a non-negative measure on* $[0, \infty)$,

(ii) the integral converges for all $t \geq 0$,

(iii) $G(t)$ *is continuous for all* $t \geq 0$.

Let

$$\mu_{-1} = \int_0^\infty G(t)\, dt = \int_0^\infty s^{-1}\, d\mu(s),$$

be finite. Let $B(t)$ *be a formal power series,*

$$B(t) = \sum_{n=0}^{\infty} \frac{\gamma_n}{n!} t^n, \tag{A.2}$$

satisfying

$$\lim_{t \to 0} \frac{1}{t^n} \left[G(t) - \sum_{k=0}^{n} \frac{\gamma_k}{k!} t^k \right] = 0, \quad n = 0, 1, 2, \ldots. \tag{A.3}$$

Then all the integrals

$$\mu_n = \int_0^\infty s^n\, d\mu(s), \quad n = 0, 1, 2, \ldots,$$

exist and take the values

$$\mu_n = (-1)^n \gamma_n, \quad n = 0, 1, 2, \ldots.$$

Proof. We prove the theorem by induction. Let P_m be the following statement: μ_n exist for $n = -1, 0, \ldots, m$ and are equal to $(-1)^n \gamma_n$ for $n = -1, 0, \ldots, m-1$. P_0 is true if we define $\gamma_{-1} = -\mu_{-1}$. It also follows that $\mu_0 = G(0)$ from (A.1) and $G(0) = \gamma_0$ from (A.3). Hence, $\mu_0 = \gamma_0$. We therefore assume that P_m is true for some $m \geq 0$ and show that

$$\text{(i) } \mu_m = (-1)^m \gamma_m, \qquad \text{(ii) } \mu_{m+1} \text{ exists.}$$

Using the integral form of the remainder in the expansion of $\exp(-st)$, we find

$$\exp(-st) = \sum_{n=0}^{m-1} \frac{(-1)^n}{n!}(st)^n + \frac{(-1)^m}{(m-1)!} \int_0^t (t-u)^{m-1} \exp(-su) s^m \, du,$$

and hence, from (A.1), we obtain

$$G(t) = \sum_{n=0}^{m-1} \frac{\gamma_n}{n!} t^n + \frac{(-1)^m}{(m-1)!} \int_0^\infty \left[\int_0^t (t-u)^{m-1} \exp(-su) \, du \right] s^m \, d\mu(s). \qquad \text{(A.4)}$$

Comparing this with (A.2) gives

$$\frac{(-1)^m}{(m-1)!} \int_0^\infty \left[\int_0^t (t-u)^{m-1} \exp(-su) \, du \right] s^m \, d\mu(s) = \frac{\gamma_m}{m!} t^m + O(t^{m+1}),$$

which implies that

$$\gamma_m = (-1)^m \lim_{t \to 0} \frac{m}{t^m} \int_0^\infty \left[\int_0^t (t-u)^{m-1} \exp(-su) \, du \right] s^m \, d\mu(s).$$

Part (i) now follows since for all $s \geq 0$, the inner integral is convergent and

$$\lim_{t \to 0} \frac{m}{t^m} \int_0^t (t-u)^{m-1} \exp(-su) \, du = 1.$$

Turning to part (ii), we note that (A.2) and (A.4) together imply

$$\frac{(-1)^{m+1}}{m!} \int_0^\infty \left[\int_0^t (t-u)^m \exp(-su) \, du \right] s^{m+1} \, d\mu(s) = O(t^{m+1}),$$

from which we have

$$I = t^{-(m+1)} \int_0^\infty \left[\int_0^t (t-u)^m \exp(-su)\, du \right] s^{m+1}\, d\mu(s) = O(1).$$

Since the inner integral, for all $s \geq 0$ and under the transformation $v = t - u$, satisfies

$$\int_0^t (t-u)^m \exp(-su)\, du = \exp(-st) \int_0^t v^m \exp(sv)\, dv \geq \exp(-st) \frac{t^{m+1}}{m+1},$$

it follows then that

$$\int_0^\infty \exp(-st) s^{m+1}\, d\mu(s) \leq (m+1) I,$$

and consequently μ_{m+1} exists proving the truth of P_{m+1}. Hence, P_m is true for all $m \geq 0$. □

BIBLIOGRAPHY

[1] N. Aronszajn and W. F. Donoghue. On exponential representations of analytic functions in the upper half-plane with positive imaginary part. *Journal d'Analyse Mathématique,* 5:321-388, 1957.

[2] H. A. Barnes, J. F. Hutton and K. Walters. *An Introduction to Rheology.* Elsevier, Amsterdam, 1989.

[3] S. N. Bernstein. Sur les fonctions absolument monotones. *Acta Mathematica,* 52:166, 1928.

[4] J. P. Boyd. *Chebyshev and Fourier Spectral Methods.* Springer- Verlag, Berlin, 1989.

[5] K. Chadan and P. C. Sabatier. *Inverse Problems in Quantum Scattering Theory.* Springer-Verlag, Berlin, 1989.

[6] T. S. Chihara. *An introduction to orthogonal polynomials.* Gordon & Breach, New York, 1978.

[7] A. R. Davies and N. J. Goulding. Wavelet regularization and the continuous relaxation spectrum. *Journal of Non-Newtonian Fluid Mechanics,* 189:19-30, 2012.

[8] M. S. P. Eastham and H. Kalf. *Schrödinger-type Operators with Continuous Spectra.* Pitman, Boston, 1982.

[9] C. L. Epstein and J. Schotland. The bad truth about Laplace's transform. *SIAM Review,* 50:504-520, 2008.

[10] W. N. Everitt. On a property of the m-coefficient of a second-order linear differential equation. *J. London Math. Soc.,* 4:443-457, 1972.

[11] J. D. Ferry. *Viscoelastic Properties of Polymers, 3rd Edition.* John Wiley and Sons, New York, 1980.

[12] L. Fox and I. B. Parker. *Chebyshev Polynomials in Numerical Analysis.* Oxford University Press, London, 1968.

[13] F. Gesztesy and B. Simon. A new approach to inverse spectral theory, II. General real potentials and the connection to the spectral measure. *Annals of Mathematics,* 152:593-643, 2000.

[14] D. Gottlieb and S. A. Orszag. *Numerical Analysis of Spectral Methods: Theory and Applications.* SIAM, Philadelphia, 1977.

[15] P. Henrici. *Applied and Computational Complex Analysis, Vol. II.* John Wiley & Sons, New York, 1977.

[16] W. B. Jones and W. J. Thron. *Continued Fractions: Analytic Theory and Applications, Encyclopedia of Mathematics and Its Applications, Vol. 11.* Addison-Wesley, Reading, 1980.

[17] B. M. Levitan. *Inverse Sturm-Liouville Problems.* VNU Science Press, Utrecht, 1987.

[18] Y. Liu. Calculation of discrete relaxation modulus and creep compliance. *Rheologica Acta,* 38:357-364, 1999.

[19] Y. Liu. A direct method for obtaining discrete relaxation spectra from creep data. *Rheologica Acta,* 40:256-260, 2001.

[20] Y. Liu. Approximaion by Dirichlet series with nonnegative coefficients. *Journal of Approximation Theory,* 112:226-234, 2001.

[21] J. C. Maxwell. On the dynamical theory of gases. *Philosophical Transactions of the Royal Society of London,* 157:49-88, 1867.

[22] D. W. Mead. Numerical interconversion of linear viscoelastic material functions. *Journal of Rheology,* 38:1769-1795, 1994.

[23] J. G. Oldroyd. On the formulation of rheological equations of state. *Proceedings of the Royal Society,* A200:523-541, 1950.

[24] B. Simon. A new approach to inverse spectral theory, I. Fundamental formalism. *Annals of Mathematics,* 150:1029-1057, 1999.

[25] R. I. Tanner and K. Walters. *Rheology: An Historical Perspective.* Elsevier, Amsterdam, 1998.

[26] J. Van Deun. The Riemann ζ function and asymptotics for Stieltjes fractions. *The Ramanujan Journal,* 21:1-16, 2010.

[27] K. Walters. *Rheometry.* Chapman and Hall, London, 1975.

[28] D. V. Widder. *The Laplace Transform.* Princeton University Press, Princeton, New Jersey, 1946.

[29] Y. Zhang. Solvability of a class of integro-differential equations and connections to one-dimensional inverse problems. *Journal of Mathematical Analysis and Applications,* 321:286-298, 2006.